Physics of thin-film ferroelectric oxides

M. Dawber*

DPMC, University of Geneva, CH-1211, Geneva 4, Switzerland

K. M. Rabe†

Department of Physics and Astronomy, Rutgers University, Piscataway, New Jersey 00854-8019, USA

J. F. Scott‡

Department of Earth Sciences, University of Cambridge, Cambridge CB2 3EQ, United Kingdom

(Published 17 October 2005)

This review covers important advances in recent years in the physics of thin-film ferroelectric oxides, the strongest emphasis being on those aspects particular to ferroelectrics in thin-film form. The authors introduce the current state of development in the application of ferroelectric thin films for electronic devices and discuss the physics relevant for the performance and failure of these devices. Following this the review covers the enormous progress that has been made in the first-principles computational approach to understanding ferroelectrics. The authors then discuss in detail the important role that strain plays in determining the properties of epitaxial thin ferroelectric films. Finally, this review ends with a look at the emerging possibilities for nanoscale ferroelectrics, with particular emphasis on ferroelectrics in nonconventional nanoscale geometries.

CONTENTS

I. Introduction 1084
II. Ferroelectric Electronic Devices 1084
A. Ferroelectric memories 1084
B. Future prospects for nonvolatile ferroelectric memories 1086
C. Ferroelectric field-effect transistors 1087
D. Replacement of gate oxides in DRAMs 1088
III. Ferroelectric Thin-Film-Device Physics 1089
A. Switching 1089
1. Ishibashi-Orihara model 1089
2. Nucleation models 1089
3. The scaling of coercive field with thickness 1090
4. Mobility of 90° domain walls 1090
5. Imaging of domain-wall motion 1090
B. Electrical characterization 1092
1. Standard measurement techniques 1092
a. Hysteresis 1092
b. Current measurements 1093
c. Dielectric permittivity 1093
2. Interpretation of dielectric permittivity data 1093
a. Depletion charge versus intrinsic response 1093
b. Domain-wall contributions 1094
c. Dielectric measurements of phase transitions 1094
3. Schottky barrier formation at metal-ferroelectric junctions 1095
4. Conduction mechanisms 1097
a. Schottky injection 1097
b. Poole-Frenkel 1098
c. Fowler-Nordheim tunneling 1098
d. Space-charge-limited currents 1098
e. Ultrathin films—direct tunneling 1098
f. Grain boundaries 1098
C. Device failure 1099
1. Electrical breakdown 1099
2. Fatigue 1100
3. Retention failure 1102
IV. First Principles 1102
A. Density-functional-theory studies of bulk ferroelectrics 1102
B. First-principles investigation of ferroelectric thin films 1104
1. First-principles methodology for thin films 1105
2. Overview of systems 1107
3. Studies of individual one-component systems 1108
a. $BaTiO_3$ 1108
b. $PbTiO_3$ 1110
c. $SrBi_2Ta_2O_9$ 1111
d. $SrTiO_3$ and $KTaO_3$ 1111
4. Studies of individual heterostructures 1112
5. First-principles modeling: methods and lessons 1113
6. Challenges for first-principles modeling 1115
V. Strain Effects 1116
VI. Nanoscale Ferroelectrics 1121
A. Quantum confinement energies 1121
B. Coercive fields in nanodevices 1121
C. Self-patterned nanoscale ferroelectrics 1121
D. Nonplanar geometries: ferroelectric nanotubes 1122
VII. Conclusions 1124
References 1124

*Electronic address: matthew.dawber@physics.unige.ch
†Electronic address: rabe@physics.rutgers.edu
‡Electronic address: jsco99@esc.cam.ac.uk

 ©2005 The American Physical Society

I. INTRODUCTION

The aim of this review is to provide an account of the progress made in the understanding of the physics of ferroelectric thin-film oxides, particularly the physics relevant to present and future technology that exploits the characteristic properties of ferroelectrics. An overview of the current state of ferroelectric devices is followed by identification and discussion of the key physics issues that determine device performance. Since technologically relevant films for ferroelectric memories are typically thicker than 120 nm, characterization and analysis of these properties can initially be carried out at comparable length scales. However, for a deeper understanding, as well as for the investigation of the behavior of ultrathin films with thickness on the order of lattice constants, it is appropriate to redevelop the analysis at the level of atomic and electronic structure. Thus, the second half of this review is devoted to a description of the state of the art in first-principles theoretical investigations of ferroelectric-oxide thin films, concluding with a discussion of experiment and theory of nanoscale ferroelectric systems.

As a starting point for the discussion, it is helpful to have a clear definition of ferroelectricity appropriate to thin films and nanoscale systems. Here we consider a ferroelectric to be a pyroelectric material with two or more stable states of different nonzero polarization. Unlike *electrets*, ferroelectrics have polarization states that are thermodynamically stable, not metastable. Furthermore, it must be possible to switch between the two states by the application of a sufficiently strong electric field, the threshold field being designated the coercive field. This field must be less than the breakdown field of the material, or the material is merely pyroelectric and not ferroelectric. Because of this switchability of the spontaneous polarization, the relationship between the electric displacement D and the electric field E is hysteretic.

For thin-film ferroelectrics the high fields that must be applied to switch the polarization state can be achieved with low voltages, making them suitable for integrated electronics applications. The ability to create high-density arrays of capacitors based on thin ferroelectric films has spawned an industry dedicated to the commercialization of ferroelectric computer memories. The classic textbooks on ferroelectricity (Fatuzzo and Merz, 1967; Lines and Glass, 1967) though good, are now over 20 years old, and predate the shift in emphasis from bulk ceramics and single crystals towards thin-film ferroelectrics. While much of the physics required to understand thin-film ferroelectrics can be developed from the understanding of bulk ferroelectrics, there is also behavior specific to thin films that cannot be readily understood in this way. This is the focus of the present review.

One of the points that will become clear is that a ferroelectric thin film cannot be considered in isolation, but rather the measured properties reflect the entire system of films, interfaces, electrodes, and substrates. We also look in detail at the effects of strain on ferroelectrics. All ferroelectrics are grown on substrates which can impose considerable strains, meaning that properties of ferroelectric thin films can often be considerably different from those of their bulk parent material. The electronic properties also have a characteristic behavior in thin-film form. While bulk ferroelectric materials are traditionally treated as good insulators, as films become thinner it becomes more appropriate to treat them as semiconductors with a fairly large band gap. These observations are key to understanding the potential and the performance of ferroelectric devices, and to understanding why they fail when they do.

In parallel with the technological developments in the field, the power of computational electronic structure theory has increased dramatically, giving us new ways of understanding ferroelectricity. Over the last 15 years, more and more complex systems have been simulated with more accuracy; and as the length scales of experimental systems decrease, there is now an overlap in size between the thinnest epitaxial films and the simulated systems. It is therefore an appropriate and exciting time to review this work, and to make connections between it and the problems considered by experimentalists and engineers.

Finally, we look at some issues and ideas in nanoscale ferroelectrics, with particular emphasis on new geometries for ferroelectric materials on the nanoscale such as ferroelectric nanotubes and self-patterned arrays of ferroelectric nanocrystals.

We do not attempt to cover some of the issues which are of great importance but instead refer readers to reviews by other authors. Some of the more important applications for ferroelectrics make use of their piezoelectric properties, for example, in actuators and microsensors; this topic has been reviewed by Muralt (2000). Relaxor ferroelectrics in which ferroelectric ordering occurs through the interaction of polar nanodomains induced by substitution are also of great interest for a number of applications and have recently been reviewed by Samara (2003).

II. FERROELECTRIC ELECTRONIC DEVICES

A. Ferroelectric memories

The idea that electronic information can be stored in the electrical polarization state of a ferroelectric material is a fairly obvious one; however, its realization is not so straightforward. The initial barrier to the development of ferroelectric memories was the necessity of making them extremely thin films because the coercive voltage of ferroelectric materials is typically of the order of several kV/cm, requiring submicron thick films to make devices that work on the voltage scale required for computing (all Si devices work at $\leqslant 5$ V). With today's deposition techniques this is no longer a problem, and now high-density arrays of nonvolatile ferroelectric memories are commercially available. However, reliability remains a key issue. The lack of good device models means that the design of ferroelectric memories is ex-

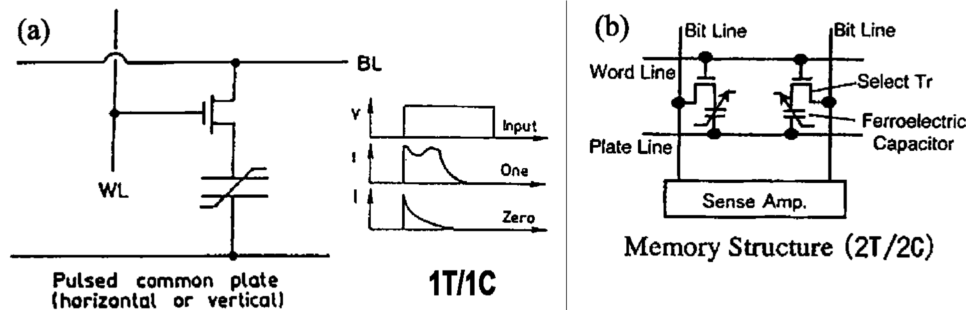

FIG. 1. (a) 1T-1C memory design. When a voltage is applied to both the word and bit line, the memory cell is addressed. Also shown is the voltage applied to the capacitor and the current output, depending on whether a one or a zero is stored. The current for the zero state is pure leakage current and by comparison to a reference capacitor can be removed. (b) A 2T-2C memory cell in which the reference capacitor is part of the memory cell.

pensive and that it is difficult to be able to guarantee that a device will still operate ten years into the future. Because competing nonvolatile memory technologies exist, ferroelectric memories can succeed only if these issues are resolved.

A ferroelectric capacitor, while capable of storing information, is not sufficient for making a nonvolatile computer memory. A pass-gate transistor is required so that a voltage above the coercive voltage is only applied to the capacitor when a voltage is applied to both the word and bit line; this is how one cell is selected from an array of memories. The current measured through a small load resistor in series with the capacitor is compared to that from a reference cell that is poled in a definite direction. If the capacitor being read is in a different state, the difference in current will be quite large where the displacement current associated with switching accounts for the difference. If the capacitor does not switch because it is already in the reference state, the difference in current between the capacitor being read and the reference capacitor is zero.

Most memories use either a 1 transistor–1 capacitor (1T-1C) design or a 2 transistor–2 capacitor (2T-2C) design (Fig. 1). The important difference is that the 1T-1C design uses a single reference cell for the entire memory for measuring the state of each bit, whereas in the 2T-2C there is a reference cell per bit. A 1T-1C design is much more space effective than a 2T-2C design, but has some significant problems, most significantly that the reference capacitor will fatigue much faster than the other capacitors, and so failure of the device occurs more quickly. In the 2T-2C design the reference capacitor in each cell fatigues at the same rate as its corresponding storage capacitor, leading to better device life. A problem with these designs is that the read operation is destructive, so every time a bit is read it needs to be written again. A ferroelectric field-effect transistor, in which a ferroelectric is used in place of the metal gate on a field-effect transistor, would both decrease the size of the memory cell and provide a nondestructive readout; however, no commercial product has yet been developed. Current efforts seem to run into serious problems with data retention.

An example of a real commercially available memory is the Samsung lead zirconate titanate-based 4 Mbit 1T-1C ferroelectric memory (Jung *et al.*, 2004). The scanning electron microscopy cross section (Fig. 2) of the device gives some indication of the complexity of design involved in a real ferroelectric memory.

Lead zirconate titanate (PZT) has long been the leading material considered for ferroelectric memories, though strontium bismuth tantalate (SBT), a layered perovskite, is also a popular choice due to its superior fatigue resistance and the fact that it is lead-free (Fig. 3). However, it requires higher-temperature processing, which creates significant integration problems. Recently progress has been made in optimizing precursors. Until recently the precursors for Sr, Bi, and Ta/Nb did not function optimally in the same temperature range, but last year Inorgtech developed Bi(mmp)3—a 2-methoxy-2-propanol propoxide that improves reaction and lowers the processing temperature for SBT, its traditional main disadvantage compared to PZT. This material also saturates the bismuth coordination number at 6. Recently several other layered perovskites, for example, bismuth titanate, have also been considered.

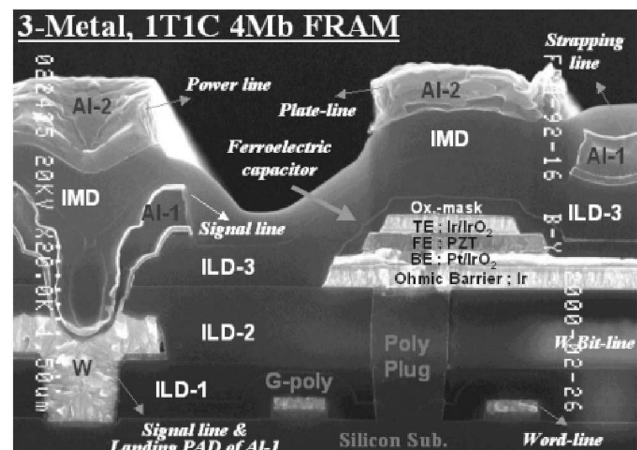

FIG. 2. Cross-sectional SEM image of the Samsung 4 Mbit 1T-1C 3 metal FRAM.

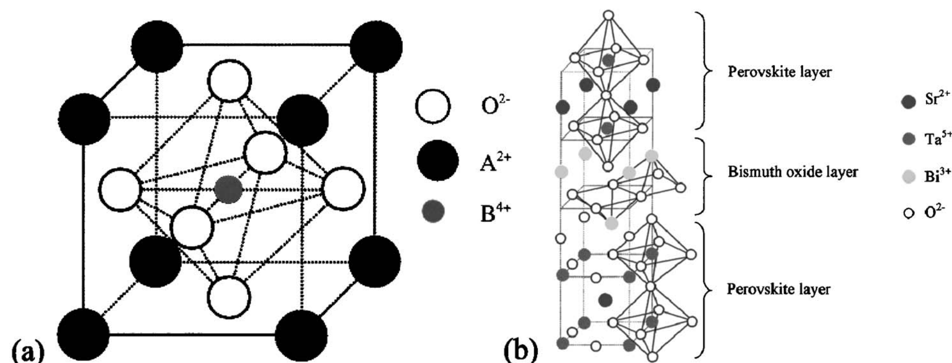

FIG. 3. (a) ABO_3 cubic perovskite structure; (b) strontium bismuth tantalate (layered perovskite structure).

As well as their applications as ferroelectric random access memories (FRAMs), ferroelectric materials have potential use in dynamic random access memories (DRAMs) because of their high dielectric constant in the vicinity of the ferroelectric phase transition, a topic which has been reviewed by Kingon, Maria, and Streiffer (2000). Barium strontium titanate (BST) is one of the leading materials in this respect since by varying the composition a transition temperature just below room temperature can be achieved, leading to a high dielectric constant over the operating temperature range.

B. Future prospects for nonvolatile ferroelectric memories

There are two basic kinds of ferroelectric random access memories in production today: (1) the free-standing RAMs and (2) fully embedded devices [usually a CPU, which may be a complementary metal-oxide semiconductor electrically erasable programmable read-only memory (CMOS EEPROM), the current generation widely used nonvolatile memory technology, plus a FRAM and an 8-bit microprocessor]. The former have reached 4 Mbit at both Samsung (using PZT) and Matsushita (using SBT). The Samsung device is not yet, as far as the authors know, in commercial production for real products, but the NEC FRAM is going into full-scale production this year in Toyama (near Kanazawa). Fujitsu clearly leads in the actual commercial use of its embedded FRAMs. The Fujitsu-embedded FRAM is that used in the SONY Playstation 2. It consists of 64 Mbit of EEPROM plus 8 kbit of RAM, 128-kbit ROM, and a 32-kbit FRAM plus security circuit. The device is manufactured with a 0.5-μm CMOS process. The capacitor is 1.6×1.9 μm^2 and the cell size is either 27.3 μm^2 for the 2T-2C design or 12.5 μm^2 for the 1T-1C.

The leading competing technologies in the long term for nonvolatile computer memories are FRAM and magnetic random access memories (MRAM). These are supposed to replace EEPROMs (electrically erasable programable read-only memories) and "Flash" memories in devices such as digital cameras. Flash, though proving highly commercially successful at the moment, is not a long-term technology, suffering from poor long-term endurance and scalability. It will be difficult for Flash to operate as the silicon logic levels decrease from 5 at present to 3.3, 1.1, and 0.5 V in the near future. The main problem for ferroelectrics is the destructive read operation, which means that each read operation must be accompanied by a write operation leading to faster degradation of the device. The operation principle of MRAMs is that the tunneling current through a thin layer sandwiched between two ferromagnetic layers is different depending on whether the ferromagnetic layers have their magnetization parallel or antiparallel to each other. The information stored in MRAMs can thus be read nondestructively, but their write operation requires high power which could be extremely undesirable in high-density applications. We present a summary of the current state of development in terms of design rule and speed of the two technologies in Table I.

Partly in recognition of the fact that there are distinct advantages for both ferroelectrics and ferromagnets, there has been a recent flurry of activity in the field of *multiferroics*, i.e., materials that display both ferroelectric and magnetic ordering, the hope being that one could develop a material with a strong enough coupling between the two kinds of ordering to create a device that can be written electrically and read magnetically. In general multiferroic materials are somewhat rare, and certainly the conventional ferroelectrics such as $PbTiO_3$ and $BaTiO_3$ will not display any magnetic behavior as the Ti-O hybridization required to stabilize the ferroelectricity in these compounds will be inhibited by the partially filled d orbitals that would be required for magnetism (Hill, 2000). However, there are other mechanisms for ferroelectricity and in materials where ferroelectricity and magnetism coexist there can be coupling between the two. For example, in $BaMnF_4$ the ferroelectricity is actually responsible for changing the antiferromagnetic ordering to a weak canted ferromagnetism (Fox *et al.*, 1980). In addition, the large magnetoelectric coupling in these materials causes large dielectric anomalies at the Néel temperature and at the in-plane spin-ordering temperature (Scott, 1977, 1979). More recent theoretical and experimental efforts have focused on $BiMnO_3$, $BiFeO_3$ (Seshadri and Hill, 2001; Moreira de Santos *et al.*, 2002; Wang *et al.*, 2003) and $YMnO_3$ (Fiebig *et al.*, 2002; Van Aken *et al.*, 2004).

TABLE I. Some clarification of the numbers presented here is required. The size of the Fujitsu FRAM memory may seem small but it is for an actual commercial device in large-scale use (in every Playstation 2), whereas the others are figures from internal sampling of unreleased devices that have not been commercialized. No MRAMs exist in any commercial device, giving FRAMs a substantial edge in this regard. The most recent commercial FRAM product actually shipped is a large-cell-area six-transistor four-capacitor (6T-4C) memory for smart credit cards and radio-frequency identification tags (RF-ID) and features nondestructive readout (Masui *et al.*, 2003). A total of 2×10^8 ferroelectric memories of all types have been sold industry wide. The Sony MRAM, though small, has submicron design rules, meaning that in principle a working device could be scaled up to Mb size.

Company	Design rule (feature size)	Speed (access time)
MRAMs		
NEC/Toshiba	1 Mb	
IBM	16 Mb	
Matsushita	4 Mb	
Sony	8kb 0.18 μm	
Cypress	256 kb	70 ns
State of the art	16 Mb 0.09 μm	25 ns
FRAMs		
Fujitsu	32 kb	100 ns
Samsung	32 Mb 0.18 μm	60 ns
Matsushita	4 Mb	60 ns
Laboratory		280 ps

C. Ferroelectric field-effect transistors

It has been known for some time that replacing the metal gate in a field-effect transistor (FET) by a ferroelectric could produce a device with nondestructive readout in which the polarization of the gate (+ for "1" and – for "0") could be sensed simply by monitoring the source-drain current magnitude. Thus such a device requires no reset operation after each READ and will experience very little fatigue in a normal frequent-read, occasional-write usage. The first mention of the idea of a ferroelectric FET is in the U.S. patent of Ross (1957) and the first realization was by Moll and Tarui (1963), while the first attempt to fabricate one on silicon was by Wu (1974). The early ferroelectric FETs utilized gates of lithium niobate (Rice University; Rabson *et al.*, 1995) or $BaMgF_4$ (Westinghouse; Sinharoy *et al.*, 1991, 1992, 1993). An example of a ferroelectric FET device as fabricated by Mathews *et al.* (1997) is shown in Fig. 4.

The optimum parameters for such a ferroelectric-gate material are extremely different from those for pass-gate-switched capacitor arrays; in particular, the latter require a remanent polarization $\sim$10 $\mu C/cm^2$, whereas the ferroelectric-gated FETs can function well with 50 times less (0.2 $\mu C/cm^2$). However, the switched capacitor array (FRAM) is very tolerant of surface traps in the ferroelectric (which may be $\sim10^{20}$ cm^{-3} in the interface

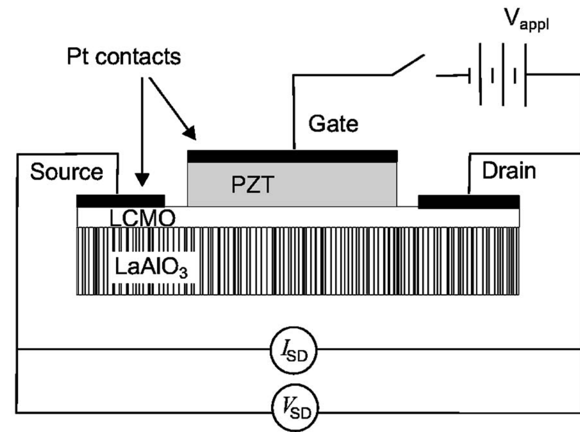

FIG. 4. Schematic diagram of an all-perovskite ferroelectric FET and measurement circuit. Reprinted with permission from Mathews *et al.*, 1997. © 1997, AAAS.

region near the electrode) since the ferroelectric makes contact only with a metal (or metal-oxide) electrode. By comparison, the ferroelectric gate in an FET contacts the Si substrate directly (metal-oxide-semiconductor field-effect-transistor channel). Thus it must be buffered from the Si to prevent charge injection. Unfortunately, if a thin buffer layer of a low-dielectric material such as SiO_2 is used, most of the applied voltage will drop across the buffer layer and not the ferroelectric gate, making it impossible to switch the gate. As a result, much of the ferroelectric FET research has employed buffer layers with relatively high dielectric constants, or else rather thick buffer layers, for example, the first $BaMnF_4$ FET made at Symetrix (Scott, 1998) used a buffer layer of $\sim$40 nm of SiO_2. Subsequent studies often used PZT (Kalkur *et al.*, 1994) although the large remanent polarization in this case ($\sim$40 $\mu C/cm^2$) is actually undesirable for a ferroelectric FET gate.

As pointed out by Yoon and Ishiwara (2001), the depolarization field in a ferroelectric gate is inevitably generated when the gate is grounded, and this makes it very difficult to obtain $>$10 year data retention in an FE-FET. Their solution is to utilize a 1T-2C capacitor geometry in which this depolarization field is suppressed by poling the two capacitors in opposite directions. With this scheme Ishiwara and his colleagues achieved an on/off source-drain current ratio of $>$1000 for a 150-nm-thick SBT film in a 5×50 μm^2 metal-oxide-semiconductor field-effect transistor channel, with Pt electrodes on the SBT capacitor.

Note that the direct contact of the ferroelectric onto Si produces a semiconductor junction that is quite different from the metal-dielectric interface discussed above. The Schottky barrier heights for this case have been calculated by Peacock and Robertson (2002). The electron screening length in the Si will be much greater than in the case of metal electrodes; in particular, this will increase the minimum ferroelectric film thickness required to stabilize the device against depolarization instabilities. Although this point was first emphasized by Batra

TABLE II. A number of the most promising gate materials under recent study, together with the buffer layers employed in each case. Studies of the $I(V)$ characteristics of such ferroelectric FETs have been given by Macleod and Ho (2001) and a disturb-free programming scheme described by Ullman *et al.* (2001).

FET gate	Buffer layer	Reference
$LiNbO_3$	none	Rabson *et al.* (1995)
SBT	$SrTa_2O_6$	Ishiwara (1993), Ishiwara *et al.* (1997), Ishiwara (2001)
SBT	CeO_2	Shimada *et al.* (2001), Haneder *et al.* (2001)
SBT	SiO_2	Okuyuma *et al.* (2001)
SBT	ZrO_2	Park and Oh (2001)
SBT	Al_2O_3	Shin *et al.* (2001)
SBT	Si_3N_4	Han *et al.* (2001)
SBT	Si_3N_4/SiO_2	Sugiyama *et al.* (2001)
SBT	poly-Si+Y_2O_3	Kalkur and Lindsey (2001)
$Pb_5Ge_3O_{11}$	none	Li and Hsu (2001)
$YMnO_3$	Y_2O_3	Cheon *et al.* (2001), Choi *et al.* (2001)
$Sr_2(Ta_{2x}Nb_{2-2x})O_7$	none	Kato (2001)
PZT	CeO_2	Xiaohua *et al.* (2001)
BST(strained)	YSZ(zirconia)	Jun and Lee (2001)
$BaMnF_4$	SiO_2	Scott (1998), Kalkur *et al.* (1994)

and Silverman (1972), it has been neglected in the more recent context of ferroelectric FETs. In our opinion, this depolarization instability for thin ferroelectric gates on FETs is a significant source of the observed retention failure in the devices but has not yet been explicitly modeled. If we are correct, the retention problem in ferroelectric FETs could be minimized by making the ferroelectric gates thicker and the Si contacts more conducting (e.g., $p+$ rather than p). See Scott (2005) for a full discussion of all-perovskite FETs.

Table II lists a number of the most promising gate materials under recent study, together with the buffer layers employed in each case. Studies of the $I(V)$ characteristics of such ferroelectric FETs have been given by Macleod and Ho (2001) and a disturb-free programming scheme described by Ullman *et al.* (2001).

Beyond its use in modulating the current in a semiconductor channel the ferroelectric field effect can also be used to modify the properties of more exotic correlated oxide systems (Ahn, Triscone, and Mannhart, 2003).

D. Replacement of gate oxides in DRAMs

At present there are three basic approaches to solving the problem of SiO_2-gate oxide replacement for DRAMs. The first is to use a high-dielectric ("high-k") material such as $SrTiO_3$ ($k=300$ is the dielectric constant; $\epsilon=k-1$ is the permittivity; for $k\gg 1$ the terms are nearly interchangeable) deposited by some form of epitaxial growth. This is the technique employed at Motorola, but the view elsewhere is that it is too expensive to become industry process worthy. The second approach is to use a material of moderate k (of order 20), with HfO_2 favored but ZrO_2 also a choice. Hafnium oxide is satisfactory in most respects but has the surprising disadvantage that it often degrades the n-channel mobility catastrophically (by as much as 10 000 times). Recently ST Microelectronics decided to use $SrTiO_3$ but with metal-organic chemical-vapor deposition from Aixtron, thus combining high dielectric constant and cheaper processing.

The specific high-k integration problems are the following four: (1) depletion effects in the polysilicon gate, (2) interface states, (3) strain effects, and (4) etching difficulties (HfO_2 is hard to wet etch). The use of a poly-Si gate instead of a metal gate produces grain-boundary stress in the poly, with resultant poor conductivity. This mobility degradation is only partly understood. The general view is that a stable amorphous HfO_2 would be a good strain-free solution. Note that HfO_2 normally crystallizes into two or three phases, one of which is monoclinic (Morrison *et al.*, 2003). Hurley in Cork has been experimenting with a liquid injection system that resembles Isobe's earlier SONY device for deposition of viscous precursors with flash evaporation at the target.

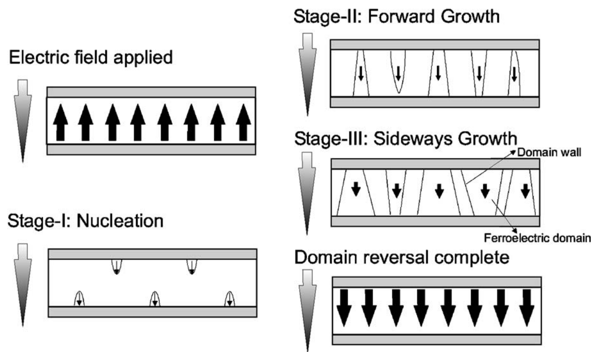

FIG. 5. The three phases of domain reversal: I, nucleation (fast); II, forward growth (fast); III, sideways growth (slow).

III. FERROELECTRIC THIN-FILM-DEVICE PHYSICS

We now turn to some of the physics questions which are relevant to ferroelectric thin-film capacitors.

A. Switching

In the ferroelectric phase, ferroelectric materials form domains where the polarization is aligned in the same direction in an effort to minimize energy. When a field is applied, the ferroelectric switches by the nucleation of domains and the movement of domain walls and not by the spontaneous reorientation of all of the polarization in a domain at once. In contrast to ferromagnets, where switching usually occurs by the sideways movement of existing domain walls, ferroelectrics typically switch by the generation of many new reverse domains at particular nucleation sites, which are not random; i.e., nucleation is inhomogeneous. The initial stage is nucleation of opposite domains at the electrode, followed by fast forward propagation of domains across the film, and then slower widening of the domains (Fig. 5). In perovskite oxides the final stage of the switching is usually much slower than the other two stages, as first established by Merz (1954). In other materials nucleation can be the slowest (rate-limiting) step.

1. Ishibashi-Orihara model

For many years the standard model to describe this process has been the Ishibashi-Orihara model (Orihara *et al.*, 1994) based on Kolomogorov-Avrami growth kinetics. In this model one considers a nucleus formed at time t' and then a domain propagating outwards from it with velocity V. In the Ishibashi-Orihara model the velocity is assumed to be dependent only on the electric field E, and not on the domain radius $r(t)$. This makes the problem analytically tractable but gives rise to unphysical fitting parameters, such as fractional dimensionality D. The fractional D is not related to fractals. It is an artifact that arises because the domain-wall velocity V is actually proportional to $1/r(t)$ for each domain and is not a constant at constant E. The volume of a domain at time t is given by

$$C(t,t') = C_D\left[\int_{t'}^{t} V(t'')dt''\right]^D, \tag{1}$$

where D is the dimensionality of the growth and C_D is a constant which depends on the dimensionality. It is also assumed within this model that the nucleation is deterministic and occurs at predefined places; i.e., this is a model of inhomogeneous nucleation. This is an important point since some researchers still use homogeneous nucleation models. These are completely inappropriate for ferroelectrics [where the nucleation is inhomogeneous, as is demonstrated by imaging experiments (Shur, 1996; Shur *et al.*, 2000; Ganpule *et al.*, 2001)].

The result of the model is that the fraction of switched charge as a function of field and frequency may be expressed as

$$Q(E,f) = 1 - \exp[-f^{-D}\Phi(E)], \tag{2}$$

where $\Phi(E)$ depends on the wave form used for switching. After some consideration and the substitution $\Phi(E)=E^k$ one obtains a useful relationship for the dependence of the field on frequency:

$$E_c = f^{D/k}. \tag{3}$$

This relationship has been used to fit data fairly well in TGS (Hashimoto *et al.*, 1994), PZT, and SBT (Scott, 1996). More recently, however, Tsurumi *et al.* (2001) and Jung *et al.* (2002) have found that over larger frequency ranges the data on several materials is better fitted by the nucleation-limited model of Du and Chen (1998a). Tagantsev *et al.* (2002) have also found that over large time ranges the Ishibashi-Orihara model is not a good description of switching-current data and that a nucleation-limited model is more appropriate. It is quite possible of course that domain-wall-limited switching (Ishibashi) is operative in one regime of time and field but that in another regime the switching is nucleation limited.

2. Nucleation models

Some of the earliest detailed studies of switching in ferroelectrics developed nucleation-limited switching models where the shape of the nucleus of the reversed domain was very important. In the work of Merz (1954) and Wieder (1956, 1957) a nucleation-limited model was used in which when dagger-shaped nuclei were assumed, the correct dependence of the switching current on electric field could be derived. This approach leads to the concept of an activation field for nucleation (somewhat different from the coercive field). Activation fields in thin-film PZT capacitors were measured by Scott *et al.* (1988); very recently, Jung *et al.* (2004) have studied the effects of microgeometry on the activation field in PZT capacitors.

The switching model of Tagantsev *et al.* (2002) is a different approach in which a number of noninteracting elementary switching regions are considered. These switch according to a broad distribution of waiting times.

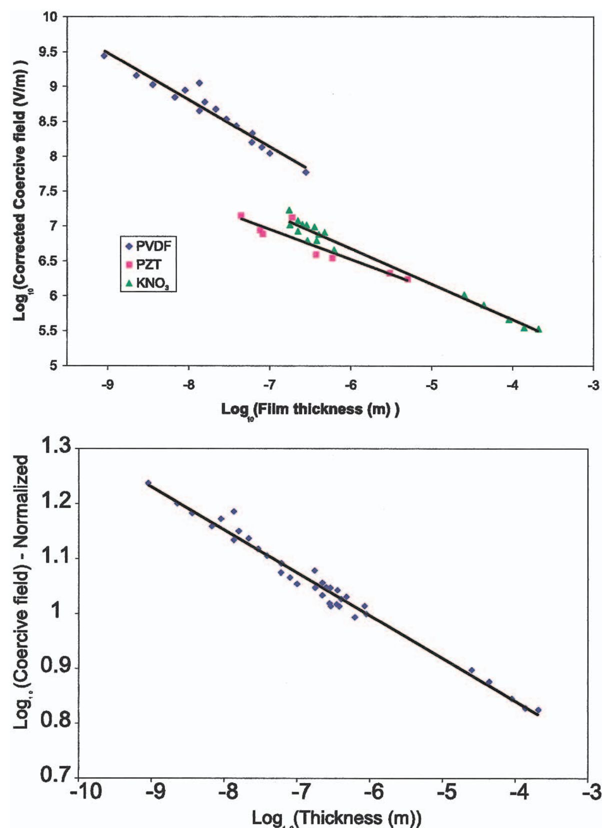

FIG. 6. (Color) The scaling of coercive field with thickness in ferroelectrics; from mm to nm scale. From Dawber, Chandra, *et al.*, 2003. The bottom is the three sets of data from the upper all normalized to the same value at $10^{-6.5}$ m.

3. The scaling of coercive field with thickness

For the last 40 years the semiempirical scaling law (Janovec, 1958; Kay and Dunn, 1962), $E_c(d) \propto d^{-2/3}$, has been used successfully to describe the thickness dependence of the coercive field in ferroelectric films ranging from 100 μm to 200 nm (Scott, 2000b). In the ultrathin PVDF films of Bune *et al.* (1998) a deviation from this relationship was seen for the thinnest films (Ducharme *et al.*, 2000). Although they attribute this to a new kind of switching taking place (simultaneous reversal of polarization, as opposed to nucleation and growth of domains), Dawber, Chandra, *et al.* (2003) have shown, to the contrary, that if the effects of a finite depolarization field due to incomplete screening in the electrode are taken into account, then the scaling law holds over six decades of thickness and the coercive field does not deviate from the value predicted by the scaling law (Fig. 6). Recently, Pertsev *et al.* (2003) measured coercive fields in very thin PZT films. Although they have used a different model to explain their data, it can be seen that in fact the scaling law describes the data very well.

4. Mobility of 90° domain walls

The mobility of domain walls, especially 90° walls, depends upon their width. In this respect the question has been controversial, with some authors claiming very wide widths (hundreds of angstroms) and immobile walls. Some recent papers show experimentally that 90° domain walls in perovskite ferroelectrics are extremely narrow (Tsai *et al.*, 1992; Stemmer *et al.*, 1995; Floquet *et al.*, 1997; Foeth *et al.*, 1999). In $PbTiO_3$ they are 1.0 ± 0.3 nm wide. This connects the general question of how wide they are and whether they are immobile. The review by Floquet and Valot (1999) is quite good. They make the point that in ceramics these 90° walls are 14.0 nm wide (an order of magnitude wider than in single crystals). This could be why theory and experiment disagree, i.e., that something special in the ceramics makes them 10–15 times wider (and less mobile?). The latter point is demonstrated clearly in experiments on $KNbO_3$, together with a theoretical model that explains geometrical pinning in polyaxial ferroelectrics in terms of electrostatic forces. In this respect the first-principles study of Meyer and Vanderbilt (2002) is extremely interesting. Not only do they show that 90° domain walls in $PbTiO_3$ are narrow and form much more easily than 180° domain walls, but that they should be much more mobile as well, the barrier for motion being so low they predict thermal fluctuation of about 12 unit cells at room temperature, which could perhaps explain why they appear to be wide.

Some experimental studies using atomic force microscopy have attempted to answer the question of whether 90° domain walls were mobile or not. In certain circumstances they were immobile (Ganpule, Nagarajan, Li, *et al.*, 2000; Ganpule, Nagarajan, Ogale, *et al.*, 2000), but in another study (Nagarajan *et al.*, 2003) the motion of 90° domain walls under an applied field was directly observed. It seems that in principle 90° domain walls can move, but this depends quite strongly on the sample conditions. Recently Shilo *et al.* (2004) and Salje and Lee (2004) have shown that domain wall widths are not a characteristic of the material *per se* but vary greatly with location in the sample due to nearby impurities. This reconciles the diverse values reported.

5. Imaging of domain-wall motion

The direct imaging of ferroelectric domain walls is an excellent method for understanding domain-wall motion and switching. At first this was carried out in materials where the domains were optically distinct such as lead germanate (Shur *et al.*, 1990), but more recently atomic force microscopy has become a powerful tool for observing domain-wall motion. The polarization at a point can be obtained from the piezoresponse detected by the tip, and the tip itself can be used to apply a field to the ferroelectric sample and initiate switching. It is thus possible to begin switching events and watch their evolution over time. Atomic force microscopy domain writing of ferroelectric domains can also be used to write extremely small domain structures in high-density arrays (Paruch *et al.*, 2001) or other devicelike structures, such as surface acoustic wave devices (Sarin Kumar *et al.*, 2004).

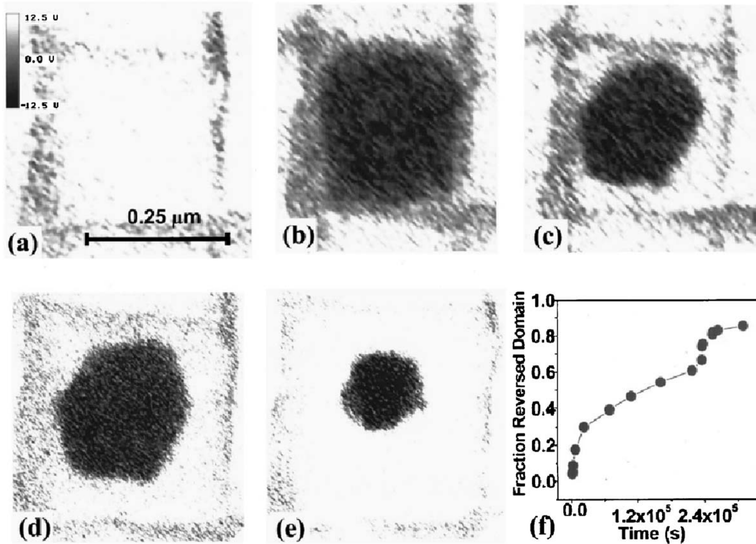

FIG. 7. Piezoresponse scans of a single cell in $PbZr_{0.2}Ti_{0.8}O_3$. (b)–(d) The spontaneous reversal of polarization within this region after wait times of (b) 1.01×10^3, (c) 1.08×10^5, (d) 1.61×10^5, and (e) 2.55×10^5 s. Faceting can be seen in (c), (d), and (e). (f) Transformation-time curve for the data in (b)–(e). From Ganpule *et al.*, 2001.

The backswitching studies of Ganpule *et al.* (2001) show two very interesting effects (Fig. 7). The first is the finding that reverse domains nucleate preferentially at antiphase boundaries. This was studied in more detail subsequently by Roelofs *et al.* (2002) who invoked a depolarization-field-mediated mechanism to explain the result. Another explanation might be that the strain is relaxed at these antiphase boundaries resulting in favorable conditions for nucleation. Second, the influence of curvature on the domain-wall relaxation is accounted for within the Kolomogorov-Avrami framework. The velocity of the domains is dependent on curvature, and, as the relaxation proceeds, the velocity decreases and the domain walls become increasingly faceted. In Fig. 7 the white polarization state is stable, whereas the black is not. The sample is poled into the black polarization state and then allowed to relax back.

A different kind of study was undertaken by Tybell *et al.* (2002), in which they applied a voltage pulse to switch a region of the ferroelectric using an atomic force microscopy tip and watched how the reversed domain grew as a function of pulse width and amplitude. They were able to show that the process was well described by a creep mechanism thought to arise due to random pinning of domain walls in a disordered system (Fig. 8). Though the exact origin of the disorder was not clear, it suggests that it is connected to oxygen vacancies, which also play a role in pinning the domain walls during a fatigue process due to their ordering (Park and Chadi, 1998; Scott and Dawber, 2000).

An unsolved puzzle is the direct observation via atomic force microscopy of domain walls penetrating grain boundaries (Gruverman *et al.*, 1997). This is contrary to some expectations and always occurs at non-normal incidence, i.e., at a small angle to the grain boundary.

One of the interesting things to come out of the work in lead germanate (where ferroelectric domains are optically distinct due to electrogyration) by Shur *et al.* (1990) is that at high applied electric fields (15 kV cm^{-1}) tiny domains are nucleated in front of the moving domain wall (Fig. 9). A very similar effect is seen in ferromagnets as observed by Randoshkin (1995) in a single-crystal iron-garnet film.

However, in ferromagnets the effect is modeled by a spin-wave mechanism (Khodenkov, 1975). This mechanism is based on the gyrotropic model of domain-wall motion in uniaxial materials (Walker, 1963). When a strong magnetic driving field (exceeding the Walker threshold) acts upon a domain wall, the magnetization vectors in the domain wall begin to precess with a frequency γH, where γ is the effective gyromagnetic ratio. By relating the precession frequency in the domain wall with the spin-wave frequency in the domain, good predictions can be made for the threshold fields at which the effect occurs. We note that the domains nucleated in

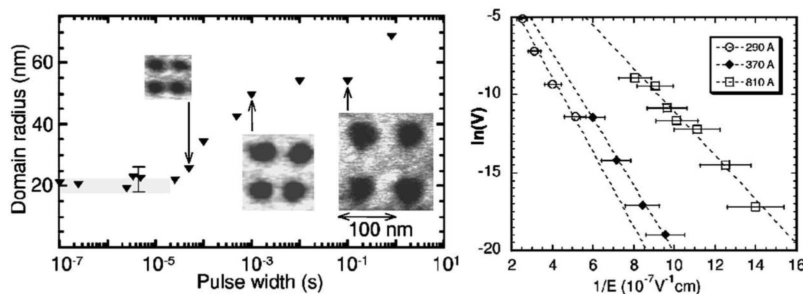

FIG. 8. (a) Domain size increases logarithmically with pulse widths longer than 20 μs and saturates for shorter times as indicated by the shaded area. (b) Domain-wall speed as a function of the inverse applied electric field for 290-, 370-, and 810-Å-thick samples. The data fit well the characteristic velocity-field relationship of a creep process. From Tybell *et al.*, 2002.

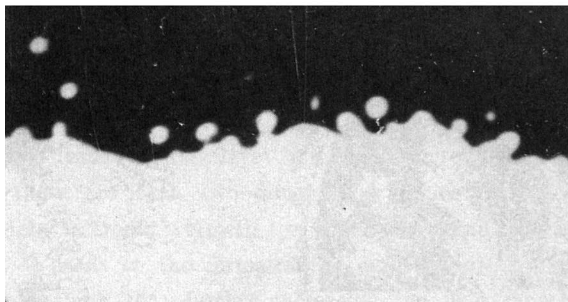

FIG. 9. Nucleation of nanodomains in front of domain wall in lead germanate at high electric field. Black and white represent the two directions of polarization. From Gruverman, 1990.

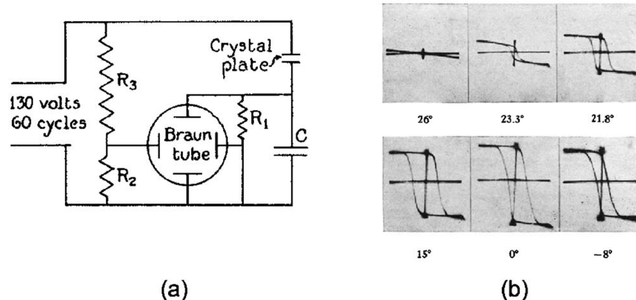

FIG. 10. (a) The original Sawyer-Tower circuit, (b) hysteresis in Rochelle salt measured using this circuit by Sawyer and Tower at various temperatures. From Sawyer and Tower, 1930.

front of the wall may be considered as vortexlike Skyrmions. The similarity between these effects is thus quite surprising and suggests that perhaps there is more in common between ferroelectric domain-wall motion and ferromagnet domain-wall motion than is usually considered. However, whereas Democritov and Kreines (1988) have shown that magnetic domain walls can be driven supersonically (resulting in a phase-matched Cherenkov-like bow wave of acoustic phonon emission), there is no direct evidence of supersonic ferroelectric domains. Processes such as the nanodomain nucleation described above seem to occur instead when the phase velocity of the domain-wall motion approaches the speed of sound. Of course the macroscopic electrical response to switching can arrive at a time $t < v/d$, where v is the sound velocity and d the film thickness, simply from domain nucleation within the interior of the film between cathode and anode.

B. Electrical characterization

1. Standard measurement techniques

Several kinds of electrical measurements are made on ferroelectric capacitors. We briefly introduce them here before proceeding to the following sections where we discuss in detail the experimental results obtained by using these techniques.

a. Hysteresis

One of the key measurements is naturally the measurement of the ferroelectric hysteresis loop. There are two measurement schemes commonly used. Traditionally a capacitance bridge as first described by Sawyer and Tower (1930) was used (Fig. 10). Although this is no longer the standard way of measuring hysteresis, the circuit is still useful (and very simple and cheap) and we have made several units which are now in use in the teaching labs in Cambridge for a demonstration in which students are able to make and test their own ferroelectric KNO_3 capacitor (Dawber, Farnan, and Scott, 2003).

This method is not very suitable in practice for many reasons, for example, the need to compensate for dielectric loss and the fact that the film is being continuously cycled. Most testing of ferroelectric capacitors is now carried out using commercial apparatus from one of two companies, Radiant Technologies and AixAcct. Both companies' testers can carry out a number of tests and measurements, and both machines use charge or current integration techniques for measuring hysteresis. Both machines also offer automated measurement of characteristics such as fatigue and retention.

In measuring $P(E)$ hysteresis loops several kinds of artifacts can arise. Some of these are entirely instrumental, and some arise from the effects of conductive (leaky) specimens.

Hysteresis circuits do not measure polarization P directly. Rather, they measure switched charge Q. For an ideal ferroelectric insulator

$$Q = 2P_r A, \tag{4}$$

where P_r is the remanent polarization and A is the electrode area for a parallel-plate capacitor. For a somewhat conductive sample

$$Q = 2P_r A + \sigma E_a t, \tag{5}$$

where σ is the electrical conductivity, E_a is the applied field, and t the measuring time. Thus Q in a pulsed measuring system depends on the pulse width.

The four basic types of apparent hysteresis curves that are artifacts are shown in Fig. 11.

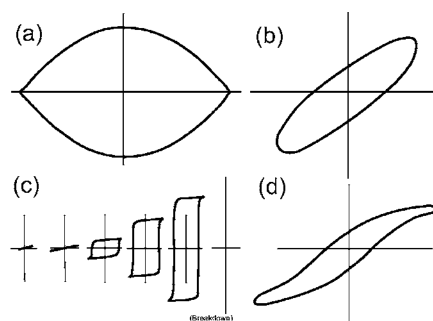

FIG. 11. Common hysteresis artifacts: (a) dead short, (b) linear lossy dielectric, (c) saturated amplifier, and (d) nonlinear lossy dielectric.

Figure 11(a) is a dead short in a Sawyer-Tower circuit or modern variant and is discussed in the instruction documentation for both the AixAcct[1] and Radiant[2] testers.

Figure 11(b) shows a linear lossy dielectric. The points where the loop crosses $V_a=0$ are often misinterpreted as P_r values. Actually this curve is a kind of Lissajous figure. It can be rotated out of the page to yield a straight line (linear dielectric response). Such a rotation can be done electrically and give a "compensated" curve. Here compensation means to compensate the phase shift caused by dielectric loss.

Figure 11(c) is more subtle. Here are two seemingly perfect square hysteresis loops obtained on the same or nominally equivalent specimens at different maximum fields. The smallest loop was run at an applied voltage of $V_a=10$ V, and yields $P_r=30$ μC cm^{-2} and the larger at $V_a=50$ V and yields $P_r=100$ μC cm^{-2}. Note that both curves are fully saturated (flat tops). This is impossible. If the dipoles of the ferroelectric are saturated at $P_r=30$ μC cm^{-2} then there are no additional dipoles to produce $P_r=100$ μC cm^{-2} in the larger loop at high voltage. What actually occurs in the illustration is saturation of the amplifier in the measuring system, not saturation of the polarization in the ferroelectric. The figure is taken from Jaffe, Cook, and Jaffe (1971) where this effect is discussed (p. 39). It will be a serious problem if conductivity is large in Eq. (5). "Large" in this sense is $\sigma > 10^{-6}$ (Ω cm)$^{-1}$ and "small" is $\sigma < 10^{-7}$ (Ω cm)$^{-1}$. This is probably the source of $P_r > 150$ μC cm^{-2} reports in $BiFeO_3$ where σ can exceed 10^{-4} (Ω cm)$^{-1}$.

Finally, Fig. 11 is a *nonlinear* lossy dielectric. If it is phase compensated it still resembles real hysteresis. One can verify whether it is real or an artifact only by varying the measuring frequency. Artifacts due to dielectric loss are apt to be highly frequency dependent. Figures 11(b) and 11(d) are discussed in Lines and Glass (1967, p. 104).

No data resembling Figs. 11(a)–11(d) should be published as ferroelectric hysteresis.

b. Current measurements

Another measurement of importance which is carried out in an automated way by these machines is the measurement of the leakage current. This is normally discussed in terms of a current-voltage (*I-V*) curve, where the current is measured at a specified voltage. It is important, however, that sufficient time is allowed for each measurement step so that the current is in fact true steady-state leakage current and not relaxation current. For this reason current-time (*I-t*) measurements can also be important (Dietz and Waser, 1995). Relaxation times in ferroelectric oxides such as barium titanate are typically 1000 s at room temperature.

[1]TF Analyzer 2000 FE-module instruction manual.
[2]http://www.ferroelectrictesters.com/html/specs.html#tut

c. Dielectric permittivity

An impedance analyzer measures the real and imaginary parts of the impedance by use of a small-amplitude ac signal which is applied to the sample. The actual measurement is then made by balancing the impedance of the sample with a set of references inside the impedance analyzer. From this the capacitance and loss can be calculated (all this is done automatically by the machine). It is possible at the same time to apply a dc bias to the sample, so the signal is now a small ac ripple superimposed on a dc voltage. Ferroelectric samples display a characteristic "butterfly loop" in their capacitance-voltage relationships, because the capacitance is different for increasing and decreasing voltage. The measurement is not exactly equivalent to the hysteresis measurement. In a capacitance-voltage measurement a static bias is applied and the capacitance measured at that bias, whereas in a hysteresis measurement the voltage is being varied in a continuous fashion. Therefore it is not strictly true that $C(V)=(d/dV)P(V)$ (area taken as unity) as claimed in some textbooks, since the frequency is not the same in measurements of C and P. Impedance spectroscopy (where the frequency of the ac signal is varied) is also a powerful tool for analysis of films, especially as it can give information on the time scales at which processes operate. Interpretation of these results must be undertaken carefully, as artifacts can arise in many circumstances and even when this is not the case many elements of the system (e.g., electrodes, grain boundaries, leads, etc.) can contribute to the impedance in complicated ways.

2. Interpretation of dielectric permittivity data

a. Depletion charge versus intrinsic response

Before looking for ferroelectric contributions to a system's electrical properties one should make sure there are not contributions due to the properties of the system unrelated to ferroelectricity. Although much is sometimes made of the dependence of capacitance on voltage, it is worth noting that metal-semiconductor-metal systems have a characteristic capacitance voltage which arises from the response of depletion layers to applied voltage (Fig. 12).

Essentially the problem boils down to the fact that there are two possible sources of the dependence of capacitance on applied field, either changes in depletion width or changes in the dielectric constant of the material, i.e.,

$$\frac{C(E)}{A} = \frac{\epsilon(E)}{d(E)}. \tag{6}$$

Several groups have assumed that the change in the capacitance with field $C(E)$ comes from change in depletion width $d(E)$ and that $\epsilon(E)$ is changing negligibly. The first to suggest this was Evans (1990), who found $d=20$ nm in PZT. Later Sandia claimed that there was no depletion ($d=0$ or $d=\infty$) (Miller *et al.*, 1990). Several authors have assumed that $d(E)$ is responsible for $C(E)$

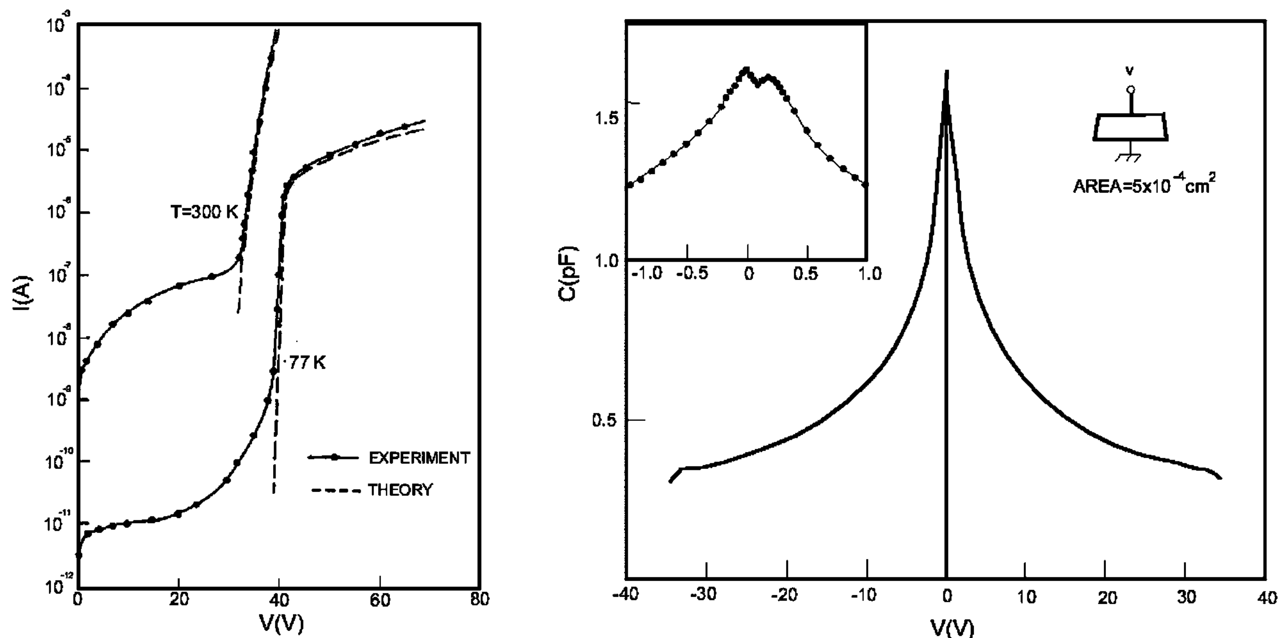

FIG. 12. Current-voltage and capacitance-voltage relationship of Pt-Si-Pt punch-through diode. The characteristics are very similar to those obtained in metal-ferroelectric-metal systems. Reprinted from Sze *et al.*, 1971, with permission from Elsevier.

(Brennan, 1992; Mihara *et al.*, 1992; Sayer *et al.*, 1992; Scott *et al.*, 1992; Hwang, 1998; Hwang *et al.*, 1998).

In contrast to the approach of explaining these characteristics using semiconductor models, Basceri *et al.* (1997) account for their results on the basis of a Landau-Ginzburg-style expansion of the polarization (Fig. 13). The change in field due to its nonlinearity has also been calculated by both Outzourhit *et al.* (1995) and Dietz *et al.* (1997). The real problem is that both pictures are feasible. One should not neglect the fact that the materials have semiconductor aspects; but at the same time it is not unreasonable to expect that the known nonlinearity of the dielectric response in these materials should be expressed in the capacitance-voltage characteristic. Probably the best approach is to avoid making any conclusions on the basis of these kinds of measurements alone, as it is quite possible that the relative sizes of the contributions will vary greatly from sample to sample, or even in the same sample under different experimental conditions.

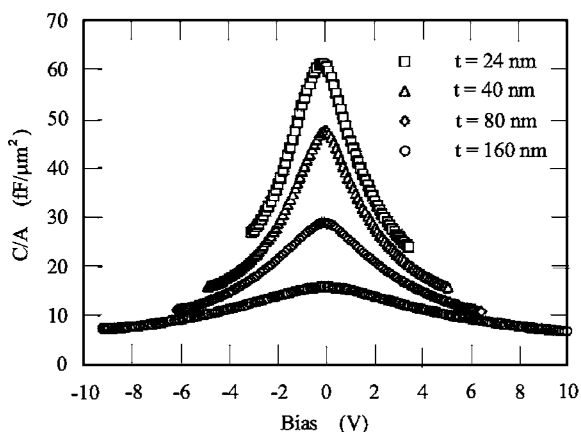

FIG. 13. Capacitance vs applied bias for BST thin films. Reprinted with permission from Basceri *et al.*, 1997. © 1997, AIP.

b. Domain-wall contributions

Below the coercive field there are also contributions to the permittivity from domain walls, as first pointed out by Fouskova (1965; Fouskova and Janousek, 1965). In PZT the contributions of domain-wall pinning to the dielectric permittivity have been studied in detail by Damjanovic and Taylor (Damjanovic, 1997; Taylor and Damjanovic, 1997, 1998), who showed that the subcoercive field contributions of the permittivity were described by a Raleigh law with both reversible and irreversible components, the irreversible component being due to domain-wall pinning.

c. Dielectric measurements of phase transitions

One of the most common approaches to measuring the transition temperature of a ferroelectric material is naturally to measure the dielectric constant and loss. However, in thin films there are significant complications. In bulk the maximum in the dielectric constant is fairly well correlated with the transition temperature, but this does not always seem to be the case in thin films. As pointed out by Vendik and Zubko (2000), a series capacitor model is required to extract the true transition temperature, which in the case of BST has been shown to be independent of thickness (Lookman *et al.*, 2004), in contrast to the temperature at which the permittivity maximum occurs, which can depend quite strongly on thickness (Fig. 14). The smearing of phase transitions due to a surface effect or a bulk inhomogeneity has re-

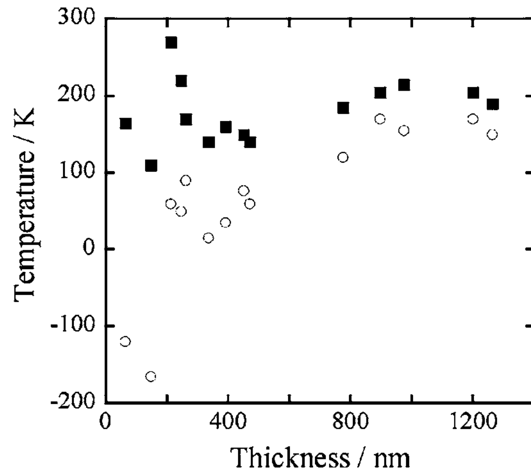

FIG. 14. Comparison between the apparent Curie temperature in BST taken from Curie-Weiss plots of raw data (empty circles) and intrinsic data after correction for interfacial capacitance (solid squares) had been performed. The intrinsic Curie temperature appears to be independent of film thickness. Reprinted with permission from Lookman *et al.*, 2004. © 2004, AIP.

cently been studied theoretically by Bratkovsky and Levanyuk (2005).

3. Schottky barrier formation at metal-ferroelectric junctions

In general, since ferroelectric materials are good insulators the majority of carriers are injected from the electrode. When a metal is attached to a ferroelectric material, a potential barrier is formed if the metal work function is greater than the electron affinity of the ferroelectric. This barrier must be overcome if charge carriers are to enter the ferroelectric. On the other hand, if the electron affinity is greater than the work function, then an Ohmic contact is formed. For the usual applications of ferroelectrics (capacitors) it is desirable to have the largest barrier possible. If a metal is brought into contact with an intrinsic pure ferroelectric and surface states do not arise (i.e., the classic metal-insulator junction), then the barrier height is simply

$$\phi_b = \phi_m - \chi. \tag{7}$$

In this case the Fermi level of the metal becomes the Fermi level of the system, as there is no charge within the insulator with which to change it. On the other hand, if there are dopants or surface states, then there can be a transfer of charge between the metal and ferroelectric, which allows the ferroelectric to bring the system Fermi level towards its own Fermi level.

Single crystals of undoped ferroelectric titanates tend to be slightly p type simply because there are greater abundances of impurities with lower valences than those of the ions for which they substitute (Na^{+} for Pb^{+2}; Fe^{+3} for Ti^{+4}) (Chan *et al.*, 1976, 1981; Smyth, 1984). In reality most ferroelectric capacitors are fine-grained polycrystalline ceramics and are almost always oxygen deficient. Typically the regions of the capacitor near the interface are more oxygen deficient than the bulk. Oxygen vacancies act as donor ions, and this means there can be a transition from n-type behavior at the interface to p-type behavior in the center of the film as is evident in the Kelvin probe study of Nowotny and Rekas (1994), who found that in bulk $BaTiO_3$ with Pt electrodes a change in work function from 2.5 ± 0.3 for surfaces to 4.4 ± 0.4 eV in the bulk of the material. The nature of the material near the surface is important since it determines whether a blocking or Ohmic contact is formed. It has been shown by Dawber and Scott (2002) that the defect concentration profile as measured by the capacitance-voltage technique may be explained by a model of combined bulk and grain-boundary diffusion of oxygen vacancies during the high-temperature processing of a film.

Regardless of the p-type or n-type nature of the material, in most oxide ferroelectrics on elemental metal electrodes the barrier height for electrons is significantly less than the barrier height for holes (Robertson and Chen, 1999), and so the dominant injected charge carriers are electrons. As the injected carriers dominate the conduction, leakage currents in ferroelectrics are electron currents and not hole currents, contrary to the suggestion of Stolichnov and Tagantsev (1998).

The first picture of barrier formation in semiconductors is due to Schottky (1938) and Mott (1938). In this picture the conduction band and valence band bend such that the vacuum levels at the interface are the same and the Fermi level is continuous through the interface, but deep within the bulk of the semiconductor it retains its original value relative to the vacuum level. This is achieved by the formation of a depletion layer which shifts the position of the Fermi level by altering the number of electrons within the interface.

Motivated by the experimental observation that many Schottky barrier heights seemed to be fairly independent of the metal used for the electrode, Bardeen (1947) proposed a different model of metal-semiconductor junctions. In this picture the Fermi level of the semiconductor is "pinned" by surface states to the original charge neutrality level. These states, as first suggested by Heine (1965), are not typically real surface states but rather states induced in the band gap of the semiconductor by the metal.

Most junctions lie somewhere between the Schottky and Bardeen limits. The metal-induced gap states can accommodate some but not all of the difference in the Fermi level between the metal and the semiconductor, and so band bending still occurs to some extent. The factor $S=d\phi_b/d\phi_m$ is used to define this, with $S=1$ being the Schottky limit and $S=0$ representing the Bardeen limit. The value of S is determined by the nature of the semiconductor; originally experimental trends linking this to the covalency or ionicity of the bonding in the material were observed (with covalent materials developing many more metal-induced gap states than ionic materials; Kurtin *et al.*, 1969). However, better correlation was found between the effective band gaps (depen-

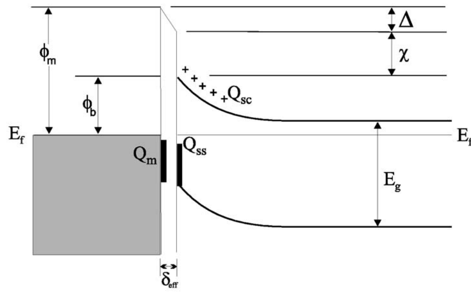

FIG. 15. Energy-band diagram of a metal n-type semiconductor contact. Adapted from Cowley and Sze, 1965.

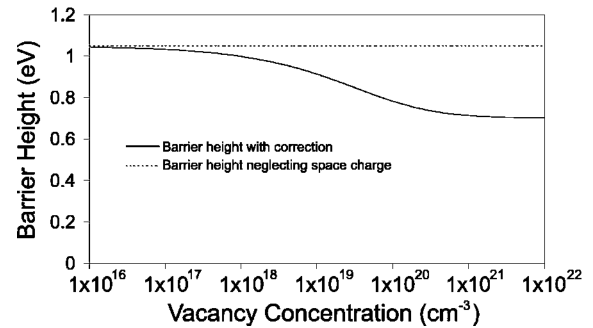

FIG. 16. Schottky barrier height of Pt-$SrTiO_3$ as a function of oxygen-vacancy concentration. Note that this may explain the variation of experimental values from ~0.7 to 1.0 eV.

dent on the electronic dielectric constant ϵ_∞; Schluter, 1978), with (Monch, 1986)

$$\frac{1}{S} - 1 = 0.1(\epsilon_\infty - 1)^2. \tag{8}$$

Although $SrTiO_3$ was invoked as one of the materials that violated the electronegativity rule by Schluter (1978), it is omitted from the plot against $\epsilon_\infty - 1$. The experimental value for S in $SrTiO_3$ can be measured from Dietz's data as approximately 0.5. This does not agree well with what one would expect from Monch's empirical relation, which gives $S=0.28$ [as used by Robertson and Chen (1999)]. Note that the use of the ionic trap-free value $S=1$ for BST gives a qualitative error. It predicts that BST on Al should be Ohmic, whereas in actuality it is a blocking junction; an S value of approximately 0.3 predicts a 0.4 eV Schottky barrier height, in agreement with experiment (Scott, 2000b).

We can extract the penetration depth for Pt states into $BaTiO_3$ from the first-principles calculation of Rao *et al.* (1997) by fitting the density of states of platinum states in the oxygen layers to an exponential relationship to extract the characteristic length as 1.68 Å.

Cowley and Sze (1965; Fig. 15) derived an expression for the barrier height for junctions between the two extremes. In this approach the screening charges in the electrode and the surface states are treated as delta functions of charge separated by an effective thickness δ_{eff}. This effective thickness takes into account both the Thomas-Fermi screening length in the metal and the penetration length of the metal-induced gap states, and is essentially an air-gap approach.

The expression for the barrier height is

$$\phi_b = S(\phi_m - \chi) + (1 - S)(E_g - \phi_0) + \zeta, \tag{9}$$

$$\zeta = \frac{S^2 C}{2} - S^{3/2}\left[C(\phi_m - \chi) + (1 - S)(E_g - \phi_0)\frac{C}{S} - \frac{C}{S}(E_g - E_f + kT) + \frac{C^2 S}{4} \right]^{1/2}. \tag{10}$$

In the above $S=1/(1+q^2\delta_{\text{eff}}D_s)$, $C=2q\varepsilon_s N_D \delta_{\text{eff}}^2$. When $\varepsilon_s \approx 10\varepsilon_0$ and $N_D < 10^{18}$ cm^{-3}, C is of the order of 0.01 eV and it is reasonable to discard the term ζ as Cowley and Sze (1965) did. Neglecting this term, as has been pointed out by Rhoderick and Williams (1988), is equivalent to neglecting the charge in the depletion width. In the systems under consideration here this term should not be neglected as it can be quite large. To demonstrate the effect on the barrier height we calculate the barrier height for a Pt-$SrTiO_3$ barrier over a wide range of vacancy concentrations (Fig. 16).

It can be seen that the effect of vacancies on barrier height becomes important for typical concentrations of vacancies encountered in ferroelectric thin films. Dawber *et al.* (2001) have addressed this issue and also the effect of introduced dopants on barrier heights. Despite their omission of the term discussed above, the work of Robertson and Chen is valuable because of their calculation of the charge neutrality levels for several ferroelectric materials, an essential parameter for the calculation of metal-ferroelectric barrier heights.

In a ferroelectric thin film this distribution of charges at the interface manifests itself in more ways than simply in the determination of the Schottky barrier height. Electric displacement in the system is screened over the entire charge distribution.

In measuring the small-signal capacitance against thickness there is always a nonzero intercept, which has been typically associated with a "dead layer" at the metal-film interface. However, in most cases this interfacial capacitance can be understood by recognizing that a finite potential exists across the charge at the interface. In the simplest approximation one neglects any charge in the ferroelectric and uses a Thomas-Fermi screening model for the metal. This was initially considered by Ku and Ullman (1964) and first applied to high-k dielectrics by Black and Welser (1999). In their work they use a large value for the dielectric constant of the oxide metal, considering it as the dielectric response of the ions stripped of their electrons. This may seem quite reasonable but is not, however, appropriate. In general we think of metals not being able to sustain fields, and in the bulk they certainly cannot, but the problem of the penetration of electric fields into metals is actually well known in a different context, that of the microwave skin depth. It is very instructive to go through the derivation as an ac current problem and then find the dc limit which will typically apply for our cases of interest.

We describe the metal in this problem using the Drude free-electron theory:

$$\sigma = \frac{\sigma_0}{1 + i\omega\tau}. \tag{11}$$

There are three key equations to describe the charge distribution in the metal: Poisson's equation for free charges,

$$\rho(z) = \frac{1}{4\pi}\frac{\partial E(z)}{\partial z}; \tag{12}$$

the continuity equation,

$$-i\omega\rho(z) = \frac{\partial j(z)}{\partial z}; \tag{13}$$

and the Einstein transport equation,

$$j = \sigma E - D\frac{\partial \rho}{\partial z}. \tag{14}$$

These are combined to give

$$\frac{\partial^2 \rho}{\partial z^2} = \frac{4\pi\sigma}{D}\left(1 + \frac{i\omega}{4\pi\sigma}\right)\rho(z). \tag{15}$$

This tells us that if at a boundary of the metal there exists a charge, it must decay with the metal exponentially with characteristic screening length λ:

$$\lambda = \left[\frac{4\pi\sigma}{D}\left(1 + \frac{i\omega}{4\pi\sigma}\right)\right]^{-1/2}. \tag{16}$$

In the dc limit (which applies for most frequencies of our interest) this length is the Thomas-Fermi screening length,

$$\lambda_0 = \left(\frac{4\pi\sigma_0}{D}\right)^{-1/2}. \tag{17}$$

So it becomes clear that the screening charge in the metal may be modeled by substituting a sheet of charge displaced from the interface by the Thomas-Fermi screening length, but that in calculating the dielectric thickness of this region the effective dielectric constant that must be used is 1, consistent with the derivation of the screening length. Had we used a form of the Poisson equation that had a nonunity dielectric constant, i.e.,

$$\rho(z) = \frac{\epsilon}{4\pi}\frac{\partial E(z)}{\partial z}, \tag{18}$$

then our screening length would be

$$\lambda_0 = \left(\frac{4\pi\sigma_0}{\epsilon D}\right)^{-1/2}, \tag{19}$$

which is not the Thomas-Fermi screening length. Thus the use of a nonunity dielectric constant for the metal is not compatible with the use of the Thomas-Fermi screening length.

Measurements on both sol-gel and chemical-vapor deposition lead zirconate titanate (PZT) films down to $\sim$60 nm thickness show that reciprocal capacitance $1/C(d)$ versus thickness d extrapolates to finite values at $d=0$, demonstrating an interfacial capacitance. However, whereas the value for the sol-gel films is consistent with the Thomas-Fermi screening approach (0.05 nm), the value of interfacial thickness (0.005 nm) for the chemical-vapor deposition films is only 10% of the interfacial capacitance that would arise from the known Fermi-Thomas screening length of 0.05 nm in the Pt electrodes (Dawber, Chandra, *et al.*, 2003). That is, if this result were interpreted in terms of a "dead layer," the dead layer would have negative width. This result may arise from a compensating "double layer" of space charge inside the semiconducting PZT dielectric; the Armstrong-Horrocks (1997) semiconductor formalism form of the earlier Helmholtz and Gouy-Chapman polar-liquid models of the double layer can be used. Such a double layer is unnecessary in PVDF because that material is highly insulating (Moreira, 2002). This explains quantitatively the difference (8 times) of interfacial capacitance in sol-gel PZT films compared with chemical-vapor deposition PZT films of the same thickness. The magnitude of the electrokinetic potential (or zeta potential) $\zeta = \sigma d'/\epsilon\epsilon_0$ that develops from the Helmholtz layer can be estimated without adjustable parameters from the oxygen-vacancy gradient data of Dey for a typical oxide perovskite, SrTiO3; using Dey's surface charge density σ of $2.8\times10^{18}\ e/\mathrm{m}^2$, a Gouy screening length in the dielectric $d'=20$ nm, and a dielectric constant of $\epsilon=1300$ yields $\zeta=0.78$ eV. Since this is comparable to the Schottky barrier height, it implies that much of the screening is provided internally by mobile oxygen vacancies. [Here $\sigma(\tau,\mu)$ is a function of time τ and mobility μ for a bimodal (ac) switching process.]

4. Conduction mechanisms

In general, conduction is undesirable in memory devices based on capacitors, and so the understanding and minimization of conduction has been a very active area of research over the years. Many mechanisms have been proposed for the conduction in ferroelectric thin films.

a. Schottky injection

Perhaps the most commonly observed currents in ferroelectrics are due to thermionic injection of electrons from the metal into the ferroelectric. The current-voltage characteristic is determined by the image force lowering of the barrier height when a potential is applied. A few points should be made about Schottky injection in ferroelectric thin films. The first is about the dielectric constant appropriate for use. In ferroelectrics the size of the calculated barrier-height lowering depends greatly on which dielectric constant, the static or the electronic, is used. The correct dielectric constant is the electronic one ($\sim$5.5), as discussed by Scott (1999) and used by Dietz and Waser (1997), and by Zafar *et al.* (1998). Dietz and Waser (1997) used the more general injection law of Murphy and Good (1956) to describe charge injection in $SrTiO_3$ films. They found that for lower fields the Schottky expression was valid, but at

higher fields numerical calculations using the general injection law were required. They did not, however, find that Fowler-Nordheim tunneling was a good description of any of the experimental data.

It has been shown by Zafar *et al.* (1998) that in fact the correct form of the Schottky equation that should be used for ferroelectric thin films is the diffusion-limited equation of Simmons. Furthermore, very recently Dawber and Scott (2004) have shown that when one considers the ferroelectric capacitor as a metal-insulator-metal system with diffusion-limited current (as opposed to a single metal-insulator junction), the leakage current is explained well; in addition, a number of unusual effects, such as the negative differential resistivity observed by Watanabe *et al.* (1998) and the PTCR effect observed by Hwang *et al.* (1997, 1998), are accounted for.

b. Poole-Frenkel

One of the standard ways of identifying a Schottky regime is to plot $\log(J/T)$ against $V^{1/2}$. In this case the plot will be linear if the current injection mechanism is Schottky injection. Confusion can arise because carriers can also be generated from internal traps by the Poole-Frenkel effect, which on the basis of this plot is indistinguishable from Schottky injection. However, if the *I-V* characteristic is asymmetric with respect to positive and negative voltages (as is usually the case) then the injection process is most probably Schottky injection. There are, however, some results that show symmetrical *I-V* curves and correctly explain their data on the basis of a Poole-Frenkel conduction mechanism (Chen *et al.*, 1998).

c. Fowler-Nordheim tunneling

Many researchers have discussed the possibility of tunneling currents in ferroelectric thin-film capacitors. For the most part they are not discussing direct tunneling through the film, which would be impossible for typical film thicknesses, but instead tunneling through the potential barrier at the electrode. The chief experimental evidence that it might indeed be possible is from Stolichnov *et al.* (1998), who have seen currents that they claim to be entirely tunneling currents in PZT films 450 nm thick at temperatures between 100 and 140 K. It should be noted, however, that they only observed tunneling currents above 2.2 MV/cm, below which they were unable to obtain data. The narrowness of the range of fields for which they have collected data is a cause for concern, since the data displayed in their paper go from 2.2 to 2.8 MV/cm. We conducted leakage-current measurements on a 70-nm BST thin film at 70 K and found that the leakage current, while of much lower magnitude, was still well described by a Schottky injection relationship; although if one fitted this data to a similarly narrow field region, it did appear to satisfy the Fowler-Nordheim relationship well (Fig. 17).

The effective masses for tunneling obtained in the studies of Stolichnov *et al.* (1999) and Baniecki *et al.* (2001) also seem to be at odds with the normal effective

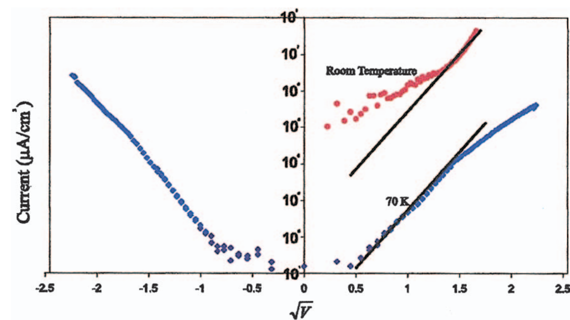

FIG. 17. (Color) Leakage-current data from Au-BST-$SrRuO_3$ film at room temperature and at $T=70$ K.

masses considered for these materials. Whereas they use effective masses of 1.0, the effective masses in perovskite oxides seem to be somewhat larger, $(5-7)m_e$ for barium titanate and strontium titanate (Scott *et al.*, 2003). Although the tunneling mass and the effective (band) mass need not be the same in general, if the tunneling is through thicknesses of >2 nm, they are nearly so. [Conley and Mahan (1967) and Schnupp (1967) also find that the tunneling mass due to light holes in GaAs fits the band mass very well.]

d. Space-charge-limited currents

The characteristic quadratic relationship between current and voltage that is the hallmark of space-charge-limited currents is often seen in ferroelectrics. Sometimes it is observed that space-charge-limited currents are seen when a sample is biased in one direction, whereas for the opposite bias Schottky injection dominates.

e. Ultrathin films—direct tunneling

Recently Rodriguez Contreras *et al.* (2003) have succeeded in producing metal-PZT-metal junctions sufficiently thin (6 nm) that it appears that direct tunneling or phonon-assisted tunneling (in contrast to Fowler-Nordheim tunneling) through the film may occur, though this result requires more thorough investigation since the authors note the barrier heights extracted from their data using a direct tuneling model are much smaller than expected. The principal result of this paper is resistive switching, which may be of considerable interest in device applications, but also requires more thorough investigation. This very interesting experimental study raises important questions about the way that metal wave functions penetrating from the electrode and ferroelectric polarization interact with each other in the thinnest ferroelectric junctions.

f. Grain boundaries

Grain boundaries are often considered to be important in leakage current because of the idea that they will provide conduction pathways through the film.

Gruverman's results [private communication, reproduced in Dawber and Scott (2001)] suggest that this is

not the case in SBT. In his experiment an atomic force microscopy tip is rastered across the surface of a polycrystalline ferroelectric film. The imaged pattern records the leakage current at each point: white areas are high-current spots; dark areas, low current. If the leakage were predominantly along grain boundaries, we should see dark polyhedral grains surrounded by white grain boundaries, which become brighter with increasing applied voltage. In fact, the opposite situation occurs. This indicates that the grains have relatively low resistivity, with high-resistivity grain boundaries. The second surprise is that the grain conduction comes in a discrete step; an individual grain suddenly “turns on” (like a light switch). Smaller grains generally conduct at lower voltages [in accord with Maier’s theory of space-charge effects being larger in small grains with higher surface-volume ratios (Lubomirsky *et al.*, 2002)].

C. Device failure

1. Electrical breakdown

The process of electrical shorting in ferroelectric PZT was first shown by Plumlee (1967) to arise from dendritelike conduction pathways through the material, initiated at the anodes and/or cathodes. These were manifest as visibly dark filamentary paths in an otherwise light material when viewed through an optical microscope. They have been thought to arise as “virtual cathodes” via the growth of ordered chains of oxygen-deficient material. This mechanism was modeled in detail by Duiker *et al.* (Duiker, 1990; Duiker and Beale, 1990; Duiker *et al.*, 1990).

To establish microscopic mechanisms for breakdown in ferroelectric oxide films one must show that the dependences of breakdown field E_B upon film thickness d, ramp rate, temperature, doping, and electrodes are satisfied. The dependence for PZT upon film thickness is most compatible with a low power-law dependence or is possibly logarithmic (Scott *et al.*, 2003). The physical models compatible with this include avalanche (logarithmic), collision ionization from electrons injected via field emission from the cathode (Forlani and Minnaja, 1964), which gives

$$E_B = Ad^{-w}, \tag{20}$$

with $1/4 < w < 1/2$, or the linked defect model of Gerson and Marshall (1959), where $w = 0.3$. The dependence on electrode material arises from the electrode work function and the ferroelectric electron affinity through the resultant Schottky barrier height. Following Von Hippel (1935) we have [Scott (2000a), p. 62]

$$eE_B\lambda = h(\Phi_M - \Phi_{\mathrm{FE}}), \tag{21}$$

where Φ_M and Φ_{FE} are the work functions of the metal and of the semiconducting ferroelectric, λ is electron mean free path, and h is a constant of order unity.

Even in films for which there is considerable Poole-Frenkel limitation of current (a bulk effect), the Schottky barriers at the electrode interfaces will still dominate breakdown behavior.

In general, electrical breakdown in ferroelectric oxides is a hybrid mechanism (like spark discharge in air) in which the initial phase is electrical but the final stage is simple thermal runaway. This makes the dependence upon temperature complicated.

There are at least three different contributions to the temperature dependence. The first is the thermal probability of finding a hopping path through the material. Following Gerson and Marshall (1959) and assuming a random isotropic distribution of traps, Scott (1995) showed that

$$E_B = G - \frac{k_B T}{B}\log A, \tag{22}$$

which gives both the dependence on temperature T and electrode area A in agreement with all experiments on PZT, BST, and SBT.

In agreement with this model the further assumption of exponential conduction (nonohmic) estimated to occur for applied field $E > 30$ MV/m (Scott, 2000a),

$$\sigma(T) = \sigma_0 \exp\left(\frac{-b}{k_B T}\right) \tag{23}$$

in these materials yields the correct dependence of breakdown time t_B upon field

$$\log t_B = c_1 - c_2 E_B \tag{24}$$

as well as the experimentally observed dependence of E_B on rise time t_c of the applied pulse:

$$E_B = c_3 t_c^{-1/2}. \tag{25}$$

Using the same assumption of exponential conduction, which is valid for

$$aeE \ll k_B T, \tag{26}$$

where a is the lattice nearest-neighbor oxygen-site hopping distance (approximately a lattice constant) and e, the electron charge, Scott (2000a) showed that the general breakdown field expression

$$C_V \frac{dT}{dt} - \nabla(K \cdot \nabla T) = \sigma E_B^2 \tag{27}$$

in the impulse approximation (in which the second term in the above equation is neglected) yields

$$E_B(T) = \left[\frac{3C_V K}{\sigma_0 b t_c}\right]^{1/2} T \exp\left(\frac{b}{2k_B T}\right), \tag{28}$$

which suffices to estimate the numerical value of breakdown field for most ferroelectric perovskite oxide films; values approximating 800 MV/m are predicted and measured.

A controversy has arisen regarding the temperature dependence of $E_B(T)$ and the possibility of avalanche (Stolichnov *et al.*, 2001). In low carrier-concentration

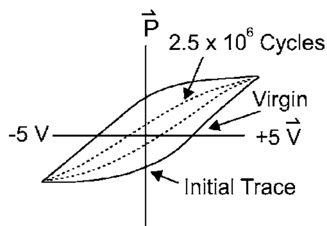

FIG. 18. Change in the polarization hysteresis loop with fatigue. Reprinted with permission from Scott and Pouligny, 1988. © 1988, AIP.

single crystals, especially Si, avalanche mechanisms give a temperature dependence that is controlled by the mean free path of the injected carriers. This is physically because at higher temperatures the mean free path λ decreases due to phonon scattering and thus one must apply a higher field E_B to achieve avalanche conditions,

$$\lambda = \lambda_0 \tanh\left(\frac{E_B}{kT}\right). \tag{29}$$

However, this effect is extremely small even for low carrier concentrations (10% change in E_B between 300 and 500 K for $n = 10^{16}\ \text{cm}^{-3}$) and negligible for higher concentrations. The change in E_B in BST between 600 and 200 K is >500% and arises from Eq. (22), not Eq. (29). Even if the ferroelectrics were single crystals, with $10^{20}\ \text{cm}^{-3}$ oxygen vacancies near the surface, any T dependence from Eq. (29) would be unmeasurably small; and for the actual fine-grained ceramics (40 nm grain diameters), the mean free path is ~1 nm and limited by grain boundaries (T independent). Thus the conclusion of Stolichnov *et al.* (2001) regarding avalanche is qualitatively and quantitatively wrong in ferroelectric oxides.

2. Fatigue

Polarization fatigue, which is the process whereby the switchable ferroelectric polarization is reduced by repetitive electrical cycling, is one of the most serious device failure mechanisms in ferroelectric thin films. It is most commonly a problem when Pt electrodes, desirable because of their high work functions, are used.

Importantly fatigue occurs through the pinning of domain walls, which pins the polarization in a particular direction, rather than any fundamental reduction of the polarization. Scott and Pouligny (1988) demonstrated in KNO_3 via Raman spectroscopy that only a very small part of the sample was converted from the ferroelectric to the nonferroelectric phase with fatigue, thus implying that fatigue must be caused by pinning of the domain walls. They also demonstrated that the domain walls could be depinned via the application of a large field, as shown in Fig. 18. The pinning of domain walls has also been observed directly with atomic force microscopy by Gruverman *et al.* (1996) and by Colla *et al.* (1998).

There is a fairly large body of evidence that oxygen vacancies play some key part in the fatigue process. Auger data of Scott *et al.* (1991) show areas of low oxygen concentration in a region near the metal electrodes, implying a region of greater oxygen-vacancy data. Scott *et al.* also reproduced Auger data from Troeger (1991) for a film that had been fatigued by 10^{10} cycles showing an increase in the width of the region with depleted oxygen near the platinum electrode (Fig. 19). There is, however, no corresponding change at the gold electrode. Gold does not form oxides. This might be an explanation of the different behavior at the two electrodes. Although some researchers believe that platinum also does not form oxides, the adsorption of oxygen onto Pt surfaces is actually a large area of research because of the important role platinum plays as a catalyst in fuel-cell electrodes. Oxygen is not normally adsorbed onto gold surfaces but can be if there is significant surface roughness (Mills *et al.*, 2003).

It has also been found experimentally that films fatigue differently in atmospheres containing different oxygen partial pressures (Brazier *et al.*, 1999). Pan *et al.*

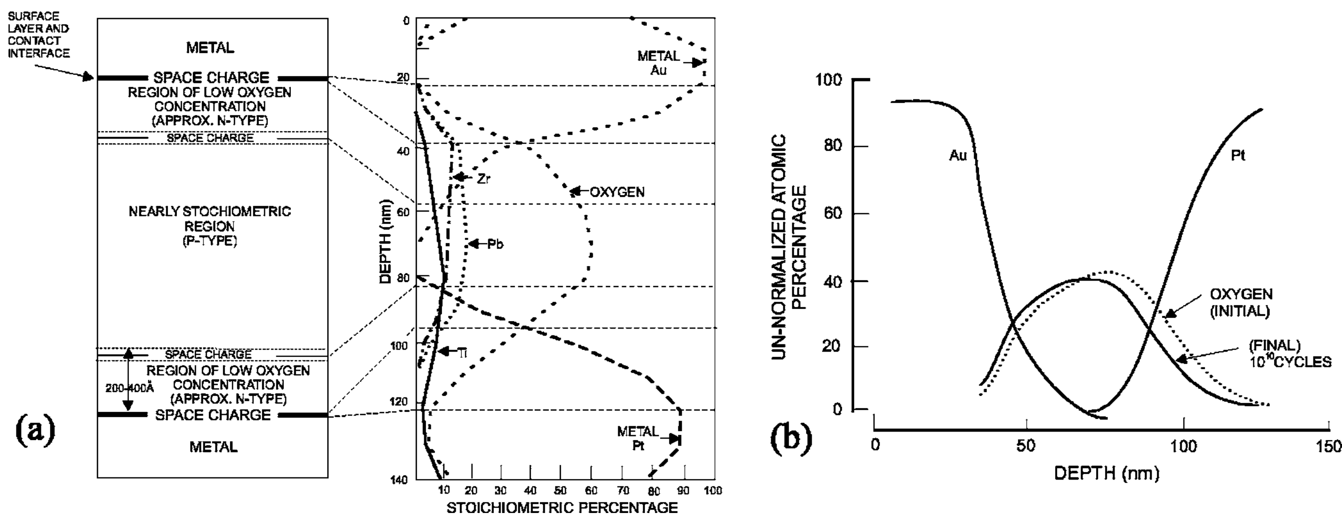

FIG. 19. (a) Auger depth profile of PZT thin-film capacitor. (b) Effect of fatigue on oxygen concentration near the electrode. Reprinted with permission from Scott *et al.*, 1991. © 1991, AIP.

(1996) claim to have seen oxygen actually leaving a ferroelectric sample during switching, though we note that Nuffer *et al.* (2001) claim this to be an experimental artifact. The results of Schloss *et al.* (2002) are very interesting in that they show directly by O^{18} tracer studies that the oxygen vacancies redistribute themselves during voltage cycling. In their original paper they concluded that the redistribution of oxygen vacancies was not the cause of fatigue because they did not see redistribution of O^{18} when the sample had been annealed. However, in a more recent publication they conclude the reason they could not see the oxygen tracer distribution was more probably due to a change in the oxygen permeability of the electrode after annealing (Schloss *et al.*, 2004).

It has been known for some time that the fatigue of PZT films can be improved by the use of oxide electrodes, such as iridium oxide or ruthenium oxides. de Araujo *et al.* (1995) explained the improved fatigue resistance by the fact that oxides of iridium and platinum can reduce or reoxidize reversibly and repeatedly without degradation. For this same reason iridium is preferred to platinum as an electrode material for medical applications, for which this property was originally studied by Robblee and Cogan (1986). This property does make the leakage-current properties of these electrodes more complicated, and generally films with Ir/IrO_2 or Ru/RuO_2 electrodes have higher leakage currents than those with platinum electrodes. Unless carefully annealed at a certain temperature RuO_2 electrodes will have elemental Ru metallic islands. Since the work function for Ru is 4.65 eV and that for RuO_2 is 4.95 eV, almost all the current will pass through the Ru islands, producing hot spots and occasional shorts (Hartmann *et al.*, 2000). By contrast, although one expects that there will be similar issues with mixtures of Ir and IrO_2 in iridium-based electrodes, when metallic Ir is oxidized to IrO_2 its work function decreases to 4.23 eV (Chalamala *et al.*, 1999).

The idea that planes of oxygen vacancies perpendicular to the polarization direction could pin domain walls is originally due to Brennan (1993). Subsequently, in a theoretical microscopic study of oxygen-vacancy defects in $PbTiO_3$, Park and Chadi (1998) showed that planes of vacancies are much more effective at pinning domain walls than single vacancies. Arlt and Neumann (1988) have discussed how under repetitive cycling in bulk ferroelectrics the vacancies can move from their originally randomly distributed sites in the perovskite structure to sites in planes parallel to the ferroelectric-electrode interface. We suspect that while this may account for fatigue in bulk ferroelectrics it is not the operative mechanism in thin films. Scott and Dawber (2000) have suggested that in thin films the vacancies can reach sufficiently high concentrations that they order themselves into planes in a similar way as occurs in Fe-doped bulk samples and on the surfaces of highly reduced specimens. Direct evidence that this occurs in bulk PZT was found using atomic force microscope imagery of PZT grains by Lupascu and Rabe (2002; Fig. 20). Recently, evidence of oxygen-vacancy ordering has also been

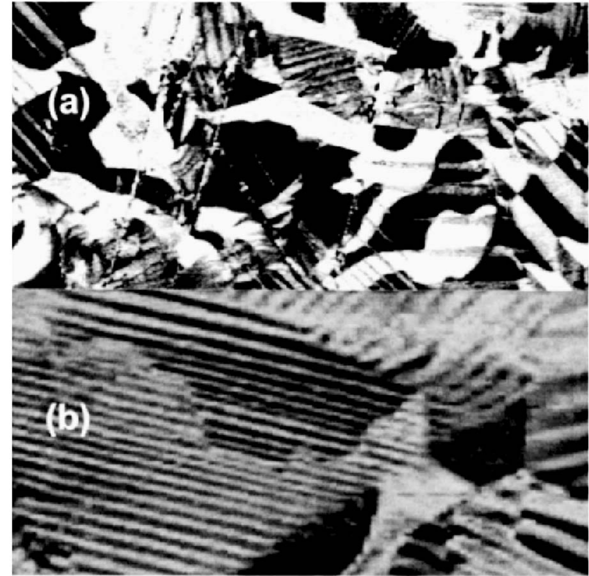

FIG. 20. Atomic force microscopy images (a) before and (b) after cycling showing evidence of planes of oxygen vacancies in the fatigued sample. Image width$=10$ μm. From Lupascu and Rabe, 2002.

found in barium titanate reduced after an accelerated life test (Woodward *et al.*, 2004).

While most researchers acknowledge that oxygen vacancies play a role in fatigue, it should be noted that Tagantsev *et al.* (2001) have aggressively championed a model of charge injection; however, since this model is not developed into a quantitative form, it is very hard to verify or falsify it. Charge injection probably does play a role in fatigue, an idea at least in part supported by the detailed experimental study of Du and Chen (1998b), but in the model of Dawber and Scott (2000) [which draws upon the basic idea of Yoo and Desu (1992) that fatigue is due to the electromigration of oxygen vacancies] it is not included; nevertheless, most of the experimental results in the literature may be accounted for. The model of Dawber and Scott (2000) basically shows that in a ferroelectric thin film under an ac field there is in fact a net migration of vacancies towards the interface and it is the high concentration of vacancies in this region that results in ordering of the vacancies and pinning of domain walls. The interfacial nature of fatigue in thin films has been demonstrated by Dimos *et al.* (1994) and by Colla *et al.* (1998).

To understand fatigue better, what are needed are more experiments that try to look at the problem in novel ways. Standard electrical measurements alone probably cannot shed a great deal of additional light on the problem, especially given the problems between comparing samples grown in different labs using different techniques. Recently, a very interesting study was undertaken by Do *et al.* (2004) using x-ray microdiffraction to observe fatigue in PZT. Using this technique they were able to see how regions of the film stopped switching as it fatigued. One of the key findings of this study was that there appear to be two fatigue effects opera-

tive, a reversible effect that occurs when low to moderate fields are used for switching and an irreversible effect which occurs under very high fields.

3. Retention failure

Clearly a nonvolatile memory that fails to retain the information stored in it will not be a successful device. Furthermore, producers of memories need to be able to guarantee retention times over much longer periods of time than they can possibly test. A better understanding of retention failure is thus required so that models can be used that allow accelerated retention tests to be carried out. The work of Kim *et al.* (2001) is a step in this direction.

It seems that imprint and retention failure are closely linked phenomena; i.e., if a potential builds up over a period of time, it can destabilize the ferroelectric polarization state and thus cause loss of information. Further comparison of retention-time data and fatigue data suggests a link between the two effects. Direct current degradation of resistance in BST seems also to be a related effect (Zafar *et al.*, 1999). The electromigration of oxygen vacancies under an applied field in a Fe-doped $SrTiO_3$ single crystal has been directly observed via electrochromic effects (Waser *et al.*, 1990). Oxygen-vacancy redistribution under an applied field has also been invoked to explain a slow relaxation of the capacitance in BST thin films (Boikov *et al.*, 2001). It would seem to make sense that whereas fatigue relates to the cumulative motion of oxygen vacancies under an ac field, resistance degradation is a result of their migration under an applied dc field, and retention failure is a result of their migration under the depolarization field or other built-in fields in the material.

IV. FIRST PRINCIPLES

With continuing advances in algorithms and computer hardware, first-principles studies of the electronic structure and structural energetics of complex oxides can now produce accurate, material-specific information relevant to the properties of thin-film ferroelectrics. In this section, we focus on first-principles studies that identify and analyze the characteristic effects specific to thin films. First, we briefly review the relevant methodological progress and the application of these methods to bulk ferroelectric materials. Next, we survey the first-principles investigations of ferroelectric thin films and superlattices reported in the literature. It will be seen that the scale of systems that can be studied directly by first-principles methods is severely limited at present by practical considerations. This can be circumvented by the construction of nonempirical models with parameters determined by fitting to the results of selected first-principles calculations. These models can be parametrized interatomic potentials, permitting molecular-dynamics studies of nonzero temperature effects, or first-principles effective Hamiltonians for appropriate degrees of freedom (usually local polarization and strain). The form of the latter strongly resembles that of a Landau-Devonshire theory, providing a connection between first-principles approaches and the extensive literature on phenomenological models for the behavior of thin-film ferroelectrics. The advantages and disadvantages of using first-principles results rather than experimental data to construct models will be considered. In addition to allowing the study of systems far more complex than those that can be considered by first principles alone, this modeling approach yields physical insight into the essential differences between bulk and thin-film behavior, which will be discussed at greater length in Sec. IV.B.5. Finally, it will be seen that, despite practical limitations, the complexity of the systems for which accurate calculations can be undertaken has steadily increased in recent years, to the point where films of several lattice constants in thickness can be considered. While this is still far thinner than the films of current technological interest, concommitent improvements in thin-film synthesis and characterizaton have made it possible to achieve a high degree of atomic perfection in comparable ultrathin films in the context of research. This progress has led to a true relevance of calculational results to experimental observations, opening a meaningful experimental-theoretical dialog. However, this progress in some ways only serves to highlight the full complexity of the physics of real ferroelectric films: as questions get answered, more questions, especially about phenomena at longer length scales and about dynamics, are put forth. These challenges will be discussed in Sec. IV.B.6.

A. Density-functional-theory studies of bulk ferroelectrics

In parallel with advances in laboratory synthesis, the past decade has seen a revolution in the atomic-scale theoretical understanding of ferroelectricity, especially in perovskite oxides, through first-principles density-functional-theory investigations. The central result of a density-functional-theory calculation is the ground-state energy computed within the Born-Oppenheimer approximation; from this the predicted ground-state crystal structure, phonon dispersion relations, and elastic constants are directly accessible. The latter two quantities can be obtained by finite-difference calculations, or, more efficiently, through the direct calculation of derivatives of the total energy through density-functional perturbation theory (Baroni *et al.*, 2001).

For the physics of ferroelectrics, the electric polarization and its derivatives, such as the Born effective charges and the dielectric and piezoelectric tensors, are as central as the structural energetics, yet proper formulation in a first-principles context long proved to be quite elusive. Expressions for derivatives of the polarization corresponding to physically measurable quantities were presented and applied in density-functional perturbation theory calculations in the late 1980s (de Gironcoli *et al.*, 1989). A key conceptual advance was establishing the correct definition of the electric polarization as a bulk property through the Berry-phase formalism of

King-Smith, Vanderbilt, and Resta (King-Smith and Vanderbilt, 1993; Resta, 1994). With this and the related Wannier function expression (King-Smith and Vanderbilt, 1994), the spontaneous polarization and its derivatives can be computed in a post-processing phase of a conventional total-energy calculation, greatly facilitating studies of polarization-related properties.

For perovskite oxides, the presence of oxygen and first-row transition metals significantly increases the computational demands of density-functional total-energy calculations compared to those for typical semiconductors. Calculations for perovskite oxides have been reported using essentially all of the available first-principles methods for accurate representation of the electronic wave functions: all-electron methods, mainly linearized augmented plane wave (LAPW) and full-potential linearized augmented plane wave (FLAPW), linear muffin-tin orbitals, norm-conserving and ultrasoft pseudopotentials, and projector-augmented wave-function potentials. The effects of different choices for the approximate density functional have been examined; while most calculations are carried out with the local-density approximation, for many systems the effects of the generalized-gradient approximation and weighted-density approximation (Wu *et al.*, 2004) have been investigated, as well as the alternative use of the Hartree-Fock approach. Most calculations being currently reported are performed with an appropriate standard package, mainly VASP (Kresse and Hafner, 1993; Kresse and Furthmuller, 1996), with ultrasoft pseudopotentials and projector-augmented wave function potentials, ABINIT (Gonze *et al.*, 2002), with norm-conserving pseudopotentials and projector-augmented wave function potentials, PWscf (Baroni *et al.*), with norm-conserving and ultrasoft pseudopotentials, SIESTA (Soler *et al.*, 2002), with norm-conserving pseudopotentials, WIEN97 (FLAPW) (Blaha *et al.*, 1990) and CRYSTAL (Hartree-Fock) (Dovesi *et al.*, 2005).

To predict ground-state crystal structures, the usual method is to minimize the total energy with respect to free structural parameters in a chosen space group, in a spirit similar to that of a Rietveld refinement in an experimental structural determination. The space group is usually implicitly specified by a starting guess for the structure. For efficient optimization, the calculation of forces on atoms and stresses on the unit cell is essential and is included now in every standard first-principles implementation following the formalism of Hellmann and Feynman (1939) for the forces and Nielsen and Martin (1985) for stresses.

The accuracy of density-functional theory for predicting the ground-state structures of ferroelectrics was first investigated for the prototypical cases of $BaTiO_3$ and $PbTiO_3$ (Cohen and Krakauer, 1990, 1992; Cohen, 1992) and then extended to a larger class of ferroelectric perovskites (King-Smith and Vanderbilt, 1994). Extensive studies of the structures of perovskite oxides and related ferroelectric-oxide structures have since been carried out (Resta, 2003). The predictive power of first-principles calculations is well illustrated by the results of Singh for $PbZrO_3$ (Singh, 1995), in which the correct energy ordering between ferroelectric and antiferroelectric structures was obtained and, furthermore, comparisons of the total energy resolved an ambiguity in the reported space group and provided an accurate determination of the oxygen positions.

It is important to note, however, that there seem to be limitations on the accuracy to which structural parameters, particularly lattice constants, can be obtained. Most obvious is the underestimation of the lattice constants within the local-density approximation, typically by about 1% (generalized-gradient approximation tends to shift lattice constants upward, sometimes substantially overcorrecting). Considering that the calculation involves no empirical input whatsoever, an error as small as 1% could be regarded not as a failure, but as a success of the method. Moreover, the fact that the underestimate varies little from compound to compound means that the relative lattice constants and thus the type of lattice mismatch (tensile/compressive) between two materials in a heterostructure is generally correctly reproduced when using computed lattice parameters. However, for certain questions, even a 1% underestimate can be problematic. The ferroelectric instability in the perovskite oxides, in particular, is known to be very sensitive to pressure (Samara, 1987) and thus to the lattice constant, so that 1% can have a significant effect on the ferroelectric instability. In addition, full optimization of all structural parameters in a low-symmetry space group can in some cases, $PbTiO_3$ being the most well-studied example, lead to an apparently spurious prediction, though fixing the lattice constants to their experimental values leads to good agreement for the other structural parameters (Saghi-Szabo *et al.*, 1998). Thus it has become acceptable, at least in certain first-principles contexts, to fix the lattice parameters or at least the volume of the unit cell, to the experimental value when this value is known.

In a first-principles structural prediction, the initial choice of space group may appear to limit the chance that a true ground-state structure will be found. In general, once a minimum is found, it can be proved (or not) to be a local minimum by computation of the full phonon dispersion and of the coupling, if allowed by symmetry, between zone-center phonons and homogeneous strain (Garcia and Vanderbilt, 1996). Of course, this does not rule out the possibility of a different local minimum with lower energy with an unrelated structure.

For ferroelectrics, the soft-mode theory of ferroelectricity provides a natural conceptual framework for the identification of low-symmetry ground-state structures and for estimating response functions. The starting point is the identification of a high-symmetry reference structure. For perovskite compounds, this is clearly the cubic perovskite structure, and for layered perovskites, it is the nonpolar tetragonal structure. The lattice instabilities of the reference structure can be readily identified from the first-principles calculation of phonon dispersion relations (Waghmare and Rabe, 1997a; Ghosez *et al.*, 1999; Sai and Vanderbilt, 2000), this being especially

efficient within density-functional perturbation theory. In simple ferroelectric perovskites, the ground-state structure is obtained to lowest order by freezing in the most unstable mode (a zone-center polar mode). This picture can still be useful for more complex ground-state structures that involve the freezing in two or more coupled modes (e.g., $PbZrO_3$) (Waghmare and Rabe, 1997b; Cockayne and Rabe, 2000), as well as for identifying low-energy structures that might be stabilized by temperature or pressure (Stachiotti *et al.*, 2000; Fennie and Rabe, 2005). The polarization induced by the soft polar mode can be obtained by computation of the Born effective charges, yielding the mode effective charge. The temperature-dependent frequency of the soft polar mode and its coupling to strain are expected largely to determine the dielectric and piezoelectric response of ferroelectric and near-ferroelectric perovskite oxides; this idea has been the basis of several calculations (Cockayne and Rabe, 1998; Garcia and Vanderbilt, 1998).

Minimization of the total energy can similarly be used to predict atomic arrangements and formation energies of point defects (Park and Chadi, 1998; Poykko and Chadi, 2000; Betsuyaku *et al.*, 2001; Man and Feng, 2002; Park, 2003; Robertson, 2003; Astala and Bristowe, 2004), domain walls (Poykko and Chadi, 2000; Meyer and Vanderbilt, 2002; He and Vanderbilt, 2003), and nonstoichiometric planar defects such as antiphase domain boundaries (Suzuki and Fujimoto, 2001; Li *et al.*, 2002), in bulk perovskite oxides. The supercell used must accommodate the defect geometry and generally must contain many bulk primitive cells to minimize the interaction of a defect with its periodically repeated images. Thus these calculations are extremely computationally intensive, and many important questions remain to be addressed.

While much of the essential physics of ferroelectrics arises from the structural energetics, the polarization, and the coupling between them, there has been increasing interest in ferroelectric oxides as electronic and optical materials, for which accurate calculations of the gap and dipole matrix elements are important. Furthermore, as we shall discuss in detail below, the band structures enter in an essential way in understanding the charge transfer and dipole layer formation of heterostructures involving ferroelectrics, other insulators, and metals. While density-functional theory provides a rigorous foundation only for the computation of Born-Oppenheimer ground-state total energies and electronic charge densities, it is also often used for investigation of electronic structure. In the vast majority of density-functional implementations, calculation of the ground-state total energy and charge density involves the computation of a band structure for independent electron states in an effective potential, following the work of Kohn and Sham (1965). This band structure is generally regarded as a useful guide to the electronic structure of materials, including perovskite and layered perovskite oxides (Cohen, 1992; Robertson *et al.*, 1996; Tsai *et al.*, 2003). It should be noted that with approximate functionals, such as the local-density approximation, the fundamental band gaps of insulators and semiconductors, including perovskite ferroelectrics, are substantially underestimated. While for narrow gap materials the system may even be erroneously found to be metallic, for wider gap systems such as most of the simple ferroelectric perovskite compounds considered here, the band gap is still nonzero and thus the structural energetics in the vicinity of the ground-state structure is unaffected. While this error might be considered to be an insuperable stumbling block to first-principles investigation of electronic structure and related properties, there is at present no widely available, computationally tractable, alternative [there are, though, some indications that the use of exact-exchange functionals can eliminate much of this error (Piskunov *et al.*, 2004); it has long been known that Hartree-Fock, i.e., exact exchange only, leads to overestimates of the gaps]. The truth is that, as will be discussed further below, these results can, with care, awareness of the possible limitations, and judicious use of experimental input, be used to extract useful information about the electronic structure and related properties in individual material systems.

At present, the computational limitations of full first-principles calculations to 70–100 atoms per supercell have stimulated considerable interest in the development and use in simulations of effective models, from which a subset of the degrees of freedom have been integrated out. Interatomic shell-model potentials have been developed for a number of perovskite-oxide systems, eliminating most of the electronic degrees of freedom except for those represented by the shells (Tinte *et al.*, 1999; Heifets, Kotonin, and Maier, 2000; Sepliarsky *et al.*, 2004). A more dramatic reduction in the number of degrees of freedom is performed to obtain effective Hamiltonians, in which typically one vector degree of freedom decribes the local polar distortion in each unit cell. This approach has proved useful for describing finite-temperature structural transitions in compounds and solid solutions (Zhong *et al.*, 1994; Rabe and Waghmare, 1995, 2002; Waghmare and Rabe, 1997a; Bellaiche *et al.*, 2000). To the extent that the parameters appearing in these potentials are determined by fitting to selected first-principles results (e.g., structures, elastic constants, phonons), these approaches can be regarded as approximate first-principles methods. They allow computation of the polarization as well as of the structural energetics, but not, however, of the electronic states. Most of the effort has been focused on $BaTiO_3$, though other perovskites, including $PbTiO_3$ and $KNbO_3$, $SrTiO_3$ and $(Ba,Sr)TiO_3$, and $Pb(Zr,Ti)O_3$, have been investigated in this way and useful results obtained.

B. First-principles investigation of ferroelectric thin films

The interest in ferroelectric thin films and superlattices lies in the fact that the properties of the system as a whole can be so different from the individual properties of the constituent material(s). Empirically, it has been observed that certain desirable bulk properties, such as a

high dielectric response, can be degraded in thin films, while in other investigations there are signs of novel interesting behavior obtained only in thin-film form.

Theoretical analysis of the observed properties of thin films presents a daunting challenge. It is well known that the process of thin-film growth itself can lead to nontrivial differences from the bulk material, as observed in studies of homoepitaxial oxide films such as $SrTiO_3$ (Klenov *et al.*, 2004). However, as synthetic methods have developed, the goal of growing nearly ideal, atomically ordered, single-crystal films and superlattices is coming within reach, and the relevance of first-principles results for perfect single-crystal films to experimental observations emerging.

As will be clear from the discussion in the rest of this section, an understanding of characteristic thin-film behavior can best be achieved by detailed quantitative examination of individual systems combined with the construction of models incorporating various aspects of the physics, from which more general organizing principles can be identified. In first-principles calculations, there is a freedom to impose constraints on structural parameters and consider hypothetical structures that goes far beyond anything possible in a real system being studied experimentally. This will allow us to isolate and examine various influences on the state of a thin film: epitaxial strain, macroscopic electric fields, surfaces and interfaces, characteristic defects associated with thin-film growth, and "true" finite-size effects, and how they change the atomic arrangements, electronic structure, polarization, vibrational properties, and responses to applied fields and stresses. While the main focus of this review is on thin films, this approach also applies naturally to multilayers and superlattices. Extending our discussion to include these latter systems will allow us to consider the effects of the influencing factors in different combinations, for example, the changing density of interfaces, the degree of mismatch strain, and the polarization mismatch. These ideas are also relevant to investigating the behavior of bulk-layered ferroelectrics, which can be regarded as natural short-period superlattices.

Within this first-principles modeling framework, we can more clearly identify specific issues and results for investigation and analysis. The focus on modeling is also key to the connection of first-principles results to the extensive literature on phenomenological analysis and to experimental observations. This makes the most effective use of first-principles calculations in developing a conceptual and quantitative understanding of characteristic thin-film properties, as manifested by thickness dependence as well as by the dependence on choice of materials for the film, substrate, and electrodes.

1. First-principles methodology for thin films

The fundamental geometry for the study of thin films, surfaces, and interfaces is that of an infinite single-crystalline planar slab. Since three-dimensional periodicity is required by most first-principles implementations, in those cases the slab is periodically repeated to produce a supercell; a few studies have been carried out with electronic wave-function basis sets that permit the study of an isolated slab. The variables to be specified include the orientation, the number of atomic layers included, choice of termination of the surfaces, and width of vacuum layer separating adjacent slabs. As in the first-principles prediction of the bulk crystal structure, choice of a space group for the supercell is usually established by the initial structure; relaxations following forces and stresses do not break space-group symmetries. The direction of the spontaneous polarization is constrained by the choice of space group, allowing comparison of unpolarized (paraelectric) films with films polarized along the normal or in the plane of the film.

As we shall see below, in most cases the slabs are very thin (ten atomic layers or fewer). It is possible to relate the results to the surface of a semi-infinite system or a coherent epitaxial film on a semi-infinite substrate by imposing certain constraints on the structures considered. In the former case, the atomic positions for interior layers are fixed to correspond to the bulk crystal structure. In the latter, the in-plane lattice parameters of the supercell are fixed to the corresponding bulk lattice parameters of the substrate, which is not otherwise explicitly included in the calculation. More sophisticated methods developed to deal with the coupling of vibrational modes at the surface with bulk modes of the substrate (Lewis and Rappe, 1996) could also be applied to ferroelectric thin films, though this has not yet been done.

The local-density approximation underestimate of the equilibrium atomic volume will in general also affect slab calculations, and similar concerns arise on the coupling of strain and the ferroelectric instability. As in the bulk crystal structure prediction, it may in some cases be appropriate to fix certain structural parameters according to experimental or bulk information. In the case of superlattices and supercells of films on substrates, it may, on the other hand, be a good choice to work consistently at the (compressed) theoretical lattice constant since the generic underestimate of the atomic volume ensures that the lattice mismatch and relative tensile/compressive strain will be correctly reproduced. This applies, for example, to the technique mentioned in the previous paragraph, in which the effects of epitaxial strain are investigated by performing slab calculations with an appropriate constraint on the in-plane lattice parameters.

As in first-principles predictions of the bulk crystal structure, the initial choice of space group constrains, to a large extent, the final "ground-state" structure. If the supercell is constructed by choosing a bulk termination, the energy minimization based on forces and stresses will preserve the initial symmetry, yielding information about surface relaxations of the unreconstructed surface. A lower-energy structure might result from breaking additional point or translational symmetries to obtain a surface reconstruction. This type of surface reconstruction could be detected by computing the Hessian matrix (coupled phonon dispersion and homogeneous strain)

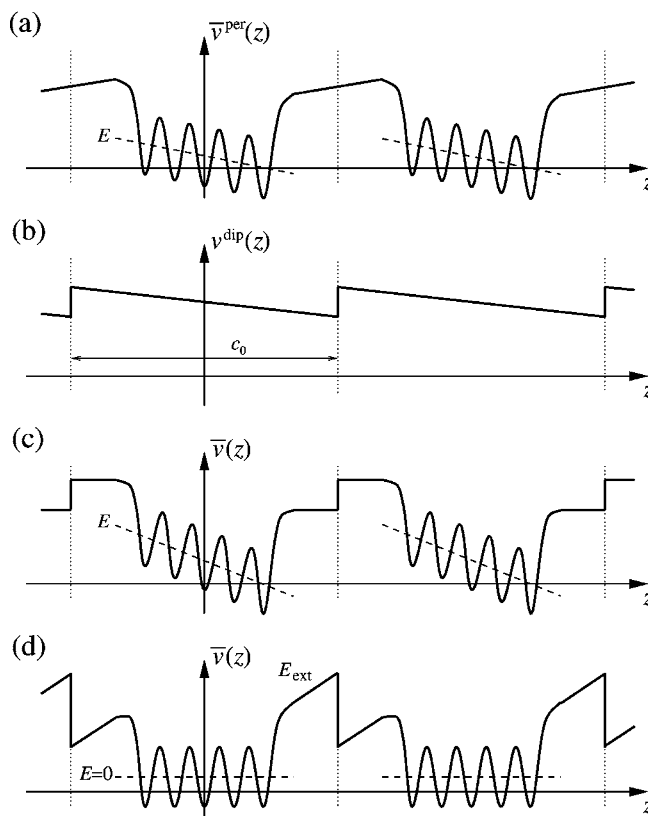

FIG. 21. Schematic picture of the planar-averaged potential $\bar{v}(z)$ for periodically repeated slabs: (a) with periodic boundary conditions, (b) potential of the dipole layer, (c) dipole-corrected slabs with vanishing external electric field, and (d) dipole-corrected slabs with vanishing internal electric field. From Meyer and Vanderbilt, 2001.

for the relaxed surface. More complex reconstructions involving adatoms, vacancies, or both would have to be studied using appropriate starting supercells. Information regarding the existence and nature of such reconstructions might be drawn from experiments and/or from known reconstructions in related materials.

One very important consideration in the theoretical prediction of stable surface orientations and terminations and of favorable surface reconstructions is that these depend on the relative chemical potential of the constituents. Fortunately, since the chemical potential couples only to the stoichiometry, the prediction of the change of relative stability with chemical potential can be made with a single total-energy calculation for each structure (see, for example, Meyer *et al.*, 1999). Because of the variation in stoichiometry for different (001) surface terminations, what is generally reported is the average surface energy of symmetric AO- and BO_2-terminated slabs.

A problem peculiar to the study of periodically repeated slabs with polarization along the normal is the appearance of electric fields in the vacuum. As shown in Fig. 21, this occurs because there is a nonzero macroscopic depolarizing field in the slab and thus a nonzero potential drop between the two surfaces of the slab. As the potential drop across the entire supercell must be zero, this inevitably leads to a nonzero electric field in the vacuum. Physically, this can be interpreted as an external field applied uniformly across the unit cell which acts partially to compensate the depolarizing field. An analogous situation arises for an asymmetrically terminated slab when the two surfaces have different work functions. To eliminate the artificial field in the vacuum, one technique is to introduce a dipole layer in the mid-vacuum region far away from the slab (Bengtsson, 1999). This can accommodate a potential drop up to a critical value, at which point electrons begin to accummulate in an artificial well in the vacuum region (see Fig. 21). This approach can also be used to compensate the depolarization field in a perpendicular polarized film, though it may happen that the maximum field that can be applied is smaller than that needed for full compensation. Alternatively, by using a first-principles implementation with a localized basis set, it is possible to perform computations for isolated slabs and thus avoid not only the spurious electric fields, but also the interaction between periodic slab images present even for symmetric nonpolar slabs. Comparison between results obtained with the two approaches is presented by Fu *et al.* (1999).

In determining the properties of an ultrathin film, the film-substrate and/or film-electrode interface plays a role at least as important as the free surface. In first-principles calculations, the atomic and electronic structure of the relevant interface(s) is most readily obtained by considering a periodic multilayer geometry identical to that used for computing the structure and properties of superlattices. To simulate a semi-infinite substrate, the in-plane lattice constant should be fixed to that of the substrate bulk. The relaxation of a large number of structural degrees of freedom requires substantial computer resources, and some strategies for efficiently generating a good starting structure will be described in the discussion of specific systems in Sec. IV.B.3.

Calculations of quantities characterizing the electronic structure are based on use of the Kohn-Sham one-electron energies and wave functions. Band structures for 1×1 (001) slabs are generally displayed in the 2D surface Brillouin zone for $k_{\text{supercell},z}=0$. One way to identify surface states is by comparison with the appropriately folded-in bulk band structure. Another analysis method is to compute the partial density of states projected onto each atom in the slab. From these plots, the dominant character of a state at a particular energy can be found. In addition, an estimate of valence-band offsets and Schottky barriers at an interface can be obtained by analyzing the partial density of states for a superlattice of the two constituents. This is done comparing the energies of the highest occupied states in the interior of the relevant constituent layers (because of the band-gap problem, the positions of the conduction bands are computed using the experimental bulk band gaps). This estimate can be refined, as described in Junquera *et al.* (2003), by computation of the average electrostatic energy difference between the relevant constituent layers.

As the computational resources required for full first-principles calculations even for the simplest slab-vacuum system are considerable, there is a strong motivation to turn to interatomic potentials and effective Hamiltonians. Interatomic potentials based on shell models fitted to bulk structural energetics are generally directly transferred to the isolated slab geometry, with no changes for the undercoordinated atoms at the surface. As discussed below, this approach seems to be successful in reproducing the relaxations observed in full first-principles studies and has been applied to far larger supercells and superlattices. In the case of effective Hamiltonians, it is, at least formally, possible simply to perform a simulation by removing unit cells and using bulk interaction parameters for the unit cells in the film. For a more accurate description, modification of the effective Hamiltonian parameters for the surface layers is advisable to restore the charge neutrality sum rule for the film (Ruini *et al.*, 1998; Ghosez and Rabe, 2000). In addition, the effects of surface relaxation would also result in modified interactions at the surface.

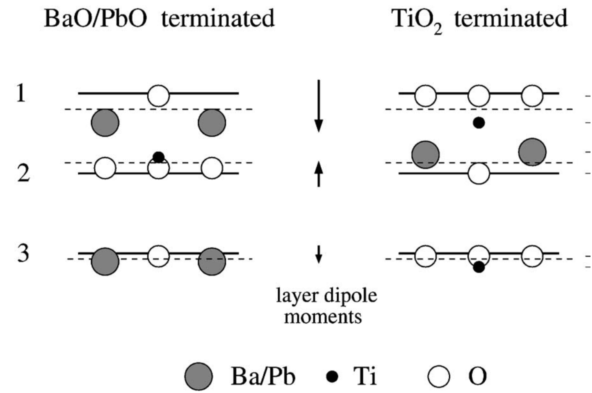

FIG. 22. Schematic illustration of the structure of the first three surface layers. From Meyer and Vanderbilt, 2001.

2. Overview of systems

In this section, we present a list of the materials and configurations that have been studied, followed by a brief overview of the quantities and properties that have been calculated in one or more of the reported studies. A more detailed description of the work on individual systems is provided in the following sections.

The configurations that have been considered to date in first-principles studies can be organized into several classes. The simplest configuration is a slab of ferroelectric material alternating with vacuum; this can be used to investigate the free surface of a semi-infinite crystal, an unconstrained thin film, or an epitaxial thin film constrained to match the lattice constant of an implicit substrate. Specific materials considered included $BaTiO_3$ [(001) surfaces (Cohen, 1996, 1997; Fu *et al.*, 1999; Heifets *et al.*, 2001a; Meyer and Vanderbilt, 2001; Krcmar and Fu, 2003) and (110) surfaces (Heifets *et al.*, 2001a)] $SrTiO_3$ (Padilla and Vanderbilt, 1998; Heifets *et al.*, 2001a, 2002a, 2002b; Kubo and Nozoye, 2003), $PbTiO_3$ (Ghosez and Rabe, 2000; Meyer and Vanderbilt, 2001; Bungaro and Rabe, 2005), $KNbO_3$ (Heifets, Kotonin, and Jacobs, 2000), and $KTaO_3$ (Li, Akhador, *et al.*, 2003). Another type of configuration of comparable complexity is obtained by replacing the vacuum by a second material. If this is another insulating perovskite oxide, the calculation can yield information on ferroelectric-dielectric [e.g., $BaTiO_3/SrTiO_3$ (Neaton and Rabe, 2003) and $KNbO_3/KTaO_3$ (Sepliarsky *et al.*, 2001, 2002)] or ferroelectric-ferroelectric interfaces and superlattices. This configuration can also be used to study the interface between the ferroelectric and a dielectric (nonferroelectric) oxide [e.g., $BaTiO_3/BaO$ and $SrTiO_3/SrO$ (Junquera *et al.*, 2003)]. Replacement of the vacuum by a conductor simulates a film with symmetrical top and bottom electrodes, e.g., $BaTiO_3/SrRuO_3$ (Junquera and Ghosez, 2003). More complex multilayer geometries including two or more different materials as well as vacuum layers have been used to simulate ferroelectric thin-film interactions with the substrate [e.g., $PbTiO_3/SrTiO_3/PbTiO_3$/vacuum (Johnston and Rabe, 2005)], and with realistic electrodes [e.g., $Pt/BaTiO_3/Pt$/vacuum (Rao *et al.*, 1997)] and $Pt/PbTiO_3/Pt$/vacuum (Sai, Kolpak, and Rappe, 2005), as well as the structure of epitaxial alkaline-earth oxide on silicon, used as a buffer layer for growth of perovskite-oxide films (McKee *et al.*, 2003).

In each class of configurations, there are corresponding quantities and properties that are generally calculated. In the single slab-vacuum configuration, for each orientation and surface termination the surface energy is obtained. While in initial studies the atomic positions were fixed according to structural information from the bulk (Cohen, 1996), in most current studies relaxations are obtained by energy minimization procedures. For the most commonly studied perovskite (001) slab, the relaxation geometry is characterized by changes in interplane spacings and rumplings quantified as shown in Fig. 22

Most studies assume bulk periodicity in the plane. For the study of surface reconstructions, it is necessary to expand the lateral unit cell, leading to a substantial additional cost in computational resources. Most attention has been focused on the paraelectric $SrTiO_3$, although recently studies have been carried out as well for $PbTiO_3$. A by-product of the total-energy calculation that is often though not universally presented is the band structure and/or density of states; the local density of states at the surface is of particular interest.

The two-component superlattice configuration can be taken to model a film on a substrate and/or with electrode layers, or to model an actual superlattice such as that obtained by molecular-beam epitaxy techniques. In these studies, the interface and coupling between the two constituents is of primary interest; combinations most considered to date are ferroelectric+paraelectric, ferroelectric+dielectric, and ferroelectric+metal, while the combination of two ferroelectrics or ferroelectric +ferromagnetic materials has been less intensively investigated. The main questions of interest are the struc-

tural rearrangements at the interface and the change in the structure, polarization, and related properties of individual layers relative to the bulk resulting from the interaction with the other constituents. Analysis of the trends with varying thickness(es) of the ferroelectric film and, in the superlattice, other constituents is particularly useful. The electronic structure of these systems can be most readily characterized by the band offset between the two materials, which should also control the charge transfer across the interface, formation of a dipole layer, and the potential difference between the two constituents. In the case of a metal, this will determine the type of contact. The existence of interface states is also very relevant to the physical behavior of the system.

At a considerable increase in computational expense but also in realism, a system with three or more components can be studied; e.g., the combination of a substrate, a film, and vacuum. The main questions of interest in the few such studies to date are the analysis of the ferroelectric instability in the film, and the film-induced changes in the substrate layers closest to the interface. As in two-component heterostructures, the partial density of states and the layer-average electrostatic potential are also useful in extracting the electronic behavior of the system.

In all of these studies, one of the main questions is that of the structure and polarization of the ferroelectric layer compared to that of the bulk. Certainly, the change of environment (electrical and mechanical boundary conditions) and the finite dimensions (film thickness, particle size) are expected to strongly affect the structure and perhaps to eliminate the ferroelectric instability entirely. Relevant quantities to examine include the relative stability of lower- and higher-symmetry phases, spatial variation in polarization, changes in the average polarization magnitude and direction, and the depth and shape of the ferroelectric double-well potential. These changes can also be expected to lead to changes in the dielectric and piezoelectric response of thin films and superlattices, which can be studied theoretically and compared with experiments. The implications of the various first-principles studies included in this review will be described below.

3. Studies of individual one-component systems

In this section, we describe a representative sampling of first-principles studies and their results. Most of the literature has concentrated on $BaTiO_3$, providing a useful comparative test of various first-principles implementations, as well as a benchmark for evaluation and analysis of results on other systems. We first consider the calculations for single slabs of pure material that focus on the properties of surfaces: surface relaxation, surface reconstructions, and surface states. Depending on the structural constraints, these calculations are relevant to the surface of a semi-infinite bulk either for a freestanding thin film or for a thin film epitaxially constrained by a substrate. This will be followed by discussions of studies of systems with two or more material components.

a. $BaTiO_3$

For $BaTiO_3$, full first-principles results have been reported primarily for the (001) orientation, with a few results for the (110) and (111) orientations. In the slab-vacuum configuration, systems up to ten atomic layers have been considered. The unpolarized slab is compared with slabs with nonzero polarization, in the plane and/or along the normal. After reviewing the results on structures, we shall describe the results of extension to larger-scale systems through the use of interatomic potentials. The discussion of $BaTiO_3$ will be concluded by a description of the first-principles results for surface electronic structure.

First-principles FLAPW calculations for the $BaTiO_3$ (001) and (111) slabs were first presented in 1995 (Cohen, 1996), and later extended using the LAPW+LO method (Cohen, 1997). The supercells contained six and seven atomic layers, corresponding to asymmetric termination and two symmetric terminations (BaO and TiO_2), and an equal vacuum thickness. The central mirror-plane symmetry $z \rightarrow -z$ symmetry is broken for the asymmetric termination even in the absence of ferroelectric distortion. The primitive cell lattice constant was fixed at the experimental cubic value 4.01 Å. Total energies of several selected paraelectric and ferroelectric structures were computed and compared: the ideal paraelectric slab and ferroelectric slabs with displacements along $\hat{z}$ corresponding to the experimental tetragonal structure. For the asymmetrically terminated slab, both the ferroelectric structure with polarization towards the BaO surface (+) and the other towards the TiO_2 surface (−) were considered. The surface layers were relaxed for the ideal and (+) ferroelectric asymmetrically terminated slabs and the ferroelectric BaO-BaO slab. It was found that the depolarization field of the ferroelectric slabs strongly destabilizes the ferroelectric state, as expected, even taking into account the energy lowering due to the surface relaxation. In all slabs considered, this consists of an inward-pointing dipole arising from the relative motion of surface cations and oxygen atoms. The average surface energy of the ideal BaO and TiO_2 surfaces is $0.0574\ \mathrm{eV/Å^2} = 0.923$ eV per surface unit cell.

Padilla and Vanderbilt (1997) reported ultrasoft pseudopotential calculations with fully relaxed atomic coordinates for symmetrically terminated (both BaO and TiO_2) seven-layer $BaTiO_3$ (001) slabs separated by two lattice constants of vacuum. The in-plane lattice constant was set equal to the theoretical equilibrium lattice constant a computed for the bulk tetragonal phase ($a = 3.94$ Å). The average surface energy of the ideal BaO and TiO_2 surfaces is 1.358 eV per surface unit cell; at least part of the difference relative by Cohen (1996) could be due to the different lattice constant. Relaxations were reported for unpolarized slabs and for polarized slabs with polarization along (100) (in the plane of the slab). Deviations from the bulk structure were confined to the first few atomic layers. The surface layer relaxes substantially inwards, and rumples such that the

cation (Ba or Ti) moves inward relative to the oxygen atoms, as in Fig. 22. While the relaxation energy was found to be much greater than the ferroelectric double-well depth, the in-plane component of the unit-cell dipole moment was relatively insensitive to the surface relaxation, with a modest enhancement at the TiO_2-terminated surface and a small reduction at the BaO-terminated surface. The relative stability of BaO and TiO_2 terminations was compared and both found to be stable depending on whether the growth was under Ba-rich or Ti-rich conditions.

This investigation was extended by Meyer and Vanderbilt (2001) to seven-layer and nine-layer polarized slabs with polarization along the normal. The problem of the artificial vacuum field in this periodically repeated slab calculation was addressed by the techniques of introducing an external dipole layer in the vacuum region of the supercell described in Sec. IV.B.1. This technique can also be used to generate an applied field that partially or fully compensates the depolarization field for $BaTiO_3$ slabs. As a function of applied field, the change in structure can be understood as arising from oppositely directed electrostatic forces on the positively charged cations and negatively charged anions, leading to corresponding changes in the rumplings of the atomic layers and field-induced increases of the layer dipoles. Analysis of the internal electric field as a function of the applied field allows determination of whether the slab is paraelectric or ferroelectric. The BaO-terminated slab is clearly ferroelectric, with vanishing internal electric field at an external field of 0.05 a.u. and a polarization of 22.9 $\mu C\,cm^{-2}$, comparable to the bulk spontaneous polarization. The ferroelectric instability is suppressed in the TiO_2-terminated slab, which appears to be marginally paraelectric.

The Hartree-Fock method was used by Cora and Catlow (1999) and by Fu *et al.* (1999). Cora and Catlow (1999) performed a detailed analysis of the bonding using tight-binding parametrization. For the 7-layer BaO-terminated slab, the reported displacement of selected Ti and O atoms is in good agreement with the results of Padilla and Vanderbilt (1997), and these calculations were extended to slabs of up to 15 layers. Fu *et al.* (1999) performed Hartree-Fock calculations for slabs of two to eight atomic layers, with symmetric and asymmetric terminations. Using a localized basis set, they were able to perform calculations for isolated slabs as well as periodically repeated slabs. Calculations of the macroscopically averaged planar charge density, surface energy, and surface dynamical charges were reported as a function of thickness and termination for a cubic lattice constant of 4.006 Å. The relative atomic positions were fixed to their bulk tetragonal structure values (note that this polarized structure in both isolated and periodic boundary conditions has a very high electrostatic energy and is not the ground-state structure). This would significantly affect the comparison of the computed surface properties with experiment. In particular, it is presumably responsible for the high value of the average surface energy reported (1.69 eV per surface unit cell). However, a useful comparison between isolated and periodic slabs is possible. It was found that the surface charge and surface dipoles of isolated slabs converge rapidly as a function of slab thickness and can be used, combined with a value of ϵ_∞ taken from the bulk, to extract a spontaneous polarization of 0.245 C/m^2 (corrected to zero field using the electronic dielectric constant $\epsilon_\infty=2.76$), compared with 0.240 C/m^2 from a Berry-phase calculation. This is only slightly less than the bulk value of 0.263 C/m^2 taken from experiment. The average surface energy for the two terminations of symmetrically terminated slabs is 0.85 eV per surface unit cell. Surface longitudinal dynamical charges differ considerably from bulk values, satisfying a sum rule that the dynamical charges at the surface planes add up to half of the corresponding bulk value (Ruini *et al.*, 1998). Convergence of all quantities with slab and vacuum thickness of periodically repeated slabs was found, in comparision, to be slow, with significant corrections due to the fictitious field in the vacuum (for polarized slabs) and the interaction between slab images.

The isolated slab was also the subject of a FLAPW study (Krcmar and Fu, 2003). The symmetric TiO_2-TiO_2 (nine-layer) and asymmetric TiO_2-BaO (ten-layer) slabs were considered in a paraelectric structure with a fixed to 4.00 Å and a polar tetragonal structure with a and c equal to 4.00 and 4.04 Å, respectively. For the cubic TiO_2-terminated slab, displacements in units of c for the surface Ti, surface O, subsurface Ba, and subsurface O are −0.021, +0.007, +0.022, and −0.009 c, to be compared with the results (Padilla and Vanderbilt, 1997; −0.0389,−0.0163,+0.0131,−0.0062) for a periodically repeated seven-layer slab with lattice constant 3.94 Å. The tetragonal phase was relaxed to a convergence criterion of 0.06 eV/Å on the atomic forces; the rumplings of the layers follow overall the same pattern as that reported by Meyer and Vanderbilt (2001), with an inward-pointing surface dipole arising from surface relaxation, though the reduction of the rumpling in the interior is not as pronounced as for the zero-applied field case by Meyer and Vanderbilt. The energy difference between the paraelectric and ferroelectric slabs was not reported.

With interatomic potentials, it is possible to study additional aspects of surface behavior in $BaTiO_3$ thin films and nanocrystals. The most important feature of interatomic studies of thin films relative to full first-principles calculations is the relative ease of extending the supercell in the lateral direction, allowing the formation of 180° domains and molecular dynamics studies of finite-temperature effects. Tinte and Stachiotti (2001) studied a 15-layer TiO_2-terminated slab periodically repeated with a vacuum region of 20 Å using interatomic potentials that had previously been benchmarked against first-principles surface relaxations and energies (Tinte and Stachiotti, 2000). The unconstrained (stress-free) slab is found to undergo a series of phase transitions with decreasing temperature, from a paraelectric phase to ferroelectric phases, first with polarization in the plane along (100), and then along (110). Enhancement of the surface

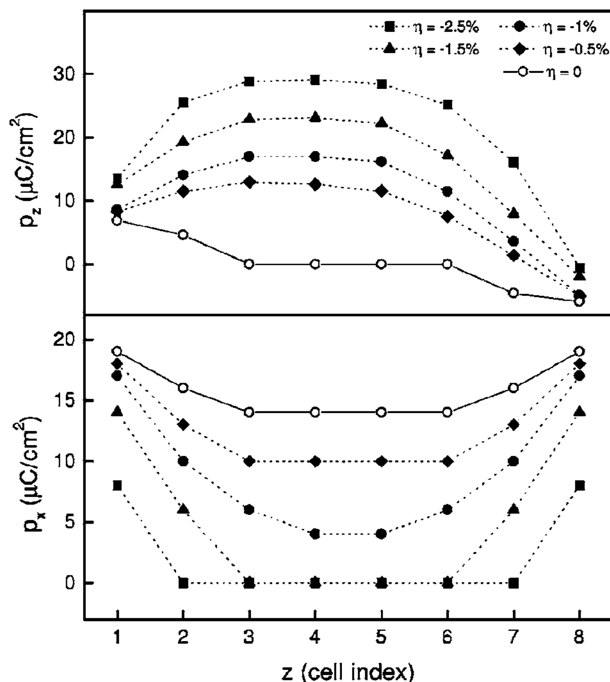

FIG. 23. Cell-by-cell out-of-plane (top panel) and in-plane (bottom panel) polarization profiles of a randomly chosen chain perpendicular to the slab surface for different misfit strains η at $T=0$ K. In the in-plane polarization profiles $p_y = p_x$. From Tinte and Stachiotti, 2001.

polarization at low temperatures appears to be linked to the existence of an intermediate temperature regime of surface ferroelectricity. For slabs with a strongly compressive epitaxial strain constraint ($\eta=-2.5\%$), there is a transition to a ferroelectric state with 180° domains and polarization along the surface normal. At the surface, the polarization has a nonzero x component and a reduced z component, giving a rotation at the surface layer. The width of the stripe domains cannot be determined, as it is limited by the lateral supercell size at least up to 10×10. Reducing the compression to $\eta=-1.0\%$ also gives a 180° domain structure in the z component of the polarization, combined with a nonzero component along [110] in the interior of the film as well as the surface, as can be seen from Fig. 23.

The thickness dependence of the transition temperature to this ferroelectric domain phase was studied at $\eta=-1.5\%$, with T_c decreasing from the 15-layer film to the 13-layer and lowest T_c 11-layer film. At and above a critical thickness of 3.6 nm, stress-free films exhibit the same ferroelectric-domain ground-state structure.

Heifets and co-workers (Heifets, Kotonin, and Maier, 2000; Heifets *et al.*, 2001a) studied BTO (001) and (110) surfaces of an isolated slab using the shell model of Heifets, Kotonin, and Maier. Between 1 and 16 atomic planes were relaxed in the electrostatic potential of a rigid slab of 20 atomic planes whose atoms were fixed in their perfect (presumably cubic) lattice sites. The relaxed structures of the two (001) terminations are in good agreement with other calculations, except for the sign of the surface dipole in the relaxation of the BaO-terminated surface, which is found to be positive (though small). The (110) surfaces are found to have much higher surface energy, except for the relaxed "asymmetric O-terminated" surface where every second-surface O atom is removed and the others occupy the same sites as in the bulk structure. In this structure, displacements of cations parallel to the surface are found to lower substantially the surface energy. A similar study of the $KNbO_3$ (110) surface (Heifets, Kotonin, and Jacobs 2000), which is the surface of most experimental interest for this 1+/5+ perovskite, showed strong relaxations extending deep below the surface, consistent with suggestions that this surface has a complicated chemistry.

Next, we consider results on the electronic structure of $BaTiO_3$ films, particularly the surface states. In the FLAPW study of Cohen, the band gap of the ideal slab is found to be reduced from the bulk. A primarily O p-occupied surface state on the TiO_2 surface was identified at M (Cohen, 1996), with a primarily Ti d surface state near the bottom of the conduction band. Analysis of the ferroelectric BaO-terminated slab showed that the macroscopic field resulted in a small charge transfer to the subsurface Ti d states from the O p and Ba p states at the other surface, making the surfaces metallic. Further study of this effect by Krcmar and Fu (2003) showed that for the symmetric TiO_2 nine-layer slab the ferroelectric distortion similarly shifts the top surface Ti states and bottom surface O state toward the bulk midgap, as in Fig. 24, resulting in a small charge transfer and a metallic character for the surfaces.

b. $PbTiO_3$

In contrast to the numerous papers on calculations on the surfaces of $BaTiO_3$, there are relatively few for the related material $PbTiO_3$. Regarding surface relaxations and energies, it was found by Meyer and Vanderbilt (2001) that the two compounds are quite similar. In perpendicularly polarized films, it seems that both terminations give ferroelectric films if the depolarization field is compensated, consistent with the stronger ferroelectric instability of $PbTiO_3$ and the microscopic model analysis of Ghosez and Rabe (2000), the latter not including the effects of surface relaxation. Because of the larger spontaneous polarization of $PbTiO_3$, it is not possible to compensate fully the depolarization field using the dipole-layer technique.

There are important differences between A-site Ba and Pb, which are evident even for the bulk. While the polarization in $BaTiO_3$ is dominated by the Ti displacements, Pb off-centering contributes substantially to the spontaneous polarization of $PbTiO_3$; this can be linked to the much richer chemistry of Pb oxides compared to alkaline-earth oxides. One downside is that it is more challenging to construct accurate interatomic potentials for perovskites with Pb than with alkaline-earth A-site cations (Sepliarsky *et al.*, 2004). In the surface, the characteristic behavior of Pb leads to an antiferrodistortive surface reconstruction of the (001) PbO-terminated sur-

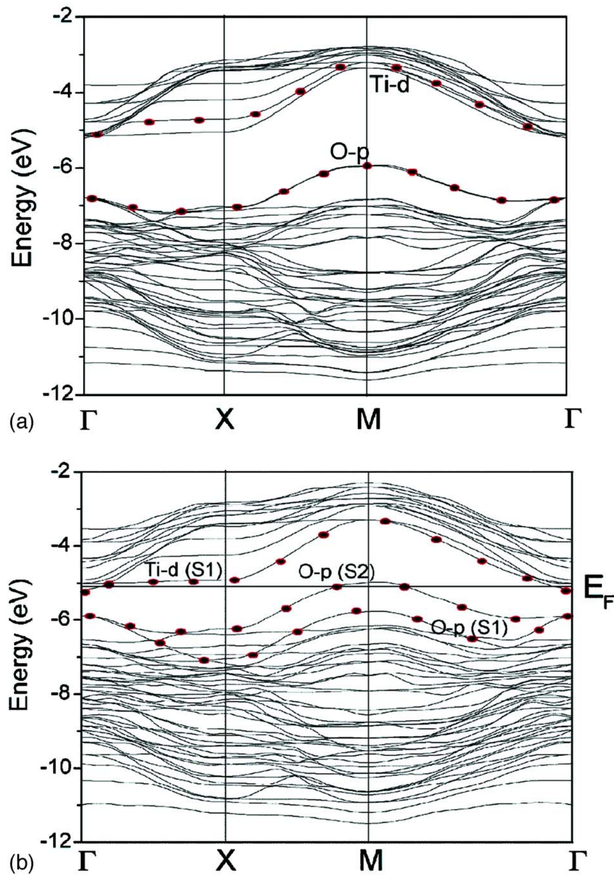

FIG. 24. (Color online) (a) Paraelectric-phase energy-band structure of a nine-layer slab of $BaTiO_3$. The surface states in (or near) the band gap are highlighted. (b) As in (a), for the ferroelectric nine-layer slab. From Krcmar and Fu, 2003.

face (Munkholm *et al.*, 2002; Bungaro and Rabe, 2005; Sepliarsky *et al.*, 2005). Specifically, first-principles calculations (Bungaro and Rabe, 2005) show that the reconstruction in the subsurface TiO_2 layer occurs only for the PbO termination and not for TiO_2 termination, and also that if the Pb in the surface layer is replaced by Ba, the reconstruction is suppressed.

c. $SrBi_2Ta_2O_9$

A first-principles study of an isolated BiO_2-terminated slab of $SrBi_2Ta_2O_9$ (SBT) one lattice constant thick (composition $SrBi_2Ta_2O_{11}$) was reported by Tsai *et al.* (2003). Spin-polarized calculations showed that such a film would be ferromagnetic as well as ferroelectric. This intriguing possibility suggests further investigation.

d. $SrTiO_3$ and $KTaO_3$

In addition to the work on true ferroelectrics, there has been interest in first-principles studies of surfaces and heterostructures of incipient ferroelectrics, mainly $SrTiO_3$ and, to a lesser extent, $KTaO_3$. As these have closely related properties that can illuminate issues in the ferroelectric perovskites, we include a description of a few representative results drawn from the very extensive literature on this subject.

Many of the studies of $BaTiO_3$ discussed above included analogous calculations for $SrTiO_3$. As already noted in the discussion of $PbTiO_3$, the (001) surface relaxations and energies of the nonpolar slab are very similar for all three materials. First-principles surface relaxation for the SrO surface is reported (in units of a =3.86 Å) for surface Sr, surface O, subsurface Ti, and subsurface O as −0.057, 0.001, 0.012, and 0.0, respectively (Padilla and Vanderbilt, 1998), to be compared with the values −0.071, 0.012, 0.016, and 0.009 (computed using a shell model with the experimental lattice constant 3.8969 Å). Similarly, first-principles surface relaxation for the TiO_2 surface is reported for surface Ti, surface O, subsurface Sr, and subsurface O as −0.034, −0.016, +0.025, and −0.005, respectively (Padilla and Vanderbilt, 1998), to be compared with the values −0.030, −0.017, +0.035, and −0.021. The average energy of the two surfaces is found to be 1.26 eV per surface unit cell. A detailed comparison of various Hartree-Fock and density-functional implementations showed generally good agreement for the surface relaxation (Heifets *et al.*, 2001b). Inward surface dipoles due to relaxation are found for both terminations, with the TiO_2 termination smaller in magnitude than $BaTiO_3$ (Heifets, Kotonin, and Maier, 2000). The possibility of an in-plane ferroelectric instability at the surface was examined and found to be quite weak (Padilla and Vanderbilt, 1998). In these studies, the antiferrodistortive instability exhibited by bulk $SrTiO_3$ at low temperatures was suppressed by the choice of a 1×1 in-plane unit cell. The surface electronic band structures show a behavior similar to that of $BaTiO_3$ described above.

For $SrTiO_3$, there is considerable evidence for a wide variety of surface reconstructions of varying stoichiometry, depending on conditions such as temperature and oxygen partial pressure as well as the relative chemical potentials of TiO_2 and SrO. Candidate structures can be obtained by creating vacancies on the surface (for example, missing rows of oxygen) and adding adatoms (Kubo and Nozoye, 2003). More drastic rearrangements of the surface atoms have also been proposed, for example, a (2×1) Ti_2O_3 reconstruction (Castell, 2002) and a (2×1) double-layer TiO_2 reconstruction with edge-sharing TiO_6 octahedra (Erdman *et al.*, 2002). As in the case of semiconductor surface reconstructions, first-principles calculations of total energies are an essential complement to experimental structural determination and can also be used to predict scanning tunneling microscope images for comparison with experiment (Johnston *et al.*, 2004). Even so, there are still many open questions about the atomic and electronic structure of $SrTiO_3$ surfaces under various conditions. The same applies to $KTaO_3$; the structures and lattice dynamics of a variety of (1×1) and (2×1) surface structures were studied by Li, Akhadov, *et al.* (2003).

As previously mentioned, the theoretical and experimental literature on $SrTiO_3$ is so extensive that it would

require a review paper in its own right to cover it fully. Since we expect the ferroelectric instability in related systems such as $BaTiO_3$ and $PbTiO_3$ to make the physics more, not less, complicated, this suggests that we have only scratched the surface in developing a complete understanding of the surfaces of perovskite ferroelectrics and the resulting effects on thin-film properties.

4. Studies of individual heterostructures

Now we turn to the description of studies of systems with two or more material components. The main structural issues are the rearrangements at the interface, the change in electrical and mechanical boundary conditions felt by each constituent layer, and how these changes modify the ferroelectric instability exhibited by the system as a whole. This geometry also allows the calculation of band offsets and/or Schottky barriers, crucial in principle to understanding the electronic behavior (though with the caveat that the measured Schottky barrier in real systems is influenced by effects such as oxidation of the electrodes that are not included in the highly idealized geometries studied theoretically). The current state of knowledge, derived from experimental measurements, is described in Sec. III.B.3.

The first combination we discuss is that of a ferroelectric thin film with metallic electrodes. Transition-metal interfaces with nonpolar BaO-terminated layers of $BaTiO_3$ were studied by Rao *et al.* (1997), specifically systems of three and seven atomic layers of $BaTiO_3$, with the lattice constant set to the bulk value of 4.00Å, combined with top and bottom monolayers of Ta, W, Ir, and Pt representing the electrodes. The preferred absorption site for the metal atoms was found to be above the O site, with calculated metal-oxygen distances ranging from 2.05 Å for Ta to 2.11 Å for Pt. The $BaTiO_3$ slabs were assumed to retain their ideal cubic structure. Analysis of the partial density of states of the heterostructure shows that the Pt and Ir Fermi energies lie in the gap of the $BaTiO_3$ layer at 0.94 and 0.64 eV, respectively, above the top of the valence band (this is, fortunately, smaller than the underestimated computed gap of 1.22 eV for the $BaTiO_3$ slab). Using the experimental gap of 3.13 eV, a Schottky barrier height of 2.19 eV for Pt and 2.49 eV for Ir is thus obtained. Experimentally, however, the Schottky barrier is known to be substantially *lower* for Ir than for Pt, illustrating the limitations mentioned in the previous paragraph.

Robertson and Chen (1999) combined first-principles calculations of the charge neutrality levels with experimental values of the band gap, electronic dielectric constant ϵ_∞, the electron affinity, and the empirical parameter S, described in Sec. III.B.3. Values for $SrTiO_3$ and PZT were reported for Pt, Au, Ti, Al, and the conduction and valence bands of Si.

To explore how the electrodes affect the ferroelectric instability of the film, Junquera and Ghosez (2003) considered a supercell of five unit cells of metallic $SrRuO_3$ and 2–10 unit cells of $BaTiO_3$, with a SrO/TiO_2 interface between $SrRuO_3$ and $BaTiO_3$. A $SrTiO_3$ substrate was treated implicitly by constraining the in-plane lattice constant of the supercell to that of bulk $SrTiO_3$. For each $BaTiO_3$ thickness, the system was relaxed assuming a nonpolar state for $BaTiO_3$, and the energy of the bulk-like tetragonal distortion was computed as a function of overall amplitude of the distortion. Above a critical thickness of six unit cells, this distortion lowered the energy, demonstrating the development of a ferroelectric instability. As discussed in Sec. IV.B.5, this finite-size effect can be largely understood by considering the imperfect screening in the metal layers.

Considerable first-principles effort has been devoted to investigating various aspects of epitaxial ferroelectric thin films on Si. As perovskite oxides cannot be grown directly on Si, an approach developed by McKee and Walker (McKee *et al.*, 1998, 2001) is to include an AO buffer layer, which apparently also results in the formation of a silicide interface phase. The constituent layers of this heterostructure should thus be considered to be $Si/ASi_2/AO/ABO_3$. The full system has not been simulated directly, but first-principles approaches have been used to investigate individual interfaces. The importance of relaxations, the additional role of the buffer layer in changing the band offset, and the analysis of electronic structure within the local-density approximation are illustrated by the following.

McKee *et al.* (2003) presented first-principles results for the atomic arrangements and electronic structure in the $Si/ASi_2/AO$ system, in conjunction with an experimental study. A strong correlation is found between the valence-band offset and the dipole associated with the A-O bond linking the A atom in the silicide to the O atom in the oxide, shown in Fig. 25. It is thus seen that the structural rearrangements in the interface are a key determining factor in the band offset.

A detailed examination of the interface between the perovskite oxide and the alkaline-oxide buffer layer, specifically $BaO/BaTiO_3$ and $SrO/SrTiO_3$, was carried out by Junquera *et al.* (2003). A periodic $1\times1\times16$ supercell was chosen with stacking of (001) atomic layers: $(AO)_n-(AO-TiO_2)_m$, with $n=6$ and $m=5$. Two mirror-symmetry planes were fixed on the central AO and BO_2 layers, and the in-plane lattice constant chosen for perfect matching to the computed local-density approximation lattice constant of Si (this epitaxial strain constraint is the only effect of the Si substrate included in the calculation). Relaxations within the highest-symmetry tetragonal space group consistent with this supercell were performed. Analysis of the partial density of states showed no interface-induced gap states. The main effect observed for relaxations was to control the size of the interface dipole, which in turn was found to control the band offsets, shown here in Fig. 26.

As in the studies described above, the conduction-band offset is obtained from the computed valence-band offset using the bulk experimental band gap. These results were combined with offsets reported for other relevant interfaces to estimate band alignments for $Si/SrO/SrTiO_3/Pt$ and $Si/BaO/BaTiO_3/SrRuO_3$ heterostructures, confirming that the AO layer introduces

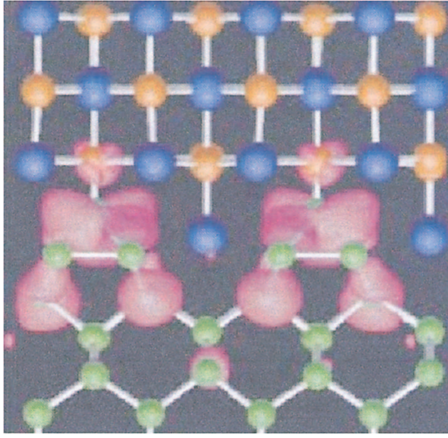

FIG. 25. (Color) Illustration of three layers of the alkaline-earth oxide on the (001) face of silicon observed in a cross section at the [110] zone axis (blue, alkaline-earth metal; yellow, oxygen; and green, silicon). A distinct interface phase can be identified as a monolayer structure between the oxide and the silicon in which the charge density in interface states is strongly localized around the silicon atoms in the interface phase. The dipole in the ionic A-O bond between the alkaline-earth metal in the silicide and the oxygen in the oxide buffers the junction against the electrostatic polarization of the interface states localized on silicon. The electron density of this valence surface state at the center of the Brillouin zone is shown with the purple isosurface ($0.3\times10^{-3}\ e$). Reprinted with permission from McKee *et al.*, 2003. © 2003, AAAS.

an electrostatic barrier of height greater than 1 eV. This is sufficient to eliminate the carrier injection from the Si into the conduction-band states of the perovskite that would occur if the two were in direct contact (Robertson and Chen, 1999).

5. First-principles modeling: methods and lessons

As discussed above, the analysis and prediction of the behavior of ferroelectric thin films and heterostructures can be carried out with direct first-principles simulations only for highly idealized configurations. However, it is possible to consider more complex and realistic situations by constructing models that incorporate certain physical ideas about the nature of these systems, with material-specific parameters determined by fitting results of first-principles calculations carefully selected for a combination of informativeness and tractability. This modeling approach also has the advantage of providing a conceptual framework for organizing the vast amount of microscopic information in large-scale first-principles calculations, and communicating those results, particularly to experimentalists. This will not diminish in importance even as such calculations become easier with continuing progress in algorithms and computer hardware.

For successful modeling of measurable physical properties, the film must be considered as part of a system (substrate+film+electrode) as all components of the system and their interaction contribute to determine properties such as the switchable polarization and the dielectric and piezoelectric responses. We start by considering the class of first-principles models in which the constituent layers (film, superlattice layers, electrodes, and substrate) are assumed to be subject to macroscopic electric fields and stresses resulting from the combination of applied fields and stresses and the effects of the other constituents, with the responses of the layers being given to lowest order by the bulk responses. For systems with constituent layer thicknesses as low as one bulk lattice constant, it seems at first unlikely that such an

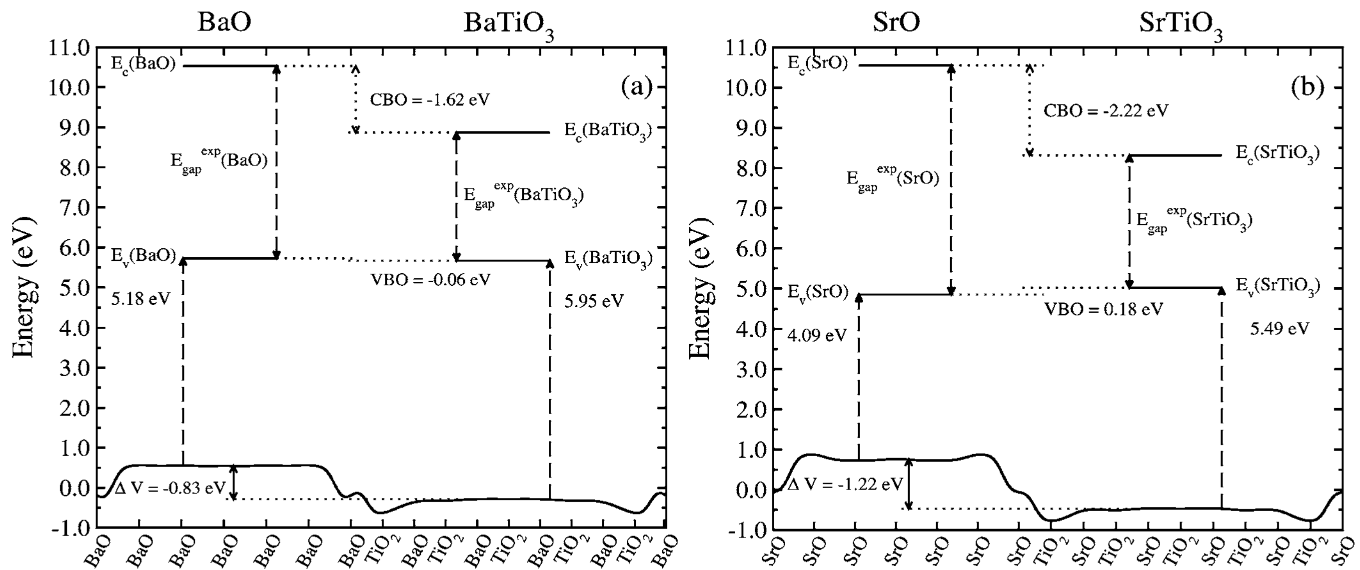

FIG. 26. Schematic representation of the valence-band offset (VBO) and the conduction-band offset (CBO) for (a) $BaO/BaTiO_3$ and (b) $SrO/SrTiO_3$ interfaces. E_v, E_c, and E_{gap}^{expt} stand for the top of the valence band, the bottom of the conduction band, and the experimental band gap, respectively. Values for E_v, measured with respect to the average of the electrostatic potential in each material, are indicated. The solid curve represents the profile of the macroscopic average of the total electrostatic potential across the interface. ΔV stands for the resulting lineup. The in-plane lattice constant was set equal to the theoretical value of Si (5.389). The size of the supercell corresponds to $n=6$ and $m=5$. From Junquera *et al.*, 2003.

approach could be useful, but in practice it has been found to be surprisingly successful.

One simple application of this approach has been used to predict and analyze the strain in nonpolar thin films and multilayers. In the construction of the reference structure for the AO/ABO_3 interfaces by Junquera *et al.* (2003), macroscopic modeling of the structure with bulk elastic constants for the constituent layers yielded accurate estimates for the lattice constants along the normal direction. In cases of large lattice mismatch, very high strains can be obtained in very thin films and nonlinear contributions to the elastic energy can become important. These can be computed with a slightly more sophisticated though still very easy-to-implement method that has been developed to study the effects of epitaixial strain more generally on the structure and properties of a particular material, described next.

As is discussed in Sec. V, the effects of epitaxial strain in ultrathin films and heterostructures have been identified as a major factor in determining polarization-related properties, and have been the subject of intense interest in both phenomenological and first-principles modeling. In particular, for ferroelectric perovskite oxides it has long been known that there is a strong coupling between strain (e.g., pressure-induced) and the ferroelectric instability, as reflected by the frequency of the soft mode and the transition temperature. In both phenomenological and first-principles studies, it has become common to study the effects of epitaxial strain induced by the substrate by studying the structural energetics of the strained bulk. Specifically, two of the lattice vectors of a bulk crystal are constrained to match the substrate and other structural degrees of freedom are allowed to relax, as described in the previous paragraph. In most cases, these calculations are performed for zero macroscopic electric field, as would be the case for a film with perfect short-circuited electrodes. Indeed, it is often the case (Pertsev *et al.*, 1998; Junquera *et al.*, 2003; Neaton and Rabe, 2003) that the strain effect is considered to be the dominant effect of the substrate, which is otherwise not included (thus greatly simplifying the calculation). At zero temperature, the sequence of phases and phase boundaries can be readily identified as a function of in-plane strain directly through total-energy calculations of the relaxed structure subject to the appropriate constraints. Atomic-scale information can be obtained for the precise atomic positions, band structure, phonon frequencies, and eigenvectors. The temperature axis in the phase diagram can be included by using effective Hamiltonian (or interatomic potential) simulations. Results for selected perovskite oxides are discussed in Sec. V; a similar analysis was reported for TiO_2 or by Montanari and Harrison (2004).

This modeling is based on the assumption that the layer stays in a single-domain state. As discussed in Sec. V, the possibility of strain relaxation through formation of multidomain structures must be allowed for. While this cannot be readily done directly in first-principles calculations, first-principles data on structural energetics for large misfit strains could be used to refine Landau parameters for use in calculations such as those by Speck and Pompe (1994), Alpay and Roytburd (1998), Bratkovsky and Levanyk (2001), and Li, Akhadov, *et al.* (2003). The effects of inhomogeneous strain due to misfit dislocations that provide elastic relaxation in thicker films have also been argued to be significant.

Next we consider the application of these "continuum" models to analyzing structures in which the macroscopic field is allowed to be nonzero. Macroscopic electrostatics is applied to the systems of interest by a coarse graining over a lattice-constant-scale window to yield a value for the local macroscopic electric potential. Despite the fact that this is not strictly within the regime of validity of the classical theory of macroscopic electrostatics, which requires slow variation over many lattice constants, this analysis turns out to be remarkably useful for first-principles results. In the simplest example, the polarization of a polar $BaTiO_3$ slab (periodically repeated in a supercell with vacuum) is accurately reproduced using bulk values for the bulk spontaneous polarization and electronic dielectric constant even for slabs as thin as two lattice constants (Junquera and Rabe, 2005).

We have already mentioned in the previous section that perpendicular (to the surface) polarization can lead to a nonzero macroscopic field that opposes the polarization (the depolarizing field). Unless compensated by fields from electrodes or applied fields, this strongly destabilizes the polarized state. In systems with two or more distinct constituent layers, this condition in the absence of free charge favors states with $\nabla \cdot \vec{P}=0$. For example, in the first-principles calculations of short-period $BaTiO_3/SrTiO_3$ superlattices, the local polarization along [001] is found to be quite uniform in the two layers (Neaton and Rabe, 2003; Johnston, Huang, *et al.*, 2005), though the in-plane component can be very different (Johnston, Huang, *et al.*, 2005). To the extent that layered ferroelectrics such as SBT can be treated in this macroscopic framework, one similarly expects that polarization along c will not tend to be energetically favored since the layers separating the polarized perovskitelike layers typically have low polarizability (Fennie and Rabe, 2005). This observation provides a theoretical framework for evaluating claims of large ferroelectric polarization along c in layered compounds (Chon *et al.*, 2002); unless there is an unusually high polarizability for the nonperovskite layers, or a strong competing contribution to the energy due, for example, to the interfaces to help stabilize a high c polarization, other reasons for the observations need to be considered (Garg *et al.*, 2003).

These considerations become particularly important for ultrathin films with metal electrodes. The limiting case of complete screening of the depolarizing field by perfect electrodes is never realized in real thin-film systems. The screening charge in real metal electrodes is spread over a characteristic screening length and is associated with a voltage drop in the electrode. For thick films, this can be neglected, but the relative size of the

voltage drop increases as the film thickness decreases. This has been identified as a dominant contribution to the relation between the applied field and the true field in the film for the thinnest films (Dawber, Chandra, *et al.*, 2003). One way this shows up is in the thickness dependence of the apparent coercive field; it is found that the true coercive field scales uniformly down to the thinnest films. Effects are also expected on the structure and polarization. While films with partial compensation of the depolarization field may still exhibit a ferroelectric instability, the polarization and the energy gain relative to the nonpolar state are expected to decrease. This simple model was developed and successfully used by Junquera and Ghosez (2003) to describe the thickness dependence of the ferroelectric instability in a $BaTiO_3$ film between $SrRuO_3$ electrodes. This analysis identified the thickness dependence of the residual depolarization field as the principal source of thickness dependence in this case. Lichtensteiger *et al.* (2005) suggest that the reduction of the uniform polarization by the residual field and its coupling to tetragonal strain is the cause of the decrease in tetragonality with decreasing thickness of $PbTiO_3$ ultrathin films.

It is well known that 180° domain formation provides an effective mechanism for compensating the depolarization field, and is expected to be favored when the screening available from electrodes is poor or nonexistent [for example, on an insulating substrate (Streiffer *et al.*, 2002)]. Instability to domain formation is discussed by Bratkovsky and Levanyuk (2000) as the result of a nonzero residual depolarization field due to the presence of a passive layer. Similarly, a phase transition from a uniform polarized state to a 180° domain state with zero net polarization is expected to occur with decreasing thickness (Junquera *et al.*, 2003).

Despite the usefulness of macroscopic models, it should not be forgotten that they are being applied far outside the regime of their formal validity (i.e., length scales of many lattice constants) and that atomistic effects can be expected to play an important role, especially at the surfaces and interfaces. The structural energetics could be substantially altered by relaxations and reconstructions (atomic rearrangements) at the surfaces and interfaces. These relaxations and reconstructions are also expected to couple to the polarization (Meyer and Vanderbilt, 2001; Bungaro and Rabe, 2005) with the possibility of either enhancing or suppressing the switchable polarization. The surfaces and the interfaces will also be primarily responsible for the asymmetry in energy between up and down directions for the polarization. For ultrathin films, the surface and interface energy can be important enough to dominate over elastic energy, leading to a possible tradeoff between lattice matching and atomic-scale matching for favorable bonding at the interface. These surface and interface energies could even be large enough to stabilize nonbulk phases with potentially improved properties. This should be especially significant for interfaces between unlike materials.

Electronic states associated with surfaces and interfaces will also contribute to determining the equilibrium configuration of electric fields and polarizations. In the simple example of periodically repeated slabs separated by vacuum, as the slab gets thicker, a breakdown is expected where the conduction-band minimum on one surface of the slab falls below the valence-band maximum on the other. In this case, charge will be transferred across the slab with the equilibrium charge (for fixed atomic positions) being determined by a combination of the macroscopic electrostatic energy and the single-particle density of states. This tends partially to screen the depolarization field. The role of interface states in screening the depolarization field in the film has been discussed in a model for $BaTiO_3$ on Ge (Reiner *et al.*, 2004). The presence of surface and interface states can be established by examination of the band structure and partial density of states, as discussed in the previous section.

Finally, we turn our attention to an analysis of what the discussion above tells us about finite-size effects in ferroelectric thin films. We have seen that many factors contribute to the thickness dependence of the ferroelectric instability: the thickness dependence of the depolarization field, the gradual relaxation of the in-plane lattice constant from full coherence with the substrate to its bulk value, and the changing weight of the influence of surfaces and interfaces. The "true" finite-size effect, i.e., the modification of the collective ferroelectric instability due to the removal of material in the film relative to the infinite bulk, could possibly be disentangled from the other factors by a carefully designed first-principles calculation, but this has not yet been done. We speculate that this effect does not universally act to suppress ferroelectricity, but could, depending on the material, enhance ferroelectricity (Ghosez and Rabe, 2000).

6. Challenges for first-principles modeling

First-principles calculations have advanced tremendously in the last decade, to the point where systems of substantial chemical and structural complexity can be addressed, and a meaningful dialog opened up between experimentalists and theorists. With these successes the bar gets set ever higher, and the push is now to make the theory of ferroelectrics truly realistic. The highest long-term priorities include making finite-temperature calculations routine, proper treatment of the effects of defects and surfaces, and the description of structure and dynamics on longer length and time scales. In addition, there are specific issues that have been raised that may be addressable in the shorter term through the interaction of theory and experiment, and the rest of this section will highlight some of these.

Many applications depend on the stability of films with a uniform switchable polarization along the film normal. This stability depends critically on compensation of the depolarization field. Understanding and controlling the compensation mechanism(s) are thus the subjects of intense current research interest. There are

two main classes of mechanism: compensation by "free" charges (in electrodes/substrate or applied fields) and compensation by the formation of polarization domains. On insulating substrates, this latter alternative has been observed and characterized in ultrathin films (Streiffer *et al.*, 2002; Fong *et al.*, 2004). It has been proposed that domain formation occurs in films on conducting substrates at very low thicknesses as well as where the finite-screening length in realistic electrodes inhibits that mechanism of compensation (Junquera *et al.*, 2003). The critical thickness for this instability depends on the domain-wall energy. This is expected to be different in thin films than in bulk, one factor being that the bulk atomic plane shifts across the domain walls.

Compensation of the depolarization field by free charges appears to be the dominant mechanism in films on conducting substrates (even relatively poor conductors) with or without a top electrode. In the latter case there must be free charge on the surface; the challenge is to understand how the charge is stabilized. There are also unresolved questions about how the charge is distributed at the substrate-film interface and how this couples to local atomic rearrangements. Asymmetry of the compensation mechanism may prove to be a significant contribution to the overall up-down asymmetry in the film discussed in the previous section. A better understanding could lead to the identification of system configurations with more complete compensation and thus an enhancement of stability.

The study of the behavior of ferroelectrics in applied electric fields also promises progress in the relatively near future. Recently, with the solution of long-standing questions of principle, it has become possible to perform density-functional-theory calculations for crystalline solids in finite electric fields (Souza *et al.*, 2002). In ferroelectrics, this allows the investigation of nonlinearities in structure and polarization at fields relevant to experiments and the possibility of more accurate modeling of constituent layers of thin-film and superlattice systems subject to nonzero fields. It is also of interest to ask what the intrinsic breakdown field would be in the absence of defects, though the question is rather academic with respect to real systems.

The nonzero conductivity of real ferroelectrics becomes particularly important for thinner films, since a higher concentration of free carriers is expected to be associated with characteristic defects in the film, and also because a given concentration of free carriers will have a more significant impact as thickness decreases. Free carriers can at least partially screen macroscopic electric fields. At the macroscopic level, the concepts of band bending and space charge arising in semiconductor physics can be applied to thin-film ferroelectrics, while a correct atomic-scale treatment of these effects could be important to describing the behavior of ultrathin films.

The physics of switching presents a significant challenge, requiring description of structure and dynamics on long length and time scales. The questions of what changes, if any, occur in switching as films become thinner continue to be debated. The possibility of switching as a whole rather than via a domain-wall mechanism has been raised for ultrathin films of PVDF (Bune *et al.*, 1998), while a different interpretation has been offered by Dawber, Chandra, *et al.* (2003). Some progress has been made using interatomic potentials for idealized defect-free films, though real systems certainly are affected by defects responsible for such phenomena as imprint and fatigue. Ongoing comparison of characteristics such as coercive fields, time scales, material sensitivity, and thickness dependence of domain-wall nucleation, formation energy, and motion with experimental studies promises that at least some of these issues will soon be better understood.

To conclude this section, we emphasize that it is not very realistic to expect first-principles calculations quantitatively to predict all aspects of the behavior of chemically and structurally complex systems such as ferroelectric thin films, although successful predictions should continue to become increasingly possible and frequent. Rather, the quantitative microscopic information and the development of a useful conceptual framework contribute in a close interaction with experiment to build an understanding of known phenomena and to propel the field into exciting new directions.

V. STRAIN EFFECTS

Macroscopic strain is an important factor in determining the structure and behavior of very thin ferroelectric films. The primary origin of homogeneous film strain is lattice mismatch between the film and the substrate. In addition, defects characteristic of thin films can produce inhomogeneous strains that can affect the properties of thicker relaxed films of technological relevance. Because of the strong coupling of both homogeneous and inhomogeneous strains to polarization, these strains have a substantial impact on the structure, ferroelectric transition temperatures, and related properties such as the dielectric and piezoelectric responses, which has been the subject of extensive experimental and theoretical investigation.

The largest effects are expected in coherent epitaxial films. These films are sufficiently thin that the areal elastic energy density for straining the film to match the substrate at the interface is less than the energy cost for introducing misfit dislocations to relax the lattice parameters back towards their unconstrained equilibrium values. [We note that for ultrathin films, the relaxed inplane lattice constant will not in general be the same as the bulk lattice constant, and the former is more appropriate for computing lattice mismatch (Rabe, 2005)]. Very high homogeneous strains, of the order of 2%, are achievable. For example, barium titanate (BTO) films on strontium titanate (STO), with a bulk mismatch of 2.2%, remain coherent in equilibrium up to a critical thickness of 2–4 nm (Sun *et al.*, 2004). With low-temperature growth techniques, the formation of misfit dislocations is kinetically inhibited and coherent films can be grown to thicknesses of two to three times the critical thickness (Choi *et al.*, 2004). Even these films, however, are much

thinner than the minimum 120 nm thickness for films used in contemporary applications, and thus much of the discussion is at present primarily of fundamental rather than technological interest.

The structure of a coherent film can be a single-crystal monodomain structure, a polydomain structure, or even possibly multiphase. We discuss the simplest single-crystal monodomain case first. The phase diagram as a function of in-plane strain will in general include lower symmetry phases due to the symmetry-breaking character of the epitaxial constraint. A nomenclature for these phases of perovskites on a surface with square symmetry [e.g., a perovskite (001) surface] has been established by Pertsev *et al.* (1998). For example, a ferroelectric perovskite rhombohedral phase will be lowered to monoclinic symmetry (called the *r* phase). For highly compressive in-plane strains, coupling between strain and the polarization tends to favor the formation of a tetragonal phase with polarization along *c* (the *c* phase) for highly compressive strains. Conversely, highly tensile strains lead to an orthorhombic phase with polarization along the cube face diagonal perpendicular to the normal (the *aa* phase) or along the in-plane Cartesian direction (the *a* phase). As a result of the added constraint, it is possible in principle to stabilize perovskite-derived phases not observed in bulk, for example, the monoclinic *r* phase and the orthorhombic *aa* phase in $PbTiO_3$. This mechanism also plays a role in the more general phenomenon of epitaxial stabilization, discussed, for example, by Gorbenko *et al.* (2002).

As discussed in Sec. IV.B.5, theoretical analysis of the in-plane-strain phase diagrams has focused on isolating the effects of strain by computing bulk single-crystal monodomain phase diagrams under the epitaxial constraint and zero macroscopic electric field using phenomenological Landau theory or first-principles methods. Phenomenological analysis based on Landau-Devonshire theory for a number of perovskite oxides has been presented by Pertsev and co-workers (Pertsev *et al.*, 1998, 1999, 2000a, 2000b, 2003; Koukhar *et al.*, 2001), with temperature-strain diagrams for $BaTiO_3$, $PbTiO_3$ (see Fig. 27), $SrTiO_3$, and $Pb(Zr,Ti)O_3$ (PZT), the latter generalized to include nonzero stress.

First-principles methods have been used to construct a temperature-strain diagram for $BaTiO_3$ (Dieguez *et al.*, 2004) and a zero-temperature–strain diagram for $PbTiO_3$ and ordered PZT (Bungaro and Rabe, 2004) and $SrTiO_3$ (Antons *et al.*, 2005). These theoretical phase diagrams have some notable features. In particular, compressive in-plane strain is found to elevate the ferroelectric (*c*) -paraelectric transition temperatures in $BaTiO_3$ and $PbTiO_3$, and tensile in-plane strain elevates the ferroelectric (*aa*) -paraelectric transition temperatures. In both cases, the transition is second order, in contrast to the first-order transition in bulk. To eliminate a possible source of confusion, we comment that zero misfit strain as defined by Pertsev *et al.* (1998) is not equivalent to an unconstrained film (the low-temperature bulk phases are in general not cubic, and

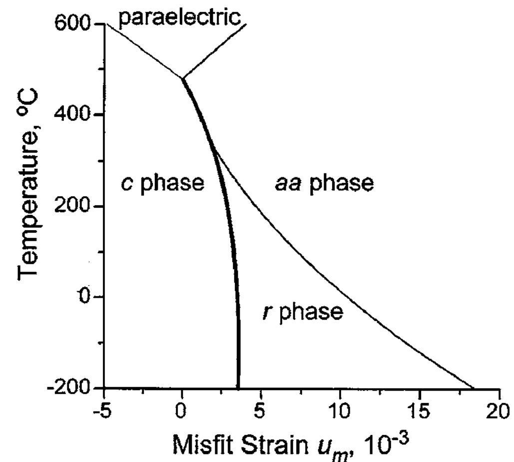

FIG. 27. Phase diagram of a (001) single-domain PbTiO3 thin film epitaxially grown on different cubic substrates providing various misfit strains in the heterostructures. The second- and first-order phase transitions are shown by thin and thick lines, respectively. From Pertsev *et al.*, 1998.

the constrained dielectric and piezoelectric responses are clamped, as will be discussed further below). The nearly vertical morphotropic phase boundary characteristic of bulk PZT is substantially modified (Li, Choudhury, *et al.*, 2003; Pertsev *et al.*, 2003). In $SrTiO_3$, ferroelectricity is found to be induced by both sufficiently compressive and tensile strains with a corresponding direction for the spontaneous polarization (*c*-type and *aa*-type) (Pertsev *et al.*, 2000a; Antons *et al.*, 2005), as shown in Fig. 28.

The enhancement of the polarization in the *c* phase by compressive in-plane strain has been noted for $BaTiO_3$ (Neaton and Rabe, 2003) and PZT (Pertsev *et al.*, 2003). For both strained $SrTiO_3$ and strained $BaTiO_3$, the ferroelectric T_c's are predicted to increase as the strain magnitudes increase (Choi *et al.*, 2004; Haeni *et al.*, 2004), as shown in Fig. 29.

The use of phenomenological bulk Landau parameters yields a very accurate description for small strains near the bulk T_c. However, different parameter sets have been shown, for example, in the case of $BaTiO_3$, to

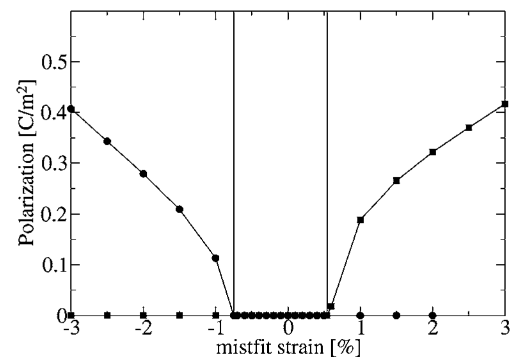

FIG. 28. Polarization of SrTiO3 as a function of in-plane strain. Solid circles and squares denote polarization along [001] and [110], respectively. From Antons *et al.*, 2005.

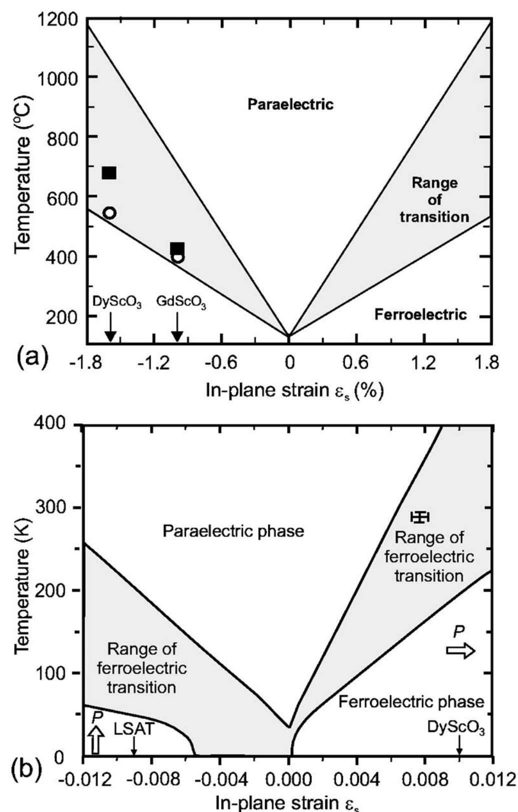

FIG. 29. Expected T_c of (a) (001) $BaTiO_3$ (reprinted with permission from Choi *et al.*, 2004; © 2004, AAAS) and (b) (001) $SrTiO_3$ (from Haeni *et al.*, 2004; © 2004, Nature Publishing Group, http: //www.nature.com) based on thermodynamic analysis. The range of transition represents the uncertainty in the predicted T_c resulting from the spread in reported property coefficients.

extrapolate to qualitatively different phase diagrams at low temperatures (Pertsev *et al.*, 1998, 1999). Quantitatively, the uncertainty in predicted phase boundaries produced by the fitting of the Landau theory parameter increases with increasing misfit strain as shown in Fig. 29 (Choi *et al.*, 2004). The Landau analysis is thus well complemented by first-principles calculations, which can provide very accurate results in the limit of zero temperature. In the case of $BaTiO_3$, the ambiguity in the low-temperature phase diagram (Pertsev *et al.*, 1998, 1999) has been resolved in this way (Dieguez *et al.*, 2004), in the case of $PbTiO_3$, the phenomenological result is confirmed (Bungaro and Rabe, 2004).

The epitaxial-strain-induced changes in structure and polarization are also expected to have a substantial effect on the dielectric and piezoelectric responses. While overall the dielectric and piezoelectric responses should be reduced by clamping to the substrate (Canedy *et al.*, 2000; Li *et al.*, 2001), these responses will tend to diverge near second-order phase boundaries (Pertsev *et al.*, 2003; Bungaro and Rabe, 2004). See Fig. 30.

Responses will also be large in phases, such as the *r* phase, in which the direction of the polarization is not fixed by symmetry, so that an applied field or stress can

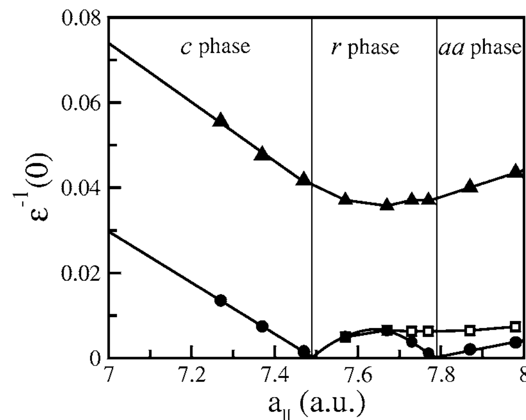

FIG. 30. Inverses of the eigenvalues of the phonon contribution to the dielectric tensor as a function of the in-plane lattice constant for the [001]-(PbTiO3)1(PbZrO3)1 superlattice. The lines are a guide to the eye. From Bungaro and Rabe, 2004.

rotate the polarization (Wu and Krakauer, 1992). This polarization rotation has been identified as a key mechanism in the colossal piezoresponse of single-crystal relaxors (Park and Shrout, 1997; Fu and Cohen, 2000). The sensitivity of the zero-field responses should also be reflected in the nonlinear response; thus the electric-field tunability of the dielectric response can be adjusted by changing the misfit strains (Chen *et al.*, 2003).

While the phase diagrams thus derived are quite rich, even the optimal single-crystal monodomain structure may be unfavorable with respect to formation of polydomain (Speck and Pompe, 1994; Bratkovsky and Levanyk, 2001; Roytburd *et al.*, 2001) or multiphase structures, which allow strain relaxation on average and reduce elastic energy. The evaluation of the energies of polydomain structures requires taking both strain and depolarization fields into account. A recent discussion of $PbTiO_3$ using a phase-field analysis (Li, Choudhury, *et al.*, 2003) suggested that including the possibility of polydomain structure formation significantly affects the phase diagram for experimentally relevant misfit strains and temperatures, as shown in Fig. 31.

For very thin films, additional effects associated with the interface between the film and substrate are also expected to contribute significantly. For example, although polydomain formation can accommodate misfit strain averaged over different variants, each domain will be mismatched to the substrate at the atomic level, with a corresponding increase in interface energy. Furthermore, the energy of a domain wall perpendicular to the substrate will be higher than the energy of the corresponding wall in the bulk due to the geometrical constraint on the allowed shifts of the atomic planes across the domain wall [as found for the bulk by Meyer and Vanderbilt (2002)] imposed by the planar interface. Different domain walls will in general be affected differently by the constraint, possibly changing the relative energy of different polydomain configurations.

With recent advances in thin-film synthesis, it is possible to grow and characterize high-quality films that are

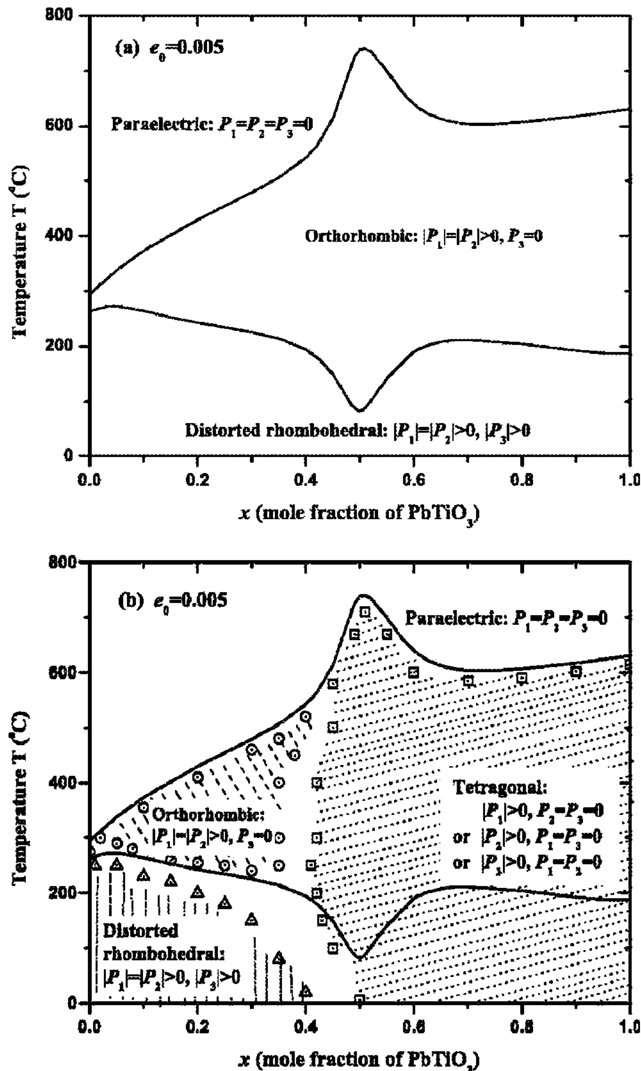

FIG. 31. (a) Phase diagram of PZT film under in-plane tensile strain of 0.005 obtained using thermodynamic calculations assuming a single-domain state. There are only two stable ferroelectric phases. The solid lines represent the boundaries separating the stability fields of the paraelectric and ferroelectric phases, or the ferroelectric-orthorhombic and distorted-rhombohedral phases. (b) Superposition of the phase diagram of a PZT film under in-plane tensile strain of 0.005 from the phase-field approach (scattered symbols) and from thermodynamic calculations assuming a single domain (solid lines). There are three stable ferroelectric phases: tetragonal, square; orthorhombic, circle; and distorted-rhombohedral, triangle according to the phase-field simulations. The scattered symbols represent the ferroelectric domain state obtained at the end of a phase-field simulation. The shaded portion surrounded by the scattered symbols label the stability regions of a single ferroelectric phase, and the nonshaded region shows a mixture of two or three ferroelectric phases. Reprinted with permission from Li, Choudhury, *et al.*, 2003. © 2003, AIP.

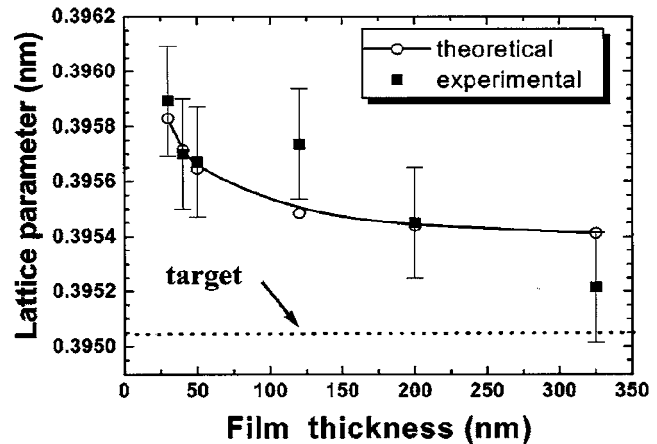

FIG. 32. Evolution of $a^{\perp}$ as a function of film thickness for $Ba_{0.6}Sr_{0.4}TiO_3$ thin films grown on $0.29(LaAlO_3):0.35(Sr_2TaAlO_6)$ substrates. Also shown is the theoretical curve, given by the open circles. The straight dashed line represents the lattice parameter of the ceramic target (a=0.395 05 nm). Reprinted with permission from Canedy *et al.*, 2000. © 2000, AIP.

sufficiently thin to be coherent or partially relaxed. Here we give a few examples of experimental observations of changes in structure and polarization in very thin films. T_c elevation in strained $PbTiO_3$ films has been reported and analyzed by Rossetti *et al.* (1991) and Streiffer *et al.* (2002). The strain-induced *r* phase has been observed in PZT films thinner than 150 nm on Ir-electroded Si wafers (Kelman *et al.*, 2002). An antiferroelectric to ferroelectric transition has been observed in thin films of $PbZrO_3$ (Ayyub *et al.*, 1998), though whether it is induced by strain or some other thin-film related effect is considered an open question. Large polarization enhancements have been observed in epitaxially strained $BaTiO_3$ films (Choi *et al.*, 2004). Most dramatically, room-temperature ferroelectricity has been achieved for $SrTiO_3$ under biaxial tensile strain induced by a $DyScO_3$ substrate (Haeni *et al.*, 2004). For thicker films, observation of polydomain structures was reported by Roytburd *et al.* (2001). It has been observed that domain formation may be suppressed by rapid cooling through the transition (Ramesh *et al.*, 1993).

For thicker films grown at high temperature, misfit dislocations will form at the growth temperature partially or completely to relax misfit strain. The degree of relaxation increases with increasing thickness, until for thick enough films the epitaxial strain is negligible. This behavior has been studied theoretically (Matthews and Blakeslee, 1974) and observed experimentally, for example, as shown in Fig. 32.

Additional strain can arise during cooling from the growth temperature if there is differential thermal expansion between the film and the substrate and the formation of misfit dislocations is kinetically inhibited. A detailed theoretical study of strain relaxation in epitaxial ferroelectric films, with discussion of the interplay of misfit dislocations, mixed domain formation, and depolarizing energy, was undertaken by Speck and Pompe (1994). It was assumed that for rapid cooling from the growth temperature the effect of misfit dislocations can be incorporated by using an effective substrate lattice parameter, while in the limit of slow cooling the system optimally accommodates misfit strain with dislocations.

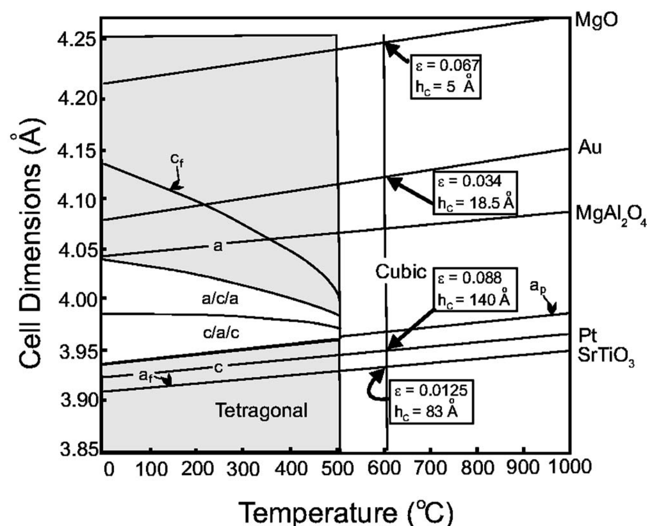

FIG. 33. Coherent temperature-dependent domain stability map for $PbTiO_3$ including the cubic lattice parameter for several common single-crystal oxide substrates. The misfit strains for epitaxial growth of $PbTiO_3$ at 600 °C are included in the insets along with the critical thickness h for misfit dislocation formation. Reprinted with permission from Speck and Pompe, 1994. © 1994, AIP.

(This assumption is valid for films with thickness of order 1 μm, while the treatment needs to be slightly modified for intermediate thicknesses where the equilibrium concentration of misfit dislocations leads to only partial strain relaxation.) Elastic domains form to relax any residual strain. Below T_c, depolarizing energy can change the relative energetics of different arrangements of polarized domains and misfit dislocations. It was suggested that the electrostatic energy should be more of a factor for smaller tetragonality systems ($BaTiO_3$ versus $PbTiO_3$) where the strain energy is less, though this could at least be partially balanced by the fact that the polarization is smaller as well. A typical coherent diagram is shown in Fig. 33.

With transmission electron microscopy it is possible to make detailed studies of the types and arrangements of misfit dislocations in perovskite thin films. Recent studies of high-quality films include Suzuki *et al.* (1999) and Sun *et al.* (2004). While strain-relaxing defects, such as misfit dislocations, reduce or eliminate the elastic energy associated with homogeneous strain, these and other defects prevalent in films do generate inhomogeneous strains. As mentioned at the beginning of this section, the inhomogeneous strains couple strongly to the polarization, and it has been shown by phenomenological analysis (Balzar *et al.*, 2002; Balzar and Popa, 2004) that their effects on T_c can be significant. They have also been argued to contribute to the degradation of the dielectric response in thin films relative to bulk values (Canedy *et al.*, 2000).

Strains and their coupling to polarization are also central to the properties exhibited by short-period superlattices of lattice-mismatched constituents. As the result of recent work on artificial superlattices of ferroelectric materials, there are some indications that improved ferroelectric properties and/or very large dielectric constants can be achieved. The most studied system at present is $BaTiO_3/SrTiO_3$ (Tabata *et al.*, 1994; Ishibashi *et al.*, 2000; Nakagawara *et al.*, 2000; Shimuta *et al.*, 2002; Jiang *et al.*, 2003; Neaton and Rabe, 2003; Rios *et al.*, 2003; Tian *et al.*, 2005). In $BaTiO_3/SrTiO_3$ superlattices lattice matched to a $SrTiO_3$ substrate, the compressive in-plane strain on the $BaTiO_3$ layer substantially raises its polarization. Theoretical studies suggest that the $SrTiO_3$ layer is polarized (and the polarization in the $BaTiO_3$ layer is reduced) by electrostatic energy considerations, which favor continuity of the component of the polarization along the normal. Overall the polarization is enhanced above that of bulk $BaTiO_3$, though not as high as that of a pure coherent $BaTiO_3$ film if it were possible to suppress the formation of strain-relaxing defects. While the natural lattice constant of $BaTiO_3/SrTiO_3$ is intermediate between the two end points, so that on a $SrTiO_3$ substrate the superlattice is under compressive in-plane stress, it has been suggested that the multilayer structure tends to inhibit the formation of misfit dislocations so that a thicker layer of coherent superlattice material can be grown. As the superlattice material thickness increases, there will be strain relaxation via misfit dislocations and the in-plane lattice constant should increase, putting the $SrTiO_3$ layer under in-plane tensile strain. In this case the $SrTiO_3$ layer is observed to have a component of polarization along [110] (Jiang *et al.*, 2003; Rios *et al.*, 2003) consistent with theoretical studies of epitaxially strained $SrTiO_3$ (Pertsev *et al.*, 2000a; Antons *et al.*, 2005) and of the $BaTiO_3/SrTiO_3$ superlattice with expanded in-plane lattice constant (Johnston, Huang, *et al.*, 2005).

The real appeal of short-periodicity ferroelectric multilayers is the potential to make "new" artificially structured materials with properties that could open the door to substantial improvements in device performance or even radically new types of devices. Perovskites are particularly promising, as individual materials possess a wide variety of structural, magnetic, and electronic properties, while their common structure allows matching at the interface to grow superlattices. Beyond the prototypical example of $BaTiO_3/SrTiO_3$ discussed in the previous paragraph, there has been work on other combinations such as $KNbO_3/KTaO_3$ (Christen *et al.*, 1996; Sepliarsky *et al.*, 2001, 2002; Sigman *et al.*, 2002), $PbTiO_3/SrTiO_3$ (Jiang *et al.*, 1999; Dawber *et al.*, 2005), $PbTiO_3/PbZrO_3$ (Bungaro and Rabe, 2002, 2004), $La_{0.6}Sr_{0.4}MnO_3/La_{0.6}Sr_{0.4}FeO_3$ (Izumi *et al.*, 1999), $CaMnO_3/CaRuO_3$ (Takahashi *et al.*, 2001), $LaCrO_3$-$LaFeO_3$ (Ueda *et al.*, 1998, 1999a), and $LaFeO_3$-$LaMnO_3$ (Ueda *et al.*, 1999b). In nearly all cases, strain plays an important role in understanding the aggregate properties of these short-period multilayers and superlattices. In addition to lattice mismatch, the layers also interact through the mismatch in polarization along the layer normal, which leads to mutual influences governed by considerations of electrostatic energy and nonzero

macroscopic electric fields. With three or more constituents, it is possible to break inversion symmetry to obtain superlattice materials with possibly favorable piezoelectric properties. This idea was first proposed theoretically (Sai *et al.*, 2000) leading to experimental studies of $CaTiO_3/SrTiO_3/BaTiO_3$ (Warusawithana *et al.*, 2003) and $LaAlO_3/(La,Sr)MnO_3/SrTiO_3$ (Yamada *et al.*, 2002; Ogawa *et al.*, 2003; Kimoto *et al.*, 2004). Perovskite superlattices combining ferroelectric and ferromagnetic layers also offer a path to the development of multiferroic materials. The identification, synthesis, and characterization of further combinations remains the subject of active research interest.

VI. NANOSCALE FERROELECTRICS

A. Quantum confinement energies

Confinement energies are a currently popular topic in nanoscale semiconductor microelectronics devices (Petroff *et al.*, 2001). The basic idea is that in a system in which the electron mean free path is long with respect to the lateral dimension(s) of the device, a quantum-mechanical increase in energy (and of the band gap) in the semiconductor will occur. In general, confinement energies exist only in the ballistic regime of conduction electrons, that is, where the electron mean free path exceeds the dimensions of the crystal. This usually requires a high-mobility semiconductor at ultralow temperatures. Such effects are both interesting and important in conventional semiconductors such as Si or Ge, GaAs and other III-V's, and perhaps in II-VI's. However, despite the fact that the commonly used oxide ferroelectrics are wide-band-gap p-type semiconductors ($3.0 < E_g < 4.5$ eV) (Waser and Smyth, 1996), neither their electron nor hole mean free paths are sufficiently long for any confinement energies to be measured. Typically the electron mean free path in an ABO_3 ferroelectric perovskite is 0.1 to 1.0 nm (Dekker, 1954) depending on applied electric field E, whereas the device size d is at least 20 nm. Therefore any confinement energy (which scales as d^{-2}) might be a meV or two, virtually unmeasurable despite a few published claims (Yu *et al.*, 1997; Kohiki *et al.*, 2000; Scott, 2000a) reporting extraordinarily large effects. In the case of Bi_2O_3 and $SrBi_2Ta_2O_9$ (SBT) these effects may arise from two-phase regions at the sample surfaces (Zhou, 1992; Switzer *et al.*, 1999). This is theoretically interesting and very important from an engineering device point of view; if it were not true the contact potential at the electrode interface in a 1T-1C device, or at the ferroelectric-Si interface in a ferroelectric-gate FET, would depend critically on the cell size, which would add a very undesirable complication to device design.

B. Coercive fields in nanodevices

One of the most pleasant surprises in the research on small-area ferroelectrics is the observation, shown in Fig. 34, that the coercive field is independent of lateral area (Alexe, 1999; Alexe *et al.*, 1999). Coercive fields in nanophase ferroelectric cells have generally been measured via atomic force microscopy (Gruverman *et al.*, 1996). Domain structures, polarization, and coercive fields of nanoscale particles of $BaTiO_3$ have been studied theoretically using interatomic potentials (Stachiotti, 2004) and a first-principles effective Hamiltonian (Fu and Bellaiche, 2003).

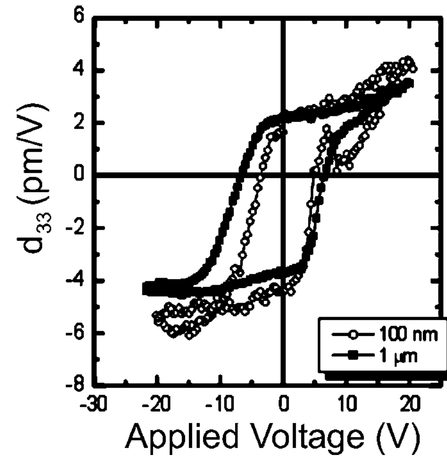

FIG. 34. Lack of significant dependence of coercive field on lateral area in nanoscale ferroelectrics. From Alexe, 1999; Alexe *et al.*, 1999.

C. Self-patterned nanoscale ferroelectrics

One approach to producing nanoscale ferroelectrics is to attempt to produce self-patterned arrays of nanocrystals, in which ordering is produced by interactions between islands through the substrate. This approach could be used to produce arrays of metallic nanoelectrodes on top of a ferroelectric film or alternatively arrays of crystals from the ferroelectric materials themselves. The first scheme was suggested by Alexe *et al.* (1998) who found that a bismuth-oxide wetting layer on top of a bismuth-titanate film formed an array of metallic bismuth-oxide nanocrystals on top of the film, which were partially registered along the crystallographic directions of the underlying substrate (Fig. 35). These nanocrystals were used successfully as electrodes to switch regions of the film (Alexe *et al.*, 1999). In the second approach one might use a material such as $PbTiO_3$ on a $SrTiO_3$ substrate, which was first demonstrated to form islands when grown epitaxially at very thin film thicknesses by Seifert *et al.* (1996). In the context of self-patterning of oxide materials, a recent work by Vasco *et al.* (2003) studied the growth of self-organized $SrRuO_3$ crystals on $LaAlO_3$.

When small amounts of materials are deposited on substrates where there is some degree of mismatch between the two materials, islands form and the repulsive interactions between them are mediated via strain fields in the substrate, as first suggested by Andreev (1981). This idea has been developed into a detailed theory by Shchukin and Bimberg (1999), however, this theory is a zero-temperature theory, whereas a thermodynamic

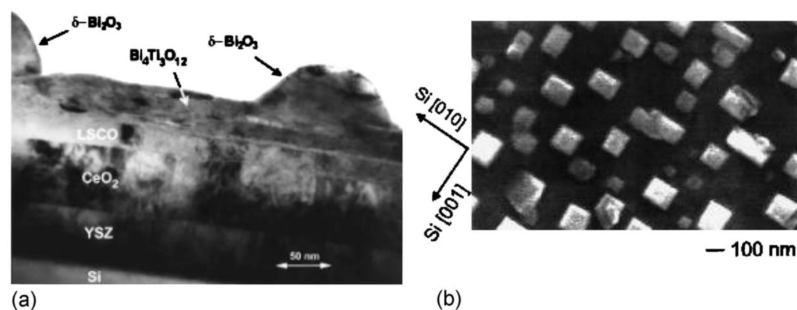

FIG. 35. Sample from Alexe *et al.*: (a) TEM cross section showing underlying layers and bismuth-oxide nanoelectrodes; (b) semiregistered array of nanoelectrodes taking their orientation from the underlying Si substrate. Reprinted with permission from Alexe *et al.*, 1998. © 1998, AIP.

theory is required to describe the crystallization processes which occur at quite high temperatures. An extension of the theory to finite temperatures has been carried out by Williams and co-workers (Williams *et al.*, 2000; Rudd *et al.*, 2003). The chief result of this theory is the prediction of three different kinds of structures (pyramids, domes, and superdomes), a volume distribution for a particular species of structure, and a shape map to describe relative populations of structures as a function of coverage and crystallization temperature. One interesting result from the experiments is that similar-shaped structures are observed in both the Volmer-Weber and Stranski-Krastanow growth modes, but on different size scales. In the work of Williams the thickness above which dome populations occur is of the order of 4–5 monolayers, corresponding to the critical thickness for misfit dislocations for Ge on Si(100). On the other hand, Capellini *et al.* (1997) studied via atomic force microscopy the growth of Ge on Si(100) in the Stanski-Krastanow growth mode and found a much larger critical structure height of 50 nm at which dislocations were introduced and the structures changed from being pyramidal in geometry to domelike. The large increase in critical thickness is due to a substantial part of the misfit strain being taken up by the substrate in the Stranski-Krastanow growth mode, as described by Eaglesham and Cerrulo (1990). The description of self-patterned ferroelectric nanocrystals by the models of Schukin and Williams has recently been undertaken by Dawber, Szafraniak, *et al.* (2003).

Prior to this two groups have grown $PbTiO_3$ nanocrystals on Pt/Si(111) substrates to measure size effects in ferroelectricity (Roelofs *et al.*, 2003; Shimizu *et al.*, 2004). These works both show a lack of piezoresponse in structures below 20 nm in lateral size (Fig. 36), though we expect that this is connected to mechanical constraints rather than any fundamental limiting size for ferroelectric systems. Chu *et al.* (2004) have highlighted the role that misfit dislocations can play in hampering ferroelectricity in small structures. Interestingly in the work of Roelofs *et al.* (2003) and Shimizu *et al.* (2004) because of the (111) orientation of their substrates, instead of square-based pyramids they obtain triangular-based structures that display hexagonal rather than cubic registration [an analogous result is observed when Ge is grown on Si(111); Capellini *et al.*, 1999]. The growth and analysis of PZT nanocrystals on $SrTiO_3$ has been carried out by Szafraniak *et al.* (2003). Ruediger *et al.* (2004) have recently reviewed size effects in ferroelectric nanocrystals.

Although there is potential to produce self-patterned arrays with greater registration by better choice of materials and processing conditions, our general conclusion is that highly registered memory arrays will not occur spontaneously in the absence of a prepatterned field.

D. Nonplanar geometries: ferroelectric nanotubes

Almost all recent work on ferroelectric-oxide films has involved planar geometries. However, both from a device engineering point of view and from theoretical considerations, it is now appropriate to analyze carefully nonplanar geometries, especially nanotubes.

Nanotubes made of oxide insulators have a variety of applications for pyroelectric detectors, piezoelectric inkjet printers, and memory capacitors that cannot be filled by other nanotubes (Herzog and Kattner, 1985; Gnade *et al.*, 2000; Averdung *et al.*, 2001; Sakamaki *et al.*, 2001; Sajeev and Busch, 2002). In the drive for increased storage density in FRAM and DRAM devices, complicated

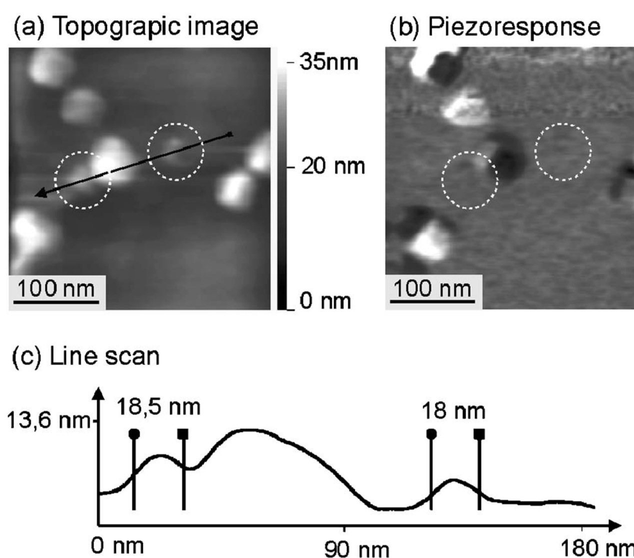

FIG. 36. (a) Topographic image of grains from 100 to 20 nm in lateral size. (b) Piezoresponse image of same grains showing the absence of piezoresponse for grains below 20 nm. From Roelofs *et al.*, 2003.

stacking geometries, 3D structures, and trenches with high aspect ratios are also being investigated to increase the dielectric surface area. The integration of ferroelectric nanotubes into Si substrates is particularly important in the construction of 3D memory devices beyond the present stacking and trenching designs, which according to the international ULSI schedule[3] must be achieved by 2008. Template synthesis of nanotubes and wires is a versatile and inexpensive technique for producing nanostructures. The size, shape, and structural properties of the assembly are simply controlled by the template used. Using carbon nanotubes as templates, tubular forms of a number of oxides including V_2O_5, SiO_2, Al_2O_3, and ZrO_2 have been generated (Patzke *et al.*, 2002). Much larger (>20 μm diameter) ferroelectric microtubes have been made by sputter deposition around polyester fibers (Fox, 1995; Pokropivny, 2001)—Fox has made them from ZnO and PZT, with a 23 μm inside diameter, about 1000 times larger than the smallest nanotubes reported in the present paper. Porous sacrificial templates as opposed to fibers have also been used. Porous anodic alumina has a polycrystalline structure with ordered domains of diameter 1–3 μm, containing self-organized 2D hexagonal tubular pore arrays with an interpore distance of 50–420 nm (Li *et al.*, 1998). This nanochannel material can therefore be used as a template for individual nanotubes but is not suitable for making an ordered array of tubes over length scales greater than a few mm. Many oxide nanotubes, such as TiO_2, In_2O_3, Ga_2O_3, $BaTiO_3$, and $PbTiO_3$, as well as nanorods of MnO_2, Co_3O_4, and TiO_2, have been made using porous alumina membranes as templates (Patzke *et al.*, 2002). Hernandez *et al.* (2002) used a sol-gel-template synthesis route to prepare $BaTiO_3$ and $PbTiO_3$ nanotube bundles by dipping alumina membranes with 200-nm pores into the appropriate sol. The $BaTiO_3$ and $PbTiO_3$ nanotubes were shown to be cubic (paraelectric) and tetragonal (ferroelectric) by x-ray diffraction, although Raman studies indicated some noncentrosymmetric phase on a local scale in $BaTiO_3$. Porous silicon materials are also available as suitable templates. Mishina *et al.* (2002) used a sol-gel dipping technique to fill nanoporous silicon with a $PbZr_{1-x}Ti_xO_3$ (PZT) sol producing nanograins and nanorods 10–20 nm in diameter. The presence of the ferroelectric PZT phase was shown by second-harmonic generation measurements. In this instance the porous silicon does not have a periodic array of pores (Smith and Collins, 1992) and as in the case for those produced by Hernandez *et al.* (2002) we emphasize that those nanotubes are not ordered arrays, but instead "spaghettilike" tangles of nanotubes that cannot be used for the Si device embodiments. A second type of porous Si template, however, consists of a very regular periodic array of pores with very high aspect ratios. By a combination of photolithography and electrochemical etching hexagonal or orthogonal arrays of pores with diameters 400 nm to a few mm and up to 100 μm deep can be formed in single-crystal Si wafers (Ottow *et al.*, 1996; Schilling *et al.*, 2001). These crystals were originally developed for application as 2D photonic crystals, but also find applications as substrates for templated growth and integration of oxides nanostructures with Si technology. Luo *et al.* (2003) recently used such crystals to produce individual, free-standing PZT and $BaTiO_3$ ferroelectric nanotubes by a polymeric wetting technique. Morrison *et al.* (2003) described the use of liquid source misted chemical deposition to fill such photonic Si crystals with a SBT precursor. During deposition, the SBT precursor was shown to coat the inside of the pores. After etching of the photonic crystal with pore diameter 2 μm for 30 sec with aqueous HF/HNO_3, the interface between the Si substrate and SBT coating is dissolved, exposing the uniform SBT tube, Fig. 37(a). The tube walls are very uniform with a thickness of ~200 nm. The same sample is shown in cross-sectional view after complete removal of the host Si walls between pores, Fig. 37(b). The result is a regular array of tubes attached to the host Si matrix only at the tube base. Although these tubes have suffered damage during handling, it is clear that the pores have been filled uniformly to the bottom, a depth of ~100 μm.

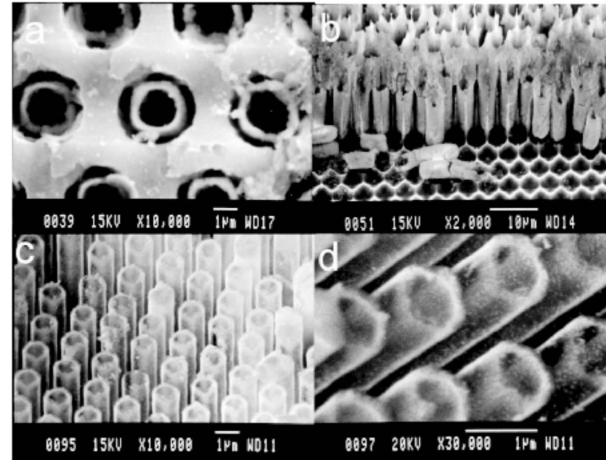

FIG. 37. (a) SEM micrograph indicating a plan view of a regular array of SBT tubes in host silicon substrate with diameter ~2 μm and wall thickness ~200 nm. (b) SBT tubes in cross-sectional view indicating coating to bottom of pore. (c) Micrograph of free-standing array of tubes with diameter ~800 nm; and (d) wall thickness <100 nm.

The second photonic crystal with pore diameter 800 nm underwent fewer depositions and after etching revealed a regular array of uniform tubes of diameter 800 nm, Fig. 37(c). The wall thickness is uniform and <100 nm, Fig. 37(d). The tubes are ~100 μm long, completely discrete, and are still attached to the host Si matrix, creating a perfectly registered hexagonal array. Free-standing tubes may be produced by completely dissolving the host Si matrix. As yet, no one has applied cylindrical electrodes to the tubes; however, Steinhart *et al.* (2003) recently used porous anodic alumina templates

[3]International Technology Roadmap for Semiconductors (ITRS) 2002 (available at http://public.itrs.net/Files/2002Update/Home.pdf).

to grow palladium nanotubes. Using a similar method it may be possible to alternately deposit Pd or Pt and SBT to produce a concentric electrode/FE/electrode structure in each nanotube. The use of the photonic crystal template with a regular array of pores has significant benefits over other porous substrates in that the coatings or tubes produced are also in a registered array ordered over several mm or even cm. This facilitates addressing of such an array for device applications. DRAMs utilize high surface-area dielectrics, and high aspect-ratio SBT coatings such as these embedded in Si could increase storage density. Current state-of-the-art deep-trenched capacitors are 0.1 mm diameter by 6 mm deep, aspect ratio 60:1. Using SBT (or other FE-oxide) nanotubes of wall thickness <100 nm and a trench (or array of trenches) of 0.1 μm diameter and 100 μm deep, an aspect ratio of $>1000:1$ is possible. Applying and addressing electrodes to an array of FE nanotubes could generate 3D FRAM structures offering high storage density with improved read/write characteristics compared to conventional planar stacks. On removal of the Si walls, the piezoelectric response (expansion or contraction under an applied field) of such an array of nanotubes could be utilized for a number of microelectromechanical systems applications. These could include (1) ink-jet printing—delivery of subpicoliter droplets for lithography-free printing of submicron circuits; (2) biomedical applications—nanosyringes, inert drug delivery implants; and (3) micropositioners or movement sensors.

Almost no theoretical work has been published on the physics of ferroelectric nanotubes. Analytical solutions for the effects on the d_{ij} piezoelectric coefficients of hollow tubes have been given both for the case in which polarization P is along the length z (Ebenezer and Ramesh, 2003) and for P radial (Ebenezer and Abraham, 2002), they did not, however, solve the azimuthal case where polarization goes around the tube. It it this latter case that has been measured as hysteresis by Luo *et al.* (2003) with a tube lying on a bottom electrode with a semicircular sputtered top electrode. Important matters such as the dependence of T_c upon tube diameter have also not been examined.

VII. CONCLUSIONS

In this review we have sought to cover the important advances in recent years in the physics of thin-film ferroelectric oxides. At present, ferroelectric thin-film memory devices have reached a point of maturity where they are beginning to appear in real commercial devices. At the same time, new directions such as the drive to faster, smaller, nanoscale devices and nonplanar geometries are evolving and new levels of physical understanding will be required. Over the next years it is expected that first-principles computational approaches will continue to develop, suggesting a new synergy between the computational modeling and experimental realizations of ferroelectric systems with new and exciting properties.

REFERENCES

Ahn, C. H., J.-M. Triscone, and J. Mannhart, 2003, Nature (London) **424**, 1015.

Alexe, M., 1999, private communication.

Alexe, M., A. Gruverman, C. Harnagea, N. D. Zakharov, A. Pignolet, D. Hesse, and J. F. Scott, 1999, Appl. Phys. Lett. **75**, 1158.

Alexe, M., J. F. Scott, C. Curran, N. D. Zakharov, D. Hesse, and A. Pignolet, 1998, Appl. Phys. Lett. **73**, 1592.

Alpay, S. P., and A. L. Roytburd, 1998, J. Appl. Phys. **83**, 4714.

Andreev, A. F., 1981, JETP Lett. **53**, 1063.

Antons, A., J. B. Neaton, K. M. Rabe, and D. Vanderbilt, 2005, Phys. Rev. B **71**, 024102.

Arlt, G., and H. Neumann, 1988, Ferroelectrics **87**, 109.

Armstrong, R. D., and B. R. Horrocks, 1997, Solid State Ionics **94**, 181.

Astala, R. K., and P. D. Bristowe, 2004, Modell. Simul. Mater. Sci. Eng. **12**, 79.

Averdung, J., *et al.*, 2001, German Patent No. DE10023456 (2 January).

Ayyub, P., S. Chattopadhyay, R. Pinto, and M. S. Multani, 1998, Phys. Rev. B **57**, R5559.

Balzar, D., and N. C. Popa, 2004, Thin Solid Films **450**, 29.

Balzar, D., P. A. Ramakrishnan, P. Spagnol, *et al.*, 2002, Jpn. J. Appl. Phys., Part 1 **41**, 6628.

Baniecki, J. D., R. B. Laibowitz, T. M. Shaw, C. Parks, J. Lian, H. Xu, and Q. Y. Ma, 2001, J. Appl. Phys. **89**, 2873.

Bardeen, J., 1947, Phys. Rev. **71**, 717.

Baroni, S., A. dal Corso, S. de Gironcoli, and P. Giannozzi, unpublished, http://www.pwscf.org

Baroni, S., S. de Gironcoli, A. D. Corso, and P. Giannozzi, 2001, Rev. Mod. Phys. **73**, 515.

Basceri, C., S. K. Streiffer, A. I. Kingon, and R. Waser, 1997, J. Appl. Phys. **82**, 2497.

Batra, I. P., and B. D. Silverman, 1973, Solid State Commun. **11**, 291.

Bellaiche, L., A. Garcia, and D. Vanderbilt, 2000, Phys. Rev. Lett. **84**, 5427.

Bengtsson, L., 1999, Phys. Rev. B **59**, 12301.

Betsuyaku, K., H. Tanaka, H. Katayama Yoshida, and T. Kawai, 2001, Jpn. J. Appl. Phys., Part 1 **40**, 6911.

Black, C. T., and J. J. Welser, 1999, IEEE Trans. Electron Devices **46**, 776.

Blaha, P., K. Schwarz, P. Sorantin, and S. B. Trickey, 1990, Comput. Phys. Commun. **59**, 399.

Boikov, Yu. A., B. M. Goltsman, V. K. Yamarkin, and V. V. Lemanov, 2001, Appl. Phys. Lett. **78**, 3866.

Bratkovsky, A. M., and A. P. Levanyuk, 2000, Phys. Rev. Lett. **84**, 3177.

Bratkovsky, A. M., and A. P. Levanyuk, 2001, Phys. Rev. Lett. **86**, 3642.

Bratkovsky, A. M., and A. P. Levanyuk, 2005, Phys. Rev. Lett. **94**, 107601.

Brazier, M., S. Mansour, and M. McElfresh 1999, Appl. Phys. Lett. **74**, 4032.

Brennan, C., 1993, Ferroelectrics **150**, 199.

Brennan, C. J., 1992, Integr. Ferroelectr. **2**, 73.

Bune, A. V., V. M. Fridkin, S. Ducharme, L. M. Blinov, S. P. Palto, A. V. Sorokin, S. G. Yudin, and A. Zlatkin, 1998, Nature (London) **391**, 1998.

Bungaro, C., and K. M. Rabe, 2002, Phys. Rev. B **65**, 224106.

Bungaro, C., and K. M. Rabe, 2004, Phys. Rev. B **69**, 184101.

Bungaro, C., and K. M. Rabe, 2005, Phys. Rev. B **71**, 035420.
Canedy, C. L., H. Li, S. P. Alpay, L. Salamanca-Riba, A. L. Roytburd, and R. Ramesh, 2000, Appl. Phys. Lett. **77**, 1695.
Capellini, G., L. Di Gaspare, and F. Evangelisti, 1997, Appl. Phys. Lett. **70**, 493.
Capellini, G., N. Motta, A. Sgarlata, and R. Calarco, 1999, Solid State Commun. **112**, 145.
Castell, M. R., 2002, Surf. Sci. **505**, 1.
Chalamala, B. R., Y. Wei, R. H. Reuss, S. Aggarwal, B. E. Gnade, R. Ramesh, J. M. Bernhard, E. D. Sosa, and D. E. Golden 1999, Appl. Phys. Lett. **74**, 1394.
Chan, N.-H., R. K. Sharma, and D. M. Smyth, 1976, J. Electrochem. Soc. **123**, 1584.
Chan, N.-H., R. K. Sharma, and D. M. Smyth, 1981, J. Am. Ceram. Soc. **64**, 556.
Chen, H.-M., S.-W. Tsaur, and Y.-M. Lee J., 1998, Jpn. J. Appl. Phys., Part 1 **137**, 4056.
Chen, L., V. Nagarajan, R. Ramesh, and A. L. Roytburd, 2003, J. Appl. Phys. **94**, 5147.
Cheon, C. I., K. Y. Yun, J. S. Kim, and J. H. Kim, 2001, Integr. Ferroelectr. **34**, 1513.
Choi, K. J., M. Biegalski, Y. L. Li, A. Sharan, J. Schubert, R. Uecker, P. Reiche, Y. B. Chen, X. Q. Pan, V. Gopalan, L.-Q. Chen, D. G. Schlom, and C. B. Eom, 2004, Science **306**, 1005.
Choi, K.-J., W.-C. Shin, and S.-G. Yoon, 2001, Integr. Ferroelectr. **34**, 1541.
Chon, U., H. M. Jang, M. G. Kim, and C. H. Chang, 2002, Phys. Rev. Lett. **89**, 087601.
Christen, H.-M., L. A. Boatner, J. D. Budai, M. F. Chisholm, L. A. Ga, P. J. Marrero, and D. P. Norton, 1996, Appl. Phys. Lett. **68**, 1488.
Chu, M.-W., I. Szafraniak, R. Scholz, C. Harnagea, D. Hesse, M. Alexe, and U. Gosele, 2004, Nat. Mater. **3**, 87.
Cockayne, E., and K. M. Rabe, 1998, in *First-Principles Calculations for Ferroelectrics*, edited by R. E. Cohen, AIP Conf. Proc. No. 436 (AIP, Woodbury, NY), p. 61.
Cockayne, E., and K. M. Rabe, 2000, J. Phys.: Condens. Matter **61**, 305.
Cohen, R. E., 1992, Nature (London) **358**, 136.
Cohen, R. E., 1996, J. Phys. Chem. Solids **57**, 1393.
Cohen, R. E., 1997, Ferroelectrics **194**, 323.
Cohen, R. E., and H. Krakauer, 1990, Phys. Rev. B **42**, 6416.
Cohen, R. E., and H. Krakauer, 1992, Ferroelectrics **136**, 65.
Colla, E. L., S. Hong, D. V. Taylor, A. K. Tagantsev, and N. Setter, 1998, Appl. Phys. Lett. **72**, 2763.
Conley, J. W., and G. D. Mahan, 1967, Phys. Rev. **161**, 681.
Cora, F., and C.R. A. Catlow, 1999, Faraday Discuss. **114**, 421.
Cowley, A. M., and S. M. Sze, 1965, J. Appl. Phys. **36**, 3212.
Damjanovic, D., 1997, Phys. Rev. B **55**, R649.
Dawber, M., P. Chandra, P. B. Littlewood, and J. F. Scott, 2003, J. Phys.: Condens. Matter **15**, L393.
Dawber, M., I. Farnan, and J. F. Scott, 2003, Am. J. Phys. **71**, 819.
Dawber, M., C. Lichtensteiger, M. Cantoni, M. Veithen, P. Ghosez, K. Johnston, K. M. Rabe, and J.-M. Triscone, 2005, Phys. Rev. Lett. (to be published).
Dawber, M., and J. F. Scott, 2000, Appl. Phys. Lett. **76**, 1060; 2000, Appl. Phys. Lett. **76**, 3655.
Dawber, M., and J. F. Scott, 2001, Integr. Ferroelectr. **38**, 161.
Dawber, M., and J. F. Scott, 2002, Jpn. J. Appl. Phys., Part 1 **41**, 6848.
Dawber, M., and J. F. Scott, 2004, J. Phys.: Condens. Matter **16**, L515.
Dawber, M., J. F. Scott, and A. J. Hartmann, 2001, J. Eur. Ceram. Soc. **21**, 1633.
Dawber, M., I. Szafraniak, M. Alexe, and J. F. Scott, 2003, J. Phys.: Condens. Matter **15**, L667.
de Araujo, C. A.-Paz, J. D. Cuchiaro, L. D. McMillan, M. C. Scott, and J. F. Scott, 1995, Nature (London) **374**, 627.
de Gironcoli, S., S. Baroni, and R. Resta, 1989, Phys. Rev. Lett. **62**, 2853.
Dekker, A. J., 1954, Phys. Rev. **94**, 1179.
Democritov, S. O., and N. M. Kreines, 1988, JETP Lett. **48**, 294.
Dieguez, O., S. Tinte, A. Antons, C. Bungaro, J. B. Neaton, K. M. Rabe, and D. Vanderbilt, 2004, Phys. Rev. B **69**, 212101.
Dietz, G. W., M. Schumacher, R. Waser, S. K. Streiffer, C. Basceri, and A. I. Kingon, 1997, J. Appl. Phys. **82**, 2359.
Dietz, G. W., and R. Waser, 1995, Integr. Ferroelectr. **9**, 317.
Dietz, G. W., and R. Waser, 1997, Thin Solid Films **299**, 53.
Dimos, D., W. L. Warren, M. B. Sinclair, B. A. Tuttle, and R. W. Schwartz, 1994, J. Appl. Phys. **76** 4305.
Do, D-H., P. G. Evans, E. D. Issacs, D. M. Kim, C. B. Eom, and E. M. Dufresne, 2004, Nat. Mater. **3**, 365.
Dovesi, R., R. Orlando, B. Civalleri, C. Roetti, V. R. Saunders, and C. M. Zichovich-Wilson, 2005, Z. Kristallogr. **220**, 571.
Du, X., and I. W. Chen, 1998a, J. Appl. Phys. **83**, 7789.
Du, X., and I. W. Chen, 1998b, in *Ferroelectric Thin Films VI*, edited by R. E. Treece *et al.*, MRS Symposia Proceedings No. 493 (Materials Research Society, Pittsburgh), p. 311.
Ducharme, S., V. M. Fridkin, A. V. Bune, S. P. Palto, L. M. Blinov, N. N. Petukhova, and S. G. Yudin, 2000, Phys. Rev. Lett. **84**, 175.
Duiker, H. M., 1990, Ph.D. thesis (University of Colorado).
Duiker, H. M., and P. D. Beale, 1990, Phys. Rev. B **41**, 490.
Duiker, H. M., P. D. Beale, J. F. Scott, C. A. Paz de Araujo, B. M. Melnick, and J. D. Cuchario, 1990, J. Appl. Phys. **68**, 5783.
Eaglesham, D. J., and M. Cerullo, 1990, Phys. Rev. Lett. **64**, 1943.
Ebenezer, D. D., and P. Abraham, 2002, Curr. Sci. **83**, 981.
Ebenezer, D. D., and R. Ramesh, 2003, Curr. Sci. **85**, 1173.
Erdman, N., K. R. Poeppelmeier, M. Asta, O. Warschkow, D. E. Ellis, and L. D. Marks, 2002, Nature (London) **419**, 55.
Evans, J., 1990.
Fatuzzo, E., and W. J. Merz, 1967, *Ferroelectricity* (North-Holland, Amsterdam).
Fennie, C. J., and K. M. Rabe, 2005, Phys. Rev. B **71**, 100102.
Feynman, R. P., 1939, Phys. Rev. **56**, 340.
Fiebig, M., T. Lottermoser, D. Frohlich, A. V. Goltsev, and R. V. Pisarev, 2002, Nature (London) **419**, 818.
Floquet, N., and C. Valot, 1999, Ferroelectrics **234**, 107.
Floquet, N., C. M. Valot, M. T. Mesnier, J. C. Niepce, L. Normand, A. Thorel, and R. Kilaas, 1997, J. Phys. III **7**, 1105.
Foeth, M., A. Sfera, P. Stadelmann, and P-A. Buffat, 1999, J. Electron Microsc. **48**, 717.
Fong, D. D., G. B. Stephenson, S. K. Streiffer, J. A. Eastman, O. Auciello, P. H. Fuoss, and C. Thompson, 2004, Science **304**, 1650.
Forlani, F., and N. Minnaja, 1964, Phys. Status Solidi **4**, 311.
Fouskova, A., 1965, J. Phys. Soc. Jpn. **20**, 1625.
Fouskova, A., and V. Janousek, 1965, J. Phys. Soc. Jpn. **20**, 1619.
Fox, D. L., D. R. Tilley, J. F. Scott, and H. J. Guggenheim, 1980, Phys. Rev. B **21**, 2926.
Fox, G. R., 1995, J. Mater. Sci. Lett. **14**, 1496.
Fu, H., and L. Bellaiche, 2003, Phys. Rev. Lett. **91**, 257601.

Fu, H. X., and R. E. Cohen, 2000, Nature (London) **403**, 281.

Fu, L., E. Yaschenko, L. Resca, and R. Resta, 1999, Phys. Rev. B **60**, 2697.

Ganpule, C. S., V. Nagarajan, H. Li, A. S. Ogale, D. E. Steinhauser, S. Aggarwal, E. Williams, R. Ramesh, and P. De Wolf, 2000, Appl. Phys. Lett. **77**, 292.

Ganpule, C. S., V. Nagarajan, S. B. Ogale, A. L. Roytburd, E. D. Williams, and R. Ramesh, 2000, Appl. Phys. Lett. **77**, 3275.

Ganpule, C. S., A. L. Roytburd, V. Nagarajan, B. K. Hill, S. B. Ogale, E. D. Williams, R. Ramesh, and J. F. Scott, 2001, Phys. Rev. B **65**, 014101.

Garcia, A., and D. Vanderbilt, 1996, Phys. Rev. B **54**, 3817.

Garcia, A., and D. Vanderbilt, 1998, Appl. Phys. Lett. **72**, 2981.

Garg, A., Z. H. Barber, M. Dawber, J. F. Scott, A. Snedden, and P. Lightfoot, 2003, Appl. Phys. Lett. **83**, 2414.

Gerson, R., and T. C. Marshall, 1959, J. Appl. Phys. **30**, 1650.

Ghosez, P., E. Cockayne, U. V. Waghmare, and K. M. Rabe, 1999, Phys. Rev. B **60**, 836.

Ghosez, P., and K. M. Rabe, 2000, Appl. Phys. Lett. **76**, 2767.

Gnade, B., *et. al*, 2000, U.S. Patent No. US6033919 (7 March).

Gonze, X., J.-M. Beuken, R. Caracas, F. Detraux, M. Fuchs, G.-M. Rignanese, L. Sindic, M. Verstraete, G. Zerah, F. Jollet, M. Torrent, A. Roy, M. Mikami, Ph. Ghosez, J.-Y. Raty, and D. C. Allan, 2002, Comput. Mater. Sci. **25**, 478. http://www.mapr.ucl.ac.be/ABINIT

Gorbenko, O. Y., S. V. Samoilenkov, I. E. Graboy, and A. R. Kaul, 2002, Chem. Mater. **14**, 4026.

Gruverman, A., 1990, Ph.D. thesis (Ural State University, Ekaterinburg, Russia).

Gruverman, A., O. Auciello, and H. Tokumoto, 1996, Appl. Phys. Lett. **69**, 3191.

Gruverman, A., H. Tokumoto, A. S. Prakash, S. Aggarwal, B. Yang, M. Wuttig, R. Ramesh, O. Auciello, and T. Venkatesan, 1997, Appl. Phys. Lett. **71**, 3492.

Haeni, J. H., *et al.*, 2004, Nature (London) **430**, 758.

Han, J.-P., X. Guo, C. C. Broadbridge, T. P. Ma, M. Cantoni, J.-M. Sallese, and P. Fazan, 2001, Integr. Ferroelectr. **34**, 1505.

Haneder, T. P., W. Hoenlein, H. Bachhofer, H. Von Philipsborn, and R. Waser, 2001, Integr. Ferroelectr. **34**, 1487.

Hartmann, A. J., M. Neilson, R. N. Lamb, K. Watanabe, and J. F. Scott, 2000, Appl. Phys. A **70**, 239.

Hashimoto, S., H. Orihara, and Y. Ishibashi, 1994, J. Phys. Soc. Jpn. **63**, 1601.

He, L. X., and D. Vanderbilt, 2003, Phys. Rev. B **68**, 134103.

Heifets, E., R. I. Eglitis, E. A. Kotonin, and G. Borstel, 2001a, in *Fundamental Physics of Ferroelectrics 2001*, edited by H. Krakauer, AIP Conf. Proc. No. 582 (AIP, Melville, NY), p. 201.

Heifets, E., R. I. Eglitis, E. A. Kotonin, and G. Borstel, 2002b, in *Fundamental Physics of Ferroelectrics 2002*, edited by R. E. Cohen, AIP Conf. Proc. No. 626 (AIP, Melville, NY), p. 285.

Heifets, E., R. I. Eglitis, E. A. Kotonin, J. Maier, and G. Borstel, 2001b, Phys. Rev. B **64**, 235417.

Heifets, E., R. I. Eglitis, E. A. Kotonin, J. Maier, and G. Borstel, 2002a, Surf. Sci. **513**, 211.

Heifets, E., E. Kotonin, and P. W. M. Jacobs, 2000, Thin Solid Films **375**, 64.

Heifets, E., E. A. Kotonin, and J. Maier, 2000, Surf. Sci. **462**, 19.

Heine, V., 1965, Phys. Rev. **138**, A1689.

Hernandez, B. A., K.-S. Chang, E. R. Fisher, and P. K. Dorhout, 2002, Chem. Mater. **14**, 481.

Herzog, K., and E. Kattner, 1985, U.S. Patent No. 4504845 (12 March).

Hill, N. A., 2000, J. Phys. Chem. B **104**, 6694.

Huffmann, M., 1995, Integr. Ferroelectr. **10**, 39.

Hwang, C. S., 1998, Mater. Sci. Eng., B **56**, 178.

Hwang, C. S., B. T. Lee, H.-J. Cho, K. H. Lee, C. S. Kang, H. Horii, S. I. Lee, and M. Y. Lee, 1997, Appl. Phys. Lett. **71**, 371.

Hwang, C. S., B. T. Lee, C. S. Kang, J. W. Kim, K. H. Lee, H.-J. Cho, H. Horii, W. D. Kim, S. I. Lee, Y. B. Roh, and M. Y. Lee, 1998, J. Appl. Phys. **83**, 3703.

Ishibashi, Y., N. Ohashi, and T. Tsurumi, 2000, Jpn. J. Appl. Phys., Part 1 **39**, 186.

Ishiwara, H., 1993, Jpn. J. Appl. Phys., Part 1 **32**, 442.

Ishiwara, H., 2001, Integr. Ferroelectr. **34**, 1451.

Ishiwara, H., T. Shimamura, and E. Tokumitsu, 1997, Jpn. J. Appl. Phys., Part 1 **36**, 1655.

Izumi, M., Y. Murakami, Y. Konishi, T. Manako, M. Kawasaki, and Y. Tokura, 1999, Phys. Rev. B **60**, 1211.

Jaffe, B., W. R. Cook, and H. Jaffe, 1971, *Piezoelectric Ceramics* (Academic, London).

Janovec, V., 1958, Czech. J. Phys., Sect. A **8**, 3.

Jiang, A. Q., J. F. Scott, H. Lu, and Z. Chen, 2003, J. Appl. Phys. **93**, 1180.

Jiang, J. C., X. Q. Pan, W. Tian, C. D. Theis, and D. G. Schlom, 1999, Appl. Phys. Lett. **74**, 2851.

Johnston, K., M. R. Castell, A. T. Paxton, and M. W. Finnis, 2004, Phys. Rev. B **70**, 085415.

Johnston, K., X. Huang, J. B. Neaton, and K. M. Rabe, 2005, Phys. Rev. B **71**, 100103.

Johnston, K., and K. M. Rabe, 2005, unpublished.

Jun, S., and J. Lee, 2001, Integr. Ferroelectr. **34**, 1579.

Jung, D. J., M. Dawber, J. F. Scott, L. J. Sinnamon, and J. M. Gregg, 2002, Integr. Ferroelectr. **48**, 59.

Jung, D. J., H. H. Kim, Y. J. Song, N. W. Jang, B. J. Koo, S. Y. Lee, S. D. Park, Y. W. Park, and K. N. Kim, 2000, IEDM 2000 Technical Digest, 801.

Jung, D. J., F. D. Morrison, M. Dawber, H. H. Kim, K. Kim, and J. F. Scott, 2004, J. Appl. Phys. **95**, 4968.

Junquera, J., and P. Ghosez, 2003, Nature (London) **422**, 506.

Junquera, J., P. Ghosez, and K. M. Rabe, 2005, unpublished.

Junquera, J., and K. M. Rabe, 2005, unpublished.

Junquera, J., M. Zimmer, P. Ordejon, and P. Ghosez, 2003, Phys. Rev. B **67**, 155327.

Kalkur, T. S., B. Jacob, and G. Argos, 1994, Integr. Ferroelectr. **5**, 177.

Kalkur, T. S., and J. Lindsey, 2001, Integr. Ferroelectr. **34**, 1587.

Kato, K., 2001, Integr. Ferroelectr. **34**, 1533.

Kay, H. F., and J. W. Dunn, 1962, Philos. Mag. **7**, 1962.

Kelman, M. B., L. F. Schloss, P. C. McIntyre, B. C. Hendrix, S. M. Bilodeau, and J. F. Roeder, 2002, Appl. Phys. Lett. **80**, 1258.

Khodenkov, G. E., 1975, Fiz. Met. Metalloved. **39**, 466.

Kim, J., C. J. Kim, and I. Chung, 2001, Integr. Ferroelectr. **33**, 133.

Kim, M., G. Duscher, N. D. Browning, K. Sohlberg, S. T. Pantelides, and S. J. Pennycock, 2001, Phys. Rev. Lett. **86**, 4056.

Kimoto, K., Y. Matsui, H. Yamada, M. Kawasaki, X. Yu, Y. Kaneko, and Y. Tokura, 2004, Appl. Phys. Lett. **84**, 5374.

King-Smith, R. D., and D. Vanderbilt, 1993, Phys. Rev. B **47**, 1651.

King-Smith, R. D., and D. Vanderbilt, 1994, Phys. Rev. B **49**,

5828.
Kingon, A. I., J. P. Maria, and S. K. Streiffer, 2000, Nature (London) **406**, 1032.
Klenov, D. O., T. R. Taylor, and S. Stemmer, 2004, J. Mater. Res. **19**, 1477.
Kohiki, S., S. Takada, A. Shmizu, K. Yamada, and M. Mitone, 2000, J. Appl. Phys. **87**, 474.
Kohn, W., and L. J. Sham, 1965, Phys. Rev. **140**, A1133.
Koukhar, V. J., N. A. Pertsev, and R. Waser, 2001, Phys. Rev. B **64**, 214103.
Krcmar, M., and C. L. Fu, 2003, Phys. Rev. B **68**, 115404.
Kresse, G., and J. Furthmuller, 1996, Phys. Rev. B **54**, 11169.
Kresse, G., and J. Hafner, 1993, Phys. Rev. B **47**, 558.
Krishnan, A., M. M. J. Treacy, M. E. Bisher, P. Chandra, and P. B. Littlewood, 2002, Integr. Ferroelectr. **43**, 31.
Ku, H. Y., and F. G. Ullman, 1964, J. Appl. Phys. **35**, 265.
Kubo, T., and H. Nozoye, 2003, Surf. Sci. **542**, 177.
Kurtin, S., T. C. McGill, and C. A. Mead, 1969, Phys. Rev. Lett. **22**, 1433.
Lewis, S. P., and A. M. Rappe, 1996, Phys. Rev. Lett. **77**, 5241.
Li, A. P., F. Muller, A. Birner, K. Nielsch, and U. Gosele, 1998, J. Appl. Phys. **84**, 6023.
Li, H., A. L. Roytburd, S. P. Alpay, T. D. Tran, L. Salamanca-Riba, and R. Ramesh, 2001, Appl. Phys. Lett. **78**, 2354.
Li, H., H. Zheng, L. Salamanca-Riba, R. Ramesh, I. Naumov, and K. Rabe, 2002, Appl. Phys. Lett. **81**, 4398.
Li, J. A., E. A. Akhadov, J. Baker, L. A. Boatner, D. Bonart, and S. A. Safron, 2003, Phys. Rev. B **68**, 045402.
Li, T., and S. T. Hsu, 2001, Integr. Ferroelectr. **34**, 1495.
Li, Y. L., S. Choudhury, Z. K. Liu, and L. Q. Chen, 2003, Appl. Phys. Lett. **83**, 1608.
Lichtensteiger, C., J. M. Triscone, J. Junquera, and P. Ghosez, 2005, Phys. Rev. Lett. **94**, 047603.
Lines, M. E., and A. M. Glass, 1967, *Principles and Applications of Ferroelectrics and Related Materials* (Clarendon, Oxford).
Lookman, A., R. M. Bowman, J. M. Gregg, J. Kut, S. Rios, M. Dawber, A. Ruediger, and J. F. Scott, 2004, J. Appl. Phys. **96**, 555.
Lubomirsky, I., J. Fleig, and J. Maier, 2002, J. Appl. Phys. **92**, 6819.
Luo, Y., I. Szafraniak, N. D. Zakharov, V. Nagarajan, M. Steinhart, R. B. Wehrspohn, J. H. Wendorff, R. Ramesh, and M. Alexe, 2003, Appl. Phys. Lett. **83**, 440.
Lupascu, D. C., and U. Rabe, 2002, Phys. Rev. Lett. **89**, 187601.
Macleod, T. C., and F. D. Ho, 2001, Integr. Ferroelectr. **34**, 1461.
Man, Z. Y., and X. Q. Feng, 2002, Solid State Commun. **123**, 333.
Masui, S., *et al.*, 2003, *Proceedings of the IEEE Custom Integrated Circuits Conference* (IEEE, New York), p. 403.
Mathews, S., R. Ramesh, T. Venkatesan, and J. Benedetto, 1997, Science **276**, 238.
Matthews, J. W., and A. E. Blakeslee, 1974, J. Cryst. Growth **27**, 118.
McKee, R. A., F. J. Walker, and M. F. Chisholm, 1998, Phys. Rev. Lett. **81**, 3014.
McKee, R. A., F. J. Walker, and M. F. Chisholm, 2001, Science **293**, 468.
McKee, R. A., F. J. Walker, M. B. Nardelli, W. A. Shelton, and G. M. Stocks, 2003, Science **300**, 1726.
McMillan, L. D., C. A. Paz de Araujo, T. Roberts, J. Cuchiaro, M. C. Scott, and J. F. Scott, 1992, Integr. Ferroelectr. **2**, 351.
Merz, W. J., 1954, Phys. Rev. **95**, 690.
Meyer, B., J. Padilla, and D. Vanderbilt, 1999, Faraday Discuss. **114**, 395.
Meyer, B., and D. Vanderbilt, 2001, Phys. Rev. B **63**, 205426.
Meyer, B. E., and D. Vanderbilt, 2002, Phys. Rev. B **65**, 104111.
Miller, S. L., R. D. Nasby, J. R. Schwank, M. S. Rodgers, and P. V. Dressendorfer, 1990, J. Appl. Phys. **68**, 6463.
Mills, G., M. S. Gordon, and H. Metiu, 2003, J. Chem. Phys. **118**, 4198.
Mihara, T., H. Watanabe, H. Yoshimori, C. A. Paz de Araujo, B. Melnick, and L. D. McMillan, 1992, Integr. Ferroelectr. **1**, 269.
Mishina, E. D., K. A. Vorotilov, V. A. Vasil'ev, A. S. Sigov, N. Ohta, and S. Nakabayashi, 2002, J. Exp. Theor. Phys. **95**, 502.
Moll, J. L., and Y. Tarui, 1963, IEEE Trans. Electron Devices **ED-10**, 338.
Monch, W., 1986, Phys. Rev. Lett. **58**, 1260.
Montanari, B., and N. M. Harrison, 2004, J. Phys.: Condens. Matter **16**, 273.
Moreira, R. L., 2002, Phys. Rev. Lett. **88**, 179701.
Moriera de Santos, A., S. Parashar, A. R. Raju, Y. S. Zhao, A. K. Cheetham, and C. N. R. Rao, 2002, Solid State Commun. **122**, 49.
Morrison, F. D., J. F. Scott, M. Alexe, T. J. Leedham, T. Tatsuta, and O. Tsuji, 2003, Microelectron. Eng. **66**, 591.
Mott, N. F., 1938, Proc. Cambridge Philos. Soc. **34**, 568.
Munkholm, A., S. K. Streiffer, M. V. R. Murty, J. A. Eastman, C. Thompson, O. Auciello, L. Thompson, J. F. Moore, and G. B. Stephenson, 2002, Phys. Rev. Lett. **88**, 016101.
Muralt, P., 2000, J. Micromech. Microeng. **10**, 136.
Murphy, E. L., and R. H. Good, 1956, Phys. Rev. **102**, 1464.
Nagarajan, V., A. Roytburd, A. Stanishevsky, S. Praserthchoung, T. Zhao, L. Chen, J. Melngailis, O. Auciello, and R. Ramesh, 2003, Nat. Mater. **2**, 43.
Nakagawara, O., T. Shimuta, T. Makino, T. Makino, and T. Makino, 2000, Appl. Phys. Lett. **77**, 3257.
Neaton, J. B., and K. M. Rabe, 2003, Appl. Phys. Lett. **82**, 1586.
Nielsen, O. H., and R. M. Martin, 1985, Phys. Rev. B **32**, 3780.
Nowotny, J., and M. Rekas, 1994, Ceram. Int. **20**, 251.
Nuffer, J., D. C. Lupascu, J. Rodel, and M. Schroeder, 2001, Appl. Phys. Lett. **79**, 3675.
Ogawa, Y., H. Yamada, T. Ogasawara, H. Yamada, and H. Yamada, 2003, Phys. Rev. Lett. **90**, 217403.
Okuyama, M., H. Sugiyama, T. Nakaiso, and M. Noda, 2001, Integr. Ferroelectr. **34**, 1477.
Orihara, H., S. Hashimoto, and Y. Ishibashi, 1994, J. Phys. Soc. Jpn. **63**, 1031.
Ottow, S., V. Lehmann, and H. Fo, 1996, Appl. Phys. A **63**, 153.
Outzourhit, A., A. Naziripour, J. U. Trefny, T. Kito, B. Yarar, R. Yandrofski, J. D. Cuchiaro, and A. M. Hermanna, 1995, Integr. Ferroelectr. **8**, 227.
Padilla, J., and D. Vanderbilt, 1997, Phys. Rev. B **56**, 1625.
Padilla, J., and D. Vanderbilt, 1998, Surf. Sci. **418**, 64.
Pan, M. J., S. F. Park, C. W. Park, K. A. Markowski, S. Yoshikawa, and C. A. Randall, 1996, J. Am. Ceram. Soc. **79**, 2971.
Park, C. H., 2003, J. Korean Phys. Soc. **42**, 1420.
Park, C. H., and D. J. Chadi, 1998, Phys. Rev. B **57**, R13961.
Park, J. D., and T. S. Oh, 2001, Integr. Ferroelectr. **34**, 1561.
Park, S. E., and T. R. Shrout, 1997, J. Appl. Phys. **82**, 1804.
Paruch, P., T. Tybell, and J.-M. Triscone, 2001, Appl. Phys.

Lett. **79**, 530.
Patzke, G. R., F. Krumeich, and R. Nesper, 2002, Angew. Chem., Int. Ed. **41**, 2446.
Peacock, P. W., and J. Robertson, 2002, J. Appl. Phys. **92**, 4712.
Pertsev, N. A., V. G. Kukhar, H. Kohlstedt, and R. Waser, 2003, Phys. Rev. B **67**, 054107.
Pertsev, N. A., J. Rodriguez Contreras, V. G. Kukhar, B. Hermanns, H. Kohlstedt, and R. Waser, 2003, Appl. Phys. Lett. **83**, 3356.
Pertsev, N. A., A. K. Tagantsev, and N. Setter, 2000a, Phys. Rev. B **61**, R825.
Pertsev, N. A., A. K. Tagantsev, and N. Setter, 2000b, Phys. Rev. Lett. **84**, 3722.
Pertsev, N. A., A. G. Zembilgotov, and A. K. Tagantsev, 1998, Phys. Rev. Lett. **80**, 1988.
Pertsev, N. A., A. G. Zembilgotov, and A. K. Tagantsev, 1999, Ferroelectrics **223**, 79.
Petroff, P. M., A. Lorke, and A. Imamoglu, 2001, Phys. Today **54** (5), 46.
Piskunov, S., E. Heifets, R. I. Eglitis, and G. Borstel, 2004, Comput. Mater. Sci. **29**, 165.
Plumlee, R., 1967, Sandia Laboratories Report No. SC-RR-67-730.
Pokropivny, V. V., 2001, Physica C **351**, 71.
Poykko, S., and D. J. Chadi, 2000, J. Phys. Chem. Solids **61**, 291.
Rabe, K. M., 2005, unpublished.
Rabe, K. M., and U. V. Waghmare, 1995, Phys. Rev. B **52**, 13236.
Rabe, K. M., and U. V. Waghmare, 2002, Phys. Rev. B **65**, 214111.
Rabson, T. A., T. A. Rost, and H. Lin, 1995, Integr. Ferroelectr. **6**, 15.
Ramesh, R., T. Sands, and V. G. Keramidas, 1993, Appl. Phys. Lett. **63**, 731.
Randoshkin, V. V., 1995, Fiz. Tverd. Tela (Leningrad) **37**, 3056.
Rao, F., M. Kim, A. J. Freeman, S. Tang, and M. Anthony, 1997, Phys. Rev. B **55**, 13953.
Reiner, J. W., F. J. Walker, R. A. McKee, C. A. Billman, J. Junquera, K. M. Rabe, and C. H. Ahn, 2004, Phys. Status Solidi B **241**, 2287.
Resta, R., 1994, Rev. Mod. Phys. **66**, 899.
Resta, R., 2003, Modell. Simul. Mater. Sci. Eng. **11**, R69.
Rhoderick, E. H., and R. H. Williams, 1988, *Metal-Semiconductor Contacts*, 2nd ed. (Oxford, Clarendon).
Rios, S., A. Ruediger, J. Q. Jiang, J. F. Scott, H. Lu, and Z. Chen, 2003, J. Phys.: Condens. Matter **15**, 305.
Robblee, L. S., and S. F. Cogan, 1986, in *Encyclopedia of Materials Science and Engineering Supplementary Vol. I*, edited by R. W. Cahn (Pergamon, Oxford), p. 276.
Robels, U., and G. Arlt, 1993, J. Appl. Phys. **73**, 3454.
Robertson, J., 2003, J. Appl. Phys. **93**, 1054.
Robertson, J., and C. W. Chen, 1999, Appl. Phys. Lett. **74**, 1168.
Robertson, J., C. W. Chen, W. L. Warren, and C. D. Gutleben, 1996, Appl. Phys. Lett. **69**, 1704.
Rodriguez Contreras, J., H. Kohlstedt, U. Poppe, and R. Waser, 2003, Appl. Phys. Lett. **83**, 4595.
Roelofs, A., N. A. Pertsev, R. Waser, F. Schlaphof, L. M. Eng, C. Ganpule, V. Nagarajan, and R. Ramesh, 2002, Appl. Phys. Lett. **80**, 1424.
Roelofs, A., T. Schneller, K. Szot, and R. Waser, 2003, Nanotechnology **14**, 250.
Ross, I. M., 1957, U.S. Patent No. 2,791,760.
Rossetti, G. A., L. E. Cross, and K. Kushida, 1991, Appl. Phys. Lett. **59**, 2524.
Roytburd, A. L., S. P. Alpay, L. A. Bendersky, V. Nagarajan, and R. Ramesh, 2001, J. Appl. Phys. **89**, 553.
Rudd, R. E., G. A. D. Briggs, A. P. Sutton, G. Medeiros-Ribeiro, and R. Stanley Williams, 2003, Phys. Rev. Lett. **90**, 146101.
Ruediger, A., T. Schneller, A. Roelofs, S. Tiedke, T. Schmitz, and R. Waser, 2004, Appl. Phys. A (to be published).
Ruini, A., R. Resta, and S. Baroni, 1998, Phys. Rev. B **57**, 5742.
Saghi-Szabo, G., R. E. Cohen, and H. Krakauer, 1998, Phys. Rev. Lett. **80**, 4321.
Sai, N., A. M. Kolpak, and A. M. Rappe, 2005 Phys. Rev. B **72**, 020101.
Sai, N., B. Meyer, and D. Vanderbilt, 2000, Phys. Rev. Lett. **84**, 5636.
Sai, N., and D. Vanderbilt, 2000, Phys. Rev. B **62**, 13942.
Sajeev, J., 2002, U.S. Patent No. US2002074537 (20 June).
Sakamaki, S., *et al.*, 2001, U.S. Patent No. 20010412.
Salje, E. K. H., and W. T. Lee, 2004, Nat. Mater. **3**, 425.
Samara, G. A., 1987, Ferroelectrics **73**, 145.
Samara, G. A., 2003, J. Phys.: Condens. Matter **15**, R367.
Sarin Kumar, A. K., P. Paruch, J.-M. Triscone, W. Daniau, S. Ballandras, L. Pellegrino, D. Marr, and T. Tybell, 2004, Appl. Phys. Lett. **85**, 1757.
Sawyer, C. B., and C. H. Tower, 1930, Phys. Rev. **35**, 269.
Sayer, M., A. Mansingh, A. K. Arora, and A. Lo, 1992, Integr. Ferroelectr. **1**, 129.
Schilling, J., F. Muller, S. Matthias, R. B. Wehrspohn, U. Gosele, and K. Busch, 2001, Appl. Phys. Lett. **78**, 1180.
Schloss, L. F., H. Kim, and P. C. McIntyre, 2004, J. Mater. Res. **19**, 1265.
Schloss, L. F., P. C. McIntyre, B. C. Hendrix, S. M. Bilodeau, J. F. Roeder, and S. R. Gilbert, 2002, Appl. Phys. Lett. **81**, 3218.
Schluter, M., 1978, Phys. Rev. B **17**, 5044.
Schnupp, P., 1967, Phys. Status Solidi **21**, 567.
Schottky, W., 1938, Naturwiss. **26**, 843.
Scott, J. F., 1977, Phys. Rev. B **16**, 2329.
Scott, J. F., 1979, Rep. Prog. Phys. **42**, 1055.
Scott, J. F., 1995, in *Science and Technology of Electroceramic Thin Films*, edited by O. Auciello and R. Waser, NATO ASI Series No. 284 (Kluwer, Dordrecht).
Scott, J. F., 1996, Integr. Ferroelectr. **12**, 71.
Scott, J. F., 1998, Ferroelectrics **1**, 82.
Scott, J. F., 1999, Ferroelectrics **232**, 905.
Scott, J. F., 2000a, *Ferroelectric Memories* (Springer-Verlag, Berlin)
Scott, J. F., 2000b, J. Appl. Phys. **88**, 6092.
Scott, J. F., 2005, Microelectron. Eng. (to be published).
Scott, J. F., C. A. Araujo, B. M. Melnick, L. D. McMillan, and R. Zuleeg, 1991, J. Appl. Phys. **70**, 382.
Scott, J. F., M. Azuma, E. Fujii, T. Otsuki, G. Kano, M. C. Scott, C. A. Paz de Araujo, L. D. McMillan, and T. Roberts, 1992, *Proceedings of ISAF 1992* (IEEE, New York), p. 356.
Scott, J. F., and M. Dawber, 2000, Appl. Phys. Lett. **76**, 3801.
Scott, J. F., A. Q. Jiang, S. A. T. Redfern, M. Zhang, and M. Dawber, 2003, J. Appl. Phys. **94**, 3333.
Scott, J. F., L. Kammerdiner, M. Parris, S. Traynor, V. Ottenbacher, A. Shawabkeh, and W. F. Oliver, 1988, J. Appl. Phys. **64**, 787.
Scott, J. F., B. M. Melnick, L. D. McMillan, and C. A. Paz de Araujo, 1993, Integr. Ferroelectr. **3**, 225.

Scott, J. F., and B. Pouligny, 1988, J. Appl. Phys. **64**, 1547.
Seifert, A., A. Vojta, J. S. Speck, and F. F. Lange, 1996, J. Mater. Res. **11**, 1470.
Sepliarsky, M., S. R. Phillpot, M. G. Stachiotti, and R. L. Migoni, 2002, J. Appl. Phys. **91**, 3165.
Sepliarsky, M., S. R. Phillpot, D. Wolf, M. G. Stachiotti, and R. L. Migoni, 2001, J. Appl. Phys. **90**, 4509.
Sepliarsky, M., M. G. Stachiotti, and R. L. Migoni, 2005, e-print cond-mat/0503524.
Sepliarsky, M., Z. Wu, A. Asthagiri, and R. E. Cohen, 2004, Ferroelectrics **301**, 55.
Seshadri R., and N. A. Hill, 2001, Chem. Mater. **13**, 2892.
Shchukin, V. A., and D. Bimberg, 1999, Rev. Mod. Phys. **71**, 1125.
Shilo, D., G. Ravichandran, and K. Bhattacharya, 2004, Nat. Mater. **3**, 453.
Shimada, Y., K. Arita, Y. Kato, K. Uchiyama, V. Joshi, and M. Lim, 2001, Integr. Ferroelectr. **34**, 1467.
Shimakawa, Y., Y. Kubo, Y. Nakagawa, T. Kamiyama, H. Asano, and F. Izumi, 1999, Appl. Phys. Lett. **74**, 1904.
Shimizu, M., H. Fujisawa, H. Nonomura, and H. Niu, 2004, Integr. Ferroelectr. **62**, 109.
Shimuta, T., O. Nakagawara, T. Makino, S. Arai, H. Tabata, and T. Kawai, 2002, Jpn. J. Appl. Phys., Part 1 **91**, 2290.
Shin, C.-H., S. Y. Cha, H. C. Lee, W.-J. Lee, B.-G. Yu, and D.-H. Kwak, 2001, Integr. Ferroelectr. **34**, 1553.
Shur, V. Ya., 1996, in *Ferroelectric Thin Films: Synthesis and Basic Properties*, edited by C. Paz de Araujo, G. W. Taylor, and J. F. Scott (Gordon and Breach, Amsterdam), pp. 153–192.
Shur, V. Ya., A. Gruverman, V. P. Kuminov, and N. A. Tonkachyova, 1990, Ferroelectrics **111**, 197.
Shur, V. Ya, A. L. Gruverman, N. Yu. Ponomarev, E. L. Rumyantsev, and N. A. Tonkacheva, 1991, JETP Lett. **53**, 615.
Shur, V. Ya., *et al.*, 2000,
Sigman, J., D. P. Norton, H. M. Christen, P. H. Fleming, and L. A. Boatner, 2002, Phys. Rev. Lett. **88**, 079601.
Simmons, J. G., 1965, Phys. Rev. Lett. **15**, 967.
Singh, D. J., 1995, Phys. Rev. B **52**, 12559.
Sinharoy, S., H. Buhay, M. H. Francombe, and D. R. Lampe, 1993, Integr. Ferroelectr. **3**, 217.
Sinharoy, S., H. Buhay, M. H. Francombe, W. J. Takei, N. J. Doyle, J. H. Rieger, D. R. Lampe, and E. Stepke, 1991, J. Vac. Sci. Technol. A **9**, 409.
Sinharoy, S., D. R. Lampe, H. Buhay, and M. H. Francombe, 1992, Integr. Ferroelectr. **2**, 377.
Smith, R. L., and S. D. Collins, 1992, J. Appl. Phys. **71**, R1.
Smyth, D. M., 1984, Prog. Solid State Chem. **15**, 145.
Soler, J. M., E. Artacho, J. D. Gale, A. Garcia, J. Junquera, P. Ordejon, and D. Sanchez-Portal, 2002, J. Phys.: Condens. Matter **14**, 2745.
Souza, I., J. Iniguez, and D. Vanderbilt, 2002, Phys. Rev. Lett. **89**, 117602.
Speck, J. S., and W. Pompe, 1994, J. Appl. Phys. **76**, 466.
Stachiotti, M. G., 2004, Appl. Phys. Lett. **84**, 251.
Stachiotti, M. G., C. O. Rodriguez, C. Ambrosch-Draxl, and N. E. Christensen, 2000, Phys. Rev. B **61**, 14434.
Steinhart, M., Z. Jia, A. K. Schaper, R. B. Wehrspohn, U. Gsele, and J. H. Wendorff, 2003, Adv. Mater. (Weinheim, Ger.) **15**, 706.
Stemmer, S., S. K. Streiffer, F. Ernst, and M. Ruhle, 1995, Philos. Mag. A **71**, 713.
Stolichnov, I., and A. K. Tagantsev, 1998, J. Appl. Phys. **84**, 3216.
Stolichnov, I., A. K. Tagantsev, E. L. Colla, and N. Setter, 1998, Appl. Phys. Lett. **73**, 1361.
Stolichnov, I., A. K. Tagantsev, E. L. Colla, and N. Setter, 1999, Ferroelectrics **225**, 125.
Stolichnov, I., A. Tagantsev, N. Setter, S. Okhonin, P. Fazan, J. S. Cross, M. Tsukada, A. Bartic, and D. Wouters, 2001, Integr. Ferroelectr. **32**, 737.
Streiffer, S. K., J. A. Eastman, D. D. Fong, C. Thompson, A. Munkholm, M. V. R. Murty, O. Auciello, G. R. Bai, and G. B. Stephenson, 2002, Phys. Rev. Lett. **89**, 067601.
Sugiyama, H., K. Kodama, T. Nakaiso, M. Noda, and M. Okuyama, 2001, Integr. Ferroelectr. **34**, 1521.
Sun, H. P., W. Tian, X. Q. Pan, J. H. Haeni, and D. G. Schlom, 2004, Appl. Phys. Lett. **84**, 3298.
Suzuki, T., and M. Fujimoto, 2001, J. Appl. Phys. **89**, 5622.
Suzuki, T., Y. Nishi, and M. Fujimoto, 1999, Philos. Mag. A **79**, 2461.
Switzer, J. A., M. G. Shumsky, and E. W. Bohannan, 1999, Science **284**, 293.
Szafraniak, I., C. Harnagea, R. Scholz, S. Bhattacharyya, D. Hesse, and M. Alexe, 2003, Appl. Phys. Lett. **83**, 2211.
Sze, S. M., D. J. Coleman, and A. Loya, 1971, Solid-State Electron. **14**, 1209.
Tabata, H., H. Tanaka, and T. Kawai, 1994, Appl. Phys. Lett. **65**, 1970.
Tagantsev, A. K., I. Stolichnov, E. L. Colla, and N. Setter, 2001, J. Appl. Phys. **90**, 1387.
Tagantsev, A. K., I. Stolichnov, N. Setter, J. S. Cross, and M. Tsukada, 2002, Phys. Rev. B **66**, 214109.
Takahashi, K. S., M. Kawasaki, and Y. Tokura, 2001, Appl. Phys. Lett. **79**, 1324.
Taylor, D. V., and D. Damjanovic, 1997, J. Appl. Phys. **82**, 1973.
Taylor, D. V., and D. Damjanovic, 1998, Appl. Phys. Lett. **73**, 2045.
Tian, W., J. C. Jiang, X. Q. Pan, J. H. Haeni, D. G. Schlom, J. B. Neaton, and K. M. Rabe, 2005, unpublished.
Tinte, S., and M. G. Stachiotti, 2000, in *Fundamental Physics of Ferroelectrics 2000*, edited by B. N. Hale and M. Kulmala, AIP Conf. Proc. No. 535 (AIP, Melville, NY), p. 273.
Tinte, S., and M. G. Stachiotti, 2001, Phys. Rev. B **64**, 235403.
Tinte, S., M. G. Stachiotti, M. Sepliarsky, R. L. Migoni, and C. O. Rodriguez, 1999, J. Phys.: Condens. Matter **11**, 9679.
Troeger, G., 1991, unpublished.
Tsai, F., V. Khiznishenko, and J. M. Cowley, 1992, Ultramicroscopy **4**, 5.
Tsai, M. H., Y. H. Tang, and S. K. Dey, 2003, J. Phys.: Condens. Matter **15**, 7901.
Tsurumi, T., S.-M. Num, Y.-B. Kil, and S. Wada, 2001, Ferroelectrics **259**, 43.
Tybell, T., P. Paruch, T. Giamarchi, and J.-M. Triscone, 2002, Phys. Rev. Lett. **89**, 097601.
Ueda, K., H. Tabata, and T. Kawai, 1998, Science **280**, 1064.
Ueda, K., H. Tabata, and T. Kawai, 1999a, Jpn. J. Appl. Phys., Part 1 **38**, 6690.
Ueda, K., H. Tabata, and T. Kawai, 1999b, Phys. Rev. B **60**, R12561.
Ullmann, M., H. Goebel, H. Hoenigschmid, and T. Haneder, 2001, Integr. Ferroelectr. **34**, 1595.
Van Aken, B. B., T. T. M. Palstra, A. Filippetti, and N. A. Spaldin, 2004, Nat. Mater. **3**, 164.

Vasco, E., R. Dittmann, S. Karthauser, and R. Waser, 2003, Appl. Phys. Lett. **82**, 2497.
Vendik, O. G., and S. P. Zubko, 2000, J. Appl. Phys. **88**, 5343.
Von Hippel, A., 1935, Ergeb. Exakten Naturwiss. **14**, 118.
Waghmare, U. V., and K. M. Rabe, 1997a, Phys. Rev. B **55**, 6161.
Waghmare, U. V., and K. M. Rabe, 1997b, Ferroelectrics **194**, 135.
Walker, L. R., 1963, in *Magnetism III*, edited by G. T. Rado and H. Suhl (Academic, New York), p. 450.
Wang, J., *et al.*, 2003, Science **299**, 1719.
Warusawithana, M. P., E. V. Colla, J. N. Eckstein, and M. B. Weissman, 2003, Phys. Rev. Lett. **90**, 036802.
Waser, R., T. Baiatu, and K.-H. Hartdl, 1990, J. Am. Ceram. Soc. **73**, 1654.
Waser, R., and D. M. Smyth, 1996, in *Ferroelectric Thin Films: Synthesis and Basic Properties*, edited by C. Paz de Araujo, G. W. Taylor, and J. F. Scott (Gordon and Breach, Amsterdam), pp. 47–92.
Watanabe, K., A. J. Hartmann, R. N. Lamb, and J. F. Scott, 1998, J. Appl. Phys. **84**, 2170.
Wieder, H. H., 1956, J. Appl. Phys. **27**, 413.
Wieder, H. H., 1957, J. Appl. Phys. **28**, 367.
Williams, R. Stanley, G. Medeiros-Ribeiro, T. I. Kamins, and D. A. A. Ohlberg, 2000, Annu. Rev. Phys. Chem. **51**, 527.
Woodward, D. I., I. M. Reaney, G. Y. Yang, E. C. Dickey, and C. A. Randall, 2004, Appl. Phys. Lett. **84**, 4650.
Wu, S.-Y., 1974, IEEE Trans. Electron Devices **21**, 8.
Wu, Z., R. E. Cohen, and D. J. Singh, 2004, Phys. Rev. B **70**, 104112.
Wu, Z., and H. Krakauer 2003, Phys. Rev. B **68**, 014112.
Xiaohua, L., J. Yin, Z. G. Liu, L. Wang, J. Li, X. H. Zhu, and K. J. Chen, 2001, Integr. Ferroelectr. **34**, 1571.
Yamada, H., M. Kawasaki, Y. Ogawa, Y. Ogawa, and Y. Ogawa, 2002, Appl. Phys. Lett. **81**, 4793.
Yoo, I. K., and S. B. Desu, 1992, Phys. Status Solidi A **133**, 565.
Yoon, S.-M., and H. Ishiwara, 2001, IEEE Trans. Electron Devices **48**, 2002.
Yu, B., C. Zhu, and F. Gan, 1997, J. Appl. Phys. **82**, 4532.
Zafar, S., B. Hradsky, D. Gentile, P. Chu, R. E. Jones, and S. Gillespie, 1999, J. Appl. Phys. **86**, 3890.
Zafar, S., R. E. Jones, B. Jiang, B. White, V. Kaushik, and S. Gillespie, 1998, Appl. Phys. Lett. **73**, 3533.
Zhong, W., D. Vanderbilt, and K. M. Rabe, 1994, Phys. Rev. Lett. **73**, 1861.
Zhou, W., 1992, J. Solid State Chem. **101**, 1.